NASA Technical Memorandum 101065

Performance and Test Section Flow Characteristics of the National Full-Scale Aerodynamics Complex 40- by 80-Foot Wind Tunnel

Peter T. Zell
Karen Flack, Ames Research Center, Moffett Field, California

February 1989

NASA

National Aeronautics and
Space Administration

Ames Research Center
Moffett Field, California 94035

CONTENTS

SYMBOLS

C_p = static pressure coefficient

I_u = axial turbulence intensity component, $I_u = u'/u$, %

I_v = lateral turbulence intensity component, $I_v = v'/v$, %

I_w = vertical turbulence intensity component, $I_w = w'/w$, %

p_s = static pressure, psf

p_t = total pressure, psf

P_s = test section static pressure from scales, psf

P_r = settling chamber reference pressure from scales, psf

q = dynamic pressure, $q = 1/2\rho U^2$, psf

q_u = uncorrected scale q, $P_r - P_s$, psf

Δq_η = compressibility correction to q

Δq_{sp} = static plate correction to scale q

Δq_{sc} = scale correction to scale q

q_{cse} = q_u corrected for scale errors only, $q_{cse} = q_u + \Delta q_{sc}$

q_s = fully corrected scale q, $q_s = q_u + \Delta q_{sc} + \Delta q_\eta + \Delta q_{sp}$

Δq_{pc} = probe correction to q

T_T = tunnel temperature, °F

T = total temperature, °F

U_{ts} = flow velocity, knots

X = streamwise coordinate, ft

Y = cross-stream coordinate, ft

Z = vertical coordinate, in. or ft

α = pitch angle (vertical plane), deg

β = yaw angle (horizontal plane), deg

ρ = air density

Subscripts:

atm = atmospheric

cl = at test section centerline

max = maximum level

pp = peak to peak

ts = test section

unc = uncorrected

w = test section wall

mm = micromanometer

Superscripts:

$\bar{}$(ex:$\bar{x}$) = mean value

SUMMARY

Results from the performance and test section flow calibration of the 40- by 80-Foot Wind Tunnel are presented. A flow calibration test was conducted in May and June 1987. The goal of the flow calibration test was to determine detailed spatial variations in the 40- by 80-ft test section flow quality throughout the tunnel operational envelope. Data were collected for test section speeds up to 300 knots and for air exchange rates of 0, 5, and 10%. The tunnel performance was also calibrated during the detailed mapping of the test section flow field.

Experimental results presented indicate that the flow quality in the test section, with the exception of temperature, is relatively insensitive to the level of dynamic pressure and the air exchange rate. The dynamic pressure variation in the test section is within ±0.5% of mean. The axial turbulence intensity is less than 0.5% up to three-quarters of the maximum test section speed, and the vertical and lateral flow angle variation is within ±0.5° at all test section velocities. Cross-stream temperature gradients in the test section caused by the air exchange system were documented, and a correction method was established. Streamwise static pressure variation on the centerline is about 1% of test section dynamic pressure over 30 ft of the test section length.

INTRODUCTION

The 40- by 80-Foot Wind Tunnel is part of the National Full-Scale Aerodynamics Complex (NFAC) located at the Ames Research Center in California (fig. 1). It is a single-return, closed test section wind tunnel. The oval test section has a maximum flow speed of approximately 300 knots (154 m/sec). Figure 2 shows a schematic of the wind tunnel circuit. The wind tunnel drive consists of six fans rated at 135,000 maximum combined horsepower (101 MW). The fans are arranged three stacked on top of three as shown in figure 3.

The 40- by 80-Foot Wind Tunnel was constructed in the 1940s and was used extensively for over three decades for a variety of large-scale subsonic tests. The tunnel was then brought off-line for modification. This was necessary to meet the current and future requirements of large-scale aerodynamic and aeroacoustic testing. The drive system was repowered to increase the test section velocity from 200 to 300 knots. A new nonreturn leg with an 80- by 120-ft test section was also added to the tunnel circuit. Figure 4 shows a schematic of the wind tunnel in the 80- by 120-Foot Wind Tunnel mode.

The 40- by 80-Foot Wind Tunnel has undergone extensive structural and aerodynamic modifications. Before research testing could resume, a performance and test section flow calibration was required. This calibration of the 40- by 80-Foot Wind Tunnel was concluded in June 1987.

This report documents the 40- by 80-Foot Wind Tunnel performance and test section flow calibration results. The results mainly take the form of tunnel performance curves and flow quality distributions.

The primary goal of the flow calibration (FLOCAL) test was to determine the detailed spatial variations in the 40- by 80-ft test section flow quality throughout the tunnel operational envelope. This was done by examining the distributions of total and static pressure; velocity, including magnitude and direction; turbulence; and temperature. Performance of the wind tunnel was also documented. The performance results consist of calibration curves of test section dynamic pressure and velocity versus fan blade angle and net power delivered to the fans.

An instrumentation boom was used as a measurement platform. The boom spanned the center 50% of the test section and was equipped with five fixed measurement stations spaced 10 ft apart. This boom was moved to three elevations during the FLOCAL. Fixed probes also provided measurement stations 10 ft from each side wall. Pressure taps were used to measure the wall pressure distribution, and fixed rakes measured the floor boundary layer. The test section measurement location grid appears in figures 5 and 6. Table 1 contains the FLOCAL test matrix.

FACILITY DESCRIPTION

The performance of the wind tunnel and the quality of the flow passing through the test chamber is determined by the quality of the flow in the entire tunnel circuit. Much experimental and theoretical work was done during the tunnel modification to improve circuit aerodynamics. The results of this work are described by Olson et al. (ref. 1).

The flow path of the 40- by 80-Foot Wind Tunnel is described here, beginning in the settling chamber just ahead of the test section and proceeding in a counterclockwise direction around the rectangular tunnel circuit. It is important to note that the 40- by 80- and 80- by 120-Foot Wind Tunnels share portions of their flow paths (figs. 2 and 4). Selection between the two tunnels is accomplished by adjusting a set of large flow valves and movable flow-deflection vanes. These valves and deflection vanes are discussed in the order that they are encountered by the flow in the 40- by 80-circuit.

Most of the flow nonuniformity and turbulence in the low-speed settling chamber is reduced by the 8:1 area ratio contraction cone ahead of the test section. There are no special flow treatment provisions (such as screens) in this area or in the rest of the circuit. Before the flow begins to accelerate through the contraction cone, it passes the reference ring of four connected wall-pressure ports. Then, just before it enters the test section, it passes the static ring of four connected wall-pressure ports. The difference in the pressure measured at these two rings is approximately equal to the test section dynamic pressure. This system is used to set the tunnel speed and will be discussed in more detail later.

The flow then enters the 40-ft-high by 80-ft-wide by 80-ft-long oval test section and can reach a speed of approximately 300 knots. The height and width have been slightly reduced from their original dimensions by the addition of a 6-in. acoustic liner on the walls, ceiling, and floor of the test section. The liner was contoured into the existing tunnel wall surface with a leading-edge ramp

with a slope of 1/3 and a trailing-edge ramp with a slope of 1/10. A description of the liner and its performance is given in reference 1.

As the flow exits the test section, it encounters a set of vortex generators which stabilize the flow field in the high-speed diffuser (2.7 area ratio). Eight airfoil-shaped fins impart a counter-clockwise rotation to the flow on the inside half of the circuit and a clockwise rotation to the flow on the outside half. The effect is an energization of the flow along the walls at the end of the diffuser. The diffuser also has 10, airfoil-shaped structural columns which extend from floor to ceiling. The first column has an enlarged structure at the base to protect the column from damage by any large pieces of debris that may come off the model in the test section. A 5-ft-high debris fence is also located at the end of the diffuser.

The flow then makes a 90° turn to the left through the fixed vertical airfoils of vane set #1 and enters a constant-area duct. The flow in the wind tunnel is heated by the energy of the fan drive. It can also be heated and contaminated by engines used in powered models. On the inside wall of the duct is the inlet for an air exchange system. This system is discussed in detail by Rossow et al. (ref. 2). The inlet consists of a streamlined cowl to guide the flow through a wall opening, and a variable-geometry door that injects outside air tangentially to the tunnel flow (fig. 7). This door can be adjusted to provide from 0 to 10% air exchange. Note that the fresh air enters on the inside of the circuit. This cool air then heats as it gradually spirals toward the outside of the tunnel circuit. The air exchange exhaust will be discussed later.

Vane set #2, which is identical to vane set #1, guides the flow through another 90° turn to the left. The flow then encounters the eight flat-plate doors of vane set #3 that serve as a large valve which closes off the 40- by 80-Foot Wind Tunnel when the 80- by 120-Foot Wind Tunnel is operated. The doors of vane set #3 are aligned with the tunnel flow (they do not turn the flow) and have structural trusses which stiffen them against bending. The trusses are constructed of aerodynamically shaped structural members. After the flow leaves vane set #3, the outside of the circuit is formed by vane set #4, which closes off the 80- by 120-Foot Wind Tunnel. Figure 8 shows the intersection of the 40- by 80- and 80- by 120-Foot Wind Tunnels.

The next vane set, vane set #5, turns the flow 45° when the tunnel is operated in 80- by 120- mode. In the 40- by 80- mode, the flow passes through vane set #5 without turning. Uniquely shaped, fixed vanes that have good drag characteristics over 55° of onset flow angle are used (ref. 1). Vane set #5 is also equipped with a 3-ft debris fence on the floor at the trailing edge.

The flow now enters the fan drive. Six fans, stacked three on top of three, have a combined power consumption at full speed of 135,000 hp (fig. 3). Each fan is approximately 40-ft in diameter and has 15 rotor blades and 23 stator blades. The fan revolutions per minute and blade angle are adjustable to alter tunnel speed. Each fan has a faired contraction and diffuser to guide the flow from the rectangular cross section ahead of the fans to the rectangular cross section after the fans.

The fan diffuser guides and slows the flow to the low-speed, south end of the tunnel. Vane set #6 is equipped with a 6-ft chord trailing-edge flap that adjusts to turn the flow 90° in the 40- by 80-mode or allows the flow to pass unturned in the 80- by 120-mode (fig. 9). The fixed portion of the vane set is acoustically treated to absorb noise from the fan drive and both test sections.

The exhaust for the 40- by 80-Foot Wind Tunnel air exchange system lies in the southwest corner of the wind tunnel. An 18-ft-wide by 125-ft-tall section of the wall is open to the atmosphere. To reduce the amount of 40- by 80- test section noise escaping through this opening, an acoustic barrier was installed between vane set #6 and the south wall, parallel to the flow exiting the tunnel (fig. 9). The remaining flow turns 90° to the left again and traverses a constant-area duct to vane set #8. Along the south side of the duct is louver #7. This set of flat plate doors, when open, allows the flow from the 80- by 120-Foot Wind Tunnel to exhaust into the atmosphere (fig. 4).

Vane set #8 guides the flow through the fourth and final 90° turn to the left and into the contraction cone again. When the flow reaches the contraction cone, the flow path of the 40- by 80-Foot Wind Tunnel is complete.

APPARATUS

Instrumentation Support Hardware

Optimum instrumentation support hardware for a flow calibration would position the instrumentation at all locations in the test chamber, instantaneously, with no interference to the flow. But in a large-scale wind tunnel, this goal is impossible to meet. The compromise is to use fixed measurement stations that are distributed as shown in figures 5 and 6.

The advantage of using fixed stations is that measurements can be made at several locations at the same time. Past problems with low-frequency variations in flow quality made it desirable to collect the data in this way. Also, because of the nature of future tests, collecting "fine grid" distributions of the flow quality was not deemed critical.

Size and flow speed of the 40- by 80-ft test section also influenced the hardware design. Deflections of large instrumentation supports caused by aerodynamic loads had to be minimized without causing significant flow interference. Cost and time restraints were also considered in the design.

Instrument boom– A fixed instrument boom with five probe stations was used to span the center 50% of the test section. This "rake" could be moved to three vertical and two streamwise positions. Photographs of the boom at the Z = 10-, 20-, and 30-ft heights are shown as figures 10, 11, and 12. The boom was mounted on the main struts of the 40- by 80-ft model support system. Aerodynamic fairings were used to cover the large cylinders of the main struts when the boom was at the Z = 20- and 30-ft heights. No fairings were used at the Z = 10-ft boom height.

The boom itself was a symmetric airfoil with a truncated trailing edge. Multiple instrument probes (multiprobes) were mounted approximately 8 ft ahead of the boom at the end of stings (fig. 13). This minimized aerodynamic measurement interference that originated from the model support struts and boom.

Wall probes– Wall mounted probe supports provided a Z = 20-ft measurement station at locations 10 ft from each wall. The wall-mounted probe supports were used only when the boom was at the 20-ft height position.

Boundary layer rakes– Two fixed rakes of pressure probes were used to measure the boundary-layer dynamic pressure and velocity profiles on the floor of the test section. The rake mounting locations are shown in figure 6. The 48-in. tall rake was mounted 36 ft upstream from the center of the turntable and 14 ft east of the tunnel centerline. A shorter, 32-in. rake was mounted 13 ft upstream and 18 ft east of the centerline.

Wall pressure taps– Nine static pressure taps were mounted on the west wall of the test section. The taps were placed in the center of a 12-in.-diameter sheet metal plate. The tap and plate surface were smooth to provide a good static pressure measurement. Distribution of the pressure plates is shown in figure 6.

Instrumentation

Standard wind tunnel instrumentation– The standard wind tunnel instrumentation is used for most tests and has become a permanent part of the facility. Most of these measurements are used to derive and set wind tunnel speed. Measurements include dynamic pressure, temperature, relative humidity, barometric pressure, fan drive power, fan revolutions per minute, and fan blade angle. Atmospheric temperature and wind conditions were also measured.

Figure 14 is a schematic of the standard wind tunnel instrumentation. Dynamic pressure is measured using static pressure rings located in the settling chamber and just ahead of the test section. The pressure is measured with a scale system and with a micromanometer pressure transducer. Tunnel temperature is measured in the settling chamber on the wind tunnel centerline. Relative humidity was measured on the floor in the test section during the flow calibration test (FLOCAL). A barometer located in the control room provides a barometric pressure measurement.

Multiprobes– The multiprobe is a compact combination of measuring instruments that was developed for the FLOCAL. It contains a pitot-static probe, a hot-wire probe, a total-temperature probe, and a set of pitch and yaw vanes. All of these components were assembled and mounted on a central sting, as shown in figure 15. Multiprobes were mounted at the measurement stations provided by the boom and the wall-mounted supports.

The pitot-static, total-temperature, and hot-wire probes used in the multiprobe were standard, commercially available instruments. The pitch and yaw vanes were developed in-house and are described in reference 3. The multiprobe was designed to rotate 180° for measuring pitch and yaw angle tares. Alignment jigs were used to set the pitch and yaw vanes at a reference zero position. An alignment jig is installed on the pitch vane of the multiprobe shown in figure 15. Specifications on all of the probes that were used for the FLOCAL are given in table 2.

Data System

Two independent data systems were used during the FLOCAL. The standard wind tunnel data system was used to collect data from pressure transducers, hot-wire anemometers, temperature probes, flow-direction vanes, and standard wind tunnel instrumentation. Most of the pressure data were collected using a stand-alone electronically scanned pressure (ESP) system. This system is described in detail in reference 4. The ESP system was run by an HP 9836 computer. Figure 16 is a data-system flow chart for a typical multiprobe.

The quality of a test section flow calibration depends on the accuracy of the measurements made. Every measurement has both fixed and random measurement errors that contribute to the overall measurement uncertainty. Practical steps were taken to reduce measurement errors during the FLOCAL. Statistical techniques presented in reference 5 were also used to estimate measurement uncertainty where appropriate.

Fixed errors occur when a measurement has a bias that stays constant for repeated measurements. Some fixed errors were accounted for by careful calibration of instrumentation. Subtracting a "starting value" from the data helped to reduce fixed errors. Monitoring the data during the test also helped to identify "bad" data and instrumentation that required repair or recalibration.

Random errors take the form of scatter or noise in the data. This type of error keeps a measurement from repeating itself. Random errors were reduced during the FLOCAL by time-averaging data. Most steady-state measurements were averaged over a 30-sec time interval. Data from repeat runs were also compared to assess the amount of data scatter.

WINDSPEED CALIBRATION

A critical element of a wind tunnel calibration is the calibration of the windspeed (velocity) measurement system. The 40- by 80-Foot Wind Tunnel system was described earlier in the Apparatus section. The method used to calibrate the wind speed system is described by Tolhurst in reference 6.

Ideally, a windspeed system would measure the velocity in the test section directly, taking into account the presence of models while being completely nonintrusive to the flow. In the 40- by 80-ft section, a measurement of dynamic pressure on the centerline of the tunnel, directly above the turntable, is used to calibrate a set of static pressure measurement rings located in the return passage and just ahead of the test section. Rae and Pope (ref. 7) suggest that this calibration should be done with the test section empty, with model support struts in, with a ground plane in, and with any other baseline test section configuration that will be used. Since a completely empty test section was not possible, this calibration was done with the instrumentation supports installed. Blockage of the supports (estimated at 2.8% at the $Z = 20$-ft height) was not accounted for in the calibration of the windspeed system.

The difference in pressure between the static pressure rings is approximately equal to the dynamic pressure just ahead of the test section. Although this measurement of dynamic pressure is not equal to the dynamic pressure in the test section, it is repeatable over the speed range of the tunnel. Corrections can be applied to adjust the reading from the rings to the dynamic pressure level on the centerline.

The first step in a windspeed calibration is to make an accurate measurement of dynamic pressure from the static rings. A mechanical bellows-type pressure transducer attached to a Toledo scale is used. The transducer is calibrated using a known variable-pressure source to account for any transducer errors. Figure 17 is a plot of the current scale correction (Δq_{sc}) plotted against the raw dynamic pressure measured with the scale (q_u). The dynamic pressure corrected for scale errors (q_{cse}) will be used as a reference pressure for flow-quality assessment. The value of q_{cse} is repeatable despite the configuration of the test section.

$$q_{cse} = q_u + \Delta q_{sc}$$

A compressibility correction (Δq_η) to the dynamic pressure is applied to correct the dynamic pressure measured by the scale. This correction is derived in reference 6. Figure 18 is a plot of Δq_η versus q_{cse}.

Corrections must also be applied to the dynamic pressure measured on the centerline with a pitot-static probe. The probe was calibrated to National Institute for Standards and Technology specifications prior to its installation in the test section. This probe correction (Δq_{pc}) is plotted against the indicated dynamic pressure on the centerline ($q_{cl,unc}$) in figure 19. The compressibility correction (Δq_η) is also applied to $q_{cl,unc}$ (fig. 18). The resulting equation for the corrected dynamic pressure on the centerline is

$$q_{cl} = q_{cl,unc} + \Delta q_{pc} + \Delta q_\eta$$

The static plate correction (Δq_{sp}) was measured during the FLOCAL. This correction is the difference between the dynamic pressure measured on the centerline (q_{cl}) and the dynamic pressure measured by the scale (corrected for scale errors and compressibility). A plot of Δq_{sp} versus q_{cse} is shown as figure 20. Several runs of the FLOCAL were averaged to obtain Δq_{sp}. This correction takes into account the increase in q due to the reduction in the tunnel cross-sectional area between the static ring location and the model mounting location.

The corrected dynamic pressure (q_s) measured by the scale is defined as

$$q_s = q_u + \Delta q_{sc} + \Delta q_\eta + \Delta q_{sp}$$

A micromanometer was connected to the pressure lines of the static pressure rings to provide a second dynamic pressure measurement source in the event of a failure of the scale system. Since the micromanometer has an internal calibration, only the compressibility and static plate corrections were used.

$$q_{s,mm} = q_{u,mm} + \Delta q_\eta + \Delta q_{sp}$$

During the FLOCAL, the centerline q probe was also positioned 15 ft forward from the center of the turntable. Because of a streamwise static pressure gradient, the static plate correction is different at this location. A plot of the static plate correction for a reference point 15 ft forward from the center of the turntable ($\Delta q_{sp'}$) versus q_{cse} is shown as figure 21.

The test section windspeed is determined from the corrected dynamic pressure, using the relationship

$$U_{ts} = (2 \cdot q_s/\rho_{ts})^{1/2}$$

The test section density (ρ_{ts}) is calculated using the method described in reference 6. The tunnel temperature, barometric pressure, relative humidity, and static pressure values in the test section are required. Locations of these measurements are shown in figure 14. The test section velocity on the centerline is used to plot performance curves for the tunnel. This information is presented in the Performance Calibration section.

PERFORMANCE CALIBRATION

A wind tunnel performance calibration was done during the FLOCAL. The variation of test section dynamic pressure and velocity with changes in fan blade angle and fan drive power were documented. These performance curves were generated for two fan drive power modes and for three air exchange rates. The rise and decay of test section dynamic pressure were also documented. Another performance factor was the rise of tunnel temperature with time. Variation of the static pressure level in the settling chamber with tunnel speed is also presented.

Two fan drive power modes are available. The induction frequency control (IFC) system, which uses a motor-generator set to provide power up to 24 MW, and the Utility power system. In the IFC mode, the fan revolution per minute and blade angle can be varied. The fan blade angle range in IFC mode is –18 to 24° (–5° is flat pitch). The Utility power system connects the fan drive motors directly to line power. When operating in Utility mode, the fans rotate at a fixed 180 rpm. The fan blade angle is adjusted between –18° and 49° to vary tunnel speed. Air exchange rates used during the calibration were 0, 5, and 10%.

A maximum fan blade angle of 44° was achieved at 0% air exchange in the Utility mode during a run to document the variations of dynamic pressure and tunnel temperature with time. Excessive wall pressures were discovered in the south end of the wind tunnel circuit during this run. Thereafter, FLOCAL testing at 0% air exchange in Utility mode was limited to a maximum fan blade angle of 24° (U_{ts} = 175 knots).

Dynamic Pressure and Velocity Versus Fan Blade Angle

The corrected dynamic pressure (q_s) on the centerline above the turntable is plotted against the fan blade angle for Utility and IFC modes in figures 22 and 23 respectively. Data are shown for the three air exchange rates (0, 5, and 10%) incorporating all of the FLOCAL runs. Scatter in the data can be mainly attributed to tunnel temperature variations. As the tunnel heats, air density and dynamic pressure decrease. The purpose of these plots is to provide an estimate of dynamic pressure for a particular fan blade angle and fan revolutions per minute.

The test section velocity (U_{ts}) is not sensitive to density variations. Figures 24 and 25 are plots of U_{ts} versus fan blade angle for Utility and IFC modes, respectively.

The 40- by 80-Foot Wind Tunnel can be run in the reverse-flow direction. The fan blade angle can be adjusted from the flat pitch position, –5°, to –18°. Running the tunnel in the reverse direction may be required to offset the flow generated by model engines during hover testing. Figures 26 and 27 show the dynamic pressure and velocity versus fan blade angle plots for reverse-flow tunnel operation. These performance curves are based on data collected at a single point, 5 ft above the floor. No information about the quality of reversed test section flow was obtained. The flow quality is probably poor because of the presence of the vortex generators near the aft end of the test section.

Dynamic Pressure and Velocity Versus Tunnel Power

The corrected dynamic pressure (q_S) is plotted against the net power delivered to the fans for Utility and IFC modes in figures 28 and 29, respectively. Data are shown for three air exchange rates (0, 5, and 10%) and incorporates all of the FLOCAL runs. Figures 30 and 31 are plots of U_{TS} versus fan drive power for Utility and IFC modes, respectively.

Dynamic Pressure Decay and Temperature Rise

The time required for the fan blade variable-pitch mechanism (VPM) system to drive the tunnel to a settled q level (and back to no flow at 0% air exchange) was measured. The rate of fall of q after a tunnel shutdown was also measured at 5 and 10% air exchange. This documented how quickly the tunnel reaches a no-flow level when the fans are suddenly turned off.

Documenting the air temperature rise with run time was done to evaluate the performance of the air exchange system. With no air-exchange, the tunnel rapidly and continuously heats. With cool atmospheric air entering through the air-exchange inlet, the tunnel temperature rises less rapidly and reaches an equilibrium value.

Temperature variation with time was measured during a tunnel "purge." A purge operation is performed to exhaust hot air and powered model engine exhaust products from the wind tunnel. The purge operation consists of opening the 40- by 80-ft test section overhead doors, opening louver 7, and bringing the fan blade angle 5° above flat pitch (0° blade angle). This operation causes a flow of cool atmospheric air through the tunnel circuit.

Data were collected at 0, 5, and 10% air exchange during tunnel heat runs. The goal of the heat runs was to document the time to reach the operational limit of 125°F or a steady-state tunnel temperature when running at maximum dynamic pressure.

The dynamic pressure measurement was made with the static pressure rings of the q-scale system. The single-point temperature measurement was made in the settling chamber ahead of the contraction cone. This was done with a thermistor mounted on vane set #8 at the tunnel centerline.

The 0% air-exchange run started with an increase of fan blade angle to 44° using the VPM system. Dynamic pressure was maintained for about 40 min. The fan blade angle was then driven down to flat pitch.

The 5 and 10% air-exchange runs started with an increase in tunnel dynamic pressure to near maximum. The runs had a duration of 63 and 32 min, respectively. A fan drive shutdown (turn off power) was performed at the end of these runs. After these runs tunnel air flow was not purged.

Time history plots of dynamic pressure were normalized with respect to the maximum value reached during the run. Temperature time histories were normalized with respect to the maximum increase in tunnel temperature achieved. The measurement of tunnel temperature that is used to calculate the tunnel speed is T_T.

Figures 32, 33, and 34 show that the VPM requires approximately 7.5 min to drive the fan blades to the maximum dynamic pressure position. Figure 32 also shows that the VPM requires approximately 7 min to drive the fans to the no-flow condition.

The 0% air-exchange temperature time history (fig. 32) shows that the tunnel temperature rose 59°F above the ambient temperature of 65°F and reached the operational limit of 125°F in 40 min of operation at maximum dynamic pressure. The temperature rise also showed no indication of slowing. After tunnel shutdown, a purge was performed. T_T first decreased as the test section doors and louver 7 were opened, allowing ambient air to enter. Then, as the purging flow started, the temperature rose again. This rise was most likely caused by the mixing of warm air that had risen to the top of the circuit with the cooler outside air. T_T then stabilized at ambient temperature.

Figure 33 shows that at 5% air exchange, the tunnel temperature rose 34°F above the ambient level and stabilized after 48 min. Figure 34 shows that at 10% air exchange, the tunnel temperature rose 25°F above the ambient level and stabilized after 32 min. After a fan drive shut-down at 5 and 10% air exchange, the tunnel q reached 5% of maximum q in 47 and 52 sec, respectively.

Static Pressure Level Variation in the Settling Chamber

The variation of static pressure level in the settling chamber with tunnel dynamic pressure is presented in figure 35. Data are shown for 0, 5, and 10% air exchange. Static pressure in the settling chamber was measured by placing a differential pressure transducer between the reference ring of the scale system (P_r) and atmosphere (P_{atm}). If P_r is used as a reference for a pressure measurement in the test section, figure 35 can be used to adjust that pressure measurement to an atmospheric reference.

TIME-AVERAGED FLOW QUALITY PARAMETERS

Pressure and Velocity Distributions

Another of the goals of the FLOCAL was to obtain the spatial distributions of total, static, and dynamic pressure in the test section. Pitot-static probes were used to measure the total and static pressure. The dynamic pressure was then calculated as total minus static pressure. These measurements were made to document variations in the level and distribution of total and static pressure caused by tunnel speed setting, air-exchange rate, tunnel geometry, power mode, or any other factors. An understanding of total, static, and dynamic pressure in a wind tunnel is required before one attempts to evaluate the results of the measurements.

Flow velocity in the test section establishes the static pressure level. If all of the flow in the test section is aligned with the tunnel centerline, then the static pressure will be uniform. Static pressure gradients are associated with flow curvature in potential flow. Sources of flow curvature in the test section may be boundary-layer growth or the flow interference of support structures. Support structures obstructing the flow also affect the overall flow velocity and thus the static pressure level.

Total pressure is a measurement of the energy of the flow. The fans generate a total pressure rise while all of the tunnel components (i.e., vane sets, contractions, diffusers, etc.) cause total pressure losses. Variations in the total pressure distribution in the test section can be caused by a wind tunnel component, such as a vane set, that has a nonuniform pressure loss. The slower flow in the boundary layer causes a total pressure gradient near the test section wall.

Levels and distributions of both total and static pressure influence the dynamic pressure level and distribution in the test section. All factors that affect the total and static pressure affect the dynamic pressure.

The pitot-static probe measurement of total pressure is not highly sensitive to probe damage or alignment. The static pressure measurement, however, may be significantly affected by such factors. Another factor affecting pressure measurement in the test section is density changes due to variations in atmospheric pressure, temperature, and humidity.

The raw total and static pressure distributions for each point of the "FLOCAL" were plotted. These plots were then analyzed to examine the data for trends in the distributions. Runs and points that illustrated any trends were then selected. These data were corrected and plotted for this report.

Total Pressure

How the total pressure on the centerline in the test section varies with tunnel q and air exchange rate is given in figure 36. The indicated total pressure on the centerline ($p_{t,cl}$–P_{atm}) is plotted against q_{cse} for 0, 5, and 10% air exchange. Figures 37 and 38 are the same plots for the $Y = 0$ ft position at the $Z = 10$ and 30-ft heights, respectively. Data from all runs of the "FLOCAL" were used to generate figures 36, 37 and 38. When $P_r - P_{atm}$ (fig. 35) is subtracted from $p_{t,cl} - P_{atm}$, the curves for 0, 5, and 10% air exchange collapse to the single curve shown as figure 39. This plot allows the user to establish the centerline total pressure level with a measurement of q_{cse} regardless of air exchange rate.

Figure 40 shows the total pressure distribution for two high-speed points at the same flow conditions at the $X = 0$ ft and $X = 15$ ft positions. These plots show that streamwise location has little effect on total pressure distribution. Figure 41 shows the same type of total pressure distributions at 5 and 10% air exchange. There appears to be no significant effect of air-exchange rate on the total pressure distribution.

Figure 42 illustrates how the absolute total pressure distribution changes with tunnel speed. Data are shown for a 10% air-exchange run at the three vertical locations. The bias of the flow toward the inside of the circuit at high speed is clearly visible in this figure. Figure 43 shows a contour plot of ($p_t - p_{t,cl}$) for the test section.

Static pressure– As previously discussed, the absolute static pressure is a difficult parameter to measure in a wind tunnel. It is affected by the blockage of the instrumentation supports, aerodynamic interference of supports, density variations, and probe geometry.

The hardware required to position the instruments at the three vertical locations had different amounts of blockage. This is illustrated in figures 10, 11, and 12. Since it was not possible to obtain data with the test section completely empty, no attempt to define absolute static pressure

levels was made. Instead, emphasis was placed on examining the distributions of static pressure only.

Findings showed that the distribution of static pressure in the test section does not vary with any tunnel variable. Figure 44 shows the static pressure coefficient distribution at the Z = 10-, 20-, and 30-ft locations. The effect of the instrumentation support fairings on the static pressure readings made at the Y = ±10-ft stations at the Z = 20-ft height is clearly visible. Since the fairings were not present at the Z = 10-ft height, and were far from the measurement locations at the Z = 30-ft height, the instrumentation support interference was negligible. A close examination of figure 44 revealed that the static pressure error produced by the fairings could be estimated by subtracting the Z= 20-ft data from the Z = 10- and 30-ft data. When the static pressure error correction is applied to the Z = 20-ft data, the distributions of C_p match closely (fig. 45).

When the instrumentation support was moved from the X = 0-ft to the X = 15-ft location, the wall-mounted probes remained at the X = 0-ft position. Since the wall-mounted probes did not move, a comparison between the static pressure level and distribution at the two streamwise stations could be made. Figure 46 shows the C_p distributions for X = 0 and X = 15 ft. Note that there is a uniform C_p difference between the two stations.

Dynamic pressure– The distributions of total and static pressure combine to produce a relatively flat dynamic pressure profile. This appears to be a characteristic of subsonic wind tunnel test section flow. While the total pressure near the walls drops because of the presence of the boundary layer, the static pressure near the wall rises because of streamline curvature. The streamline curvature near the wall is caused by boundary-layer growth and by the shape of the tunnel walls. No significant effect of tunnel speed or air-exchange rate on the distribution of dynamic pressure was found.

The accuracy of a pitot-static probe was quoted by the manufacturer to be around ±0.5% of full scale. For this reason, small variations in the dynamic pressure distribution were believed to be caused by differences in the errors of the individual probes. To provide an in situ calibration of each pitot-static probe, a separate pitot-static probe was moved to each location. Calibration curves between the "reference probe" and each pitot-static probe were generated. These final corrections were applied, and the final dynamic pressure distribution was plotted (fig. 47). The dynamic pressure distribution was found to be within ±0.5% of the mean.

Velocity– The velocity at each measurement location was also calculated from the measured pressures. A typical distribution of test section velocity is shown as figure 48. The velocity distribution is within ±0.4% of the mean.

Streamwise Static Pressure Distribution

The streamwise wall pressure distribution in the test section was measured along the west wall (fig. 6). Static pressure measurements were also made on the tunnel centerline at the two streamwise boom positions, 15 ft apart.

The wall pressure distribution was not affected by tunnel speed, boom position, or the air-exchange rate. Figure 49 is a representative plot of wall static pressure coefficient versus the streamwise location (X). Data are shown for 5 and 10% air-exchange runs with the boom in the

forward and aft position at maximum tunnel speed (four data points). The wall static pressure coefficient was referenced to scale system pressures and is defined as

$$C_{p,w} = (p_{s,w} - P_s)/(q_{cse})$$

$C_{p,w}$ is close to zero at the left side of the plot because the first wall static pressure tap was located near the static ring of the scale system.

Measurements of the static pressure coefficient on the centerline ($C_{p,cl}$), both directly above and 15 ft ahead of the center of the turntable, are also plotted on figure 49. This coefficient is also referenced to the scale system and is defined as

$$C_{p,cl} = (p_{s,cl} - P_s)/(q_{cse})$$

The nine wall-pressure taps were placed on the side wall where the largest variation in static pressure was expected because of the shape of the test section. Forward and rear pressure spikes in the wall-pressure distribution are caused by the acoustic liner ramps and the curvature of the walls at the start and end of the test section. These pressure spikes are local wall effects and also appear in numerical flow code models of the test section. The flow code models also show that the spikes decay rapidly as distance from the wall increases and they are not discernible on the tunnel centerline.

The purpose for determining the streamwise static pressure distribution in the test section is to make corrections to model drag data. Wall static pressure distributions reflect what is present in the local area near the wall, but it is the streamwise gradient in static pressure on the centerline that is required to make drag data corrections. It is difficult to say what the static pressure gradient is over the usable length of the test section with the limited number of streamwise locations tested during the FLOCAL. The centerline static pressure gradient in figure 49 shows a 0.48% of q_{cse} decrease over 15 ft of test section length. By linear interpolation, that equals approximately a 1% of q_{cse} gradient over 30 ft.

Flow Angle Distributions

Pitch and yaw flow angles were measured using the free-trailing flow direction vanes described earlier. Flow angle measurements were made at the locations shown in figures 5 and 6 for all points in the test matrix (table 1).

The sign convention used for flow angle measurements made during the FLOCAL was as follows. A positive pitch angle indicates upflow in the test section. A positive yaw angle indicates flow angled toward the outside of the tunnel circuit. The pitch and yaw angles are absolute angles. The pitch angle was referenced to the local gravitational waterline with a propeller protractor. The yaw angle was referenced to the geometric centerline of the test section.

Several factors affected the average flow angle data quality during the FLOCAL. Corrections were made to account for structural misalignments of the large probe support structure, aerodynamic affects on the vane fin, and drifts in the output of the vanes due to temperature. Deflection of the support structure under load and flow angles induced by the probe support structure was not accounted for and contributed to data inaccuracy.

Review of the data showed significant data scatter. A combination of instrumentation errors and other errors discussed earlier in this section caused this scatter. It was impossible to resolve the small variations in the flow angle distributions due to individual tunnel speed settings or air exchange rates. For this reason, flow angle data collected at each boom position were divided into three speed ranges and averaged to obtain the overall free-stream angle distributions. Data from the X = 0- and 15-ft boom positions were averaged. The speed ranges were 0 to 100 knots, 100 to 200 knots, and 200 to 300 knots. A statistical analysis performed on a set of repeat data points taken at fixed conditions indicated that the mean flow angle was within ±10% of the sample range 90% of the time.

FLOCAL flow angle results indicate that the mean flow angle is within ±0.5° at tunnel speeds above 200 knots for all air-exchange settings. Figure 50 shows the pitch-angle distributions for the Z = 10-, 20-, and 30-ft boom heights at U_{ts} > 200 knots. A curve is drawn through the mean value at each location and bars show the range of data scatter. Figure 51 shows the same series of plots for the yaw angle.

The pitch and yaw angle distributions for the three speed ranges at the Z = 20-ft boom height are shown as figures 52 and 53, respectively. As shown, the data scatter bars become smaller with increasing tunnel speed. The mean value however, does not vary much with increasing U_{ts}.

Figure 54 summarizes the pitch-angle distribution results for the FLOCAL. The three plots show data collected at the three speed ranges. Each plot has three curves that represent the mean flow angle values collected at the three boom heights. Figure 55 shows the same series of plots for the yaw angle.

The pitch-angle distributions at the Z = 10-, 20-, and 30-ft boom heights show an upflow of approximately 0.5° in the test section. The Z = 30-ft boom height shows the most upflow, and the Z = 10-ft height shows the least. Part of this upflow, particularly at high U_{ts}, may be caused by deflection of the instrumentation boom under aerodynamic load.

Upflow also results if the test section is not level with respect to the local gravitational water-line. A survey of the test section showed that the ceiling is inclined 0.22° and the floor is inclined -0.05° over the length of the test section. A positive angle indicates upflow in the test section. The increase in test section area is to account for thickening boundary layers. The survey indicated that the upflow caused by this inclination of the test section amounts to 0.01°, 0.08°, and 0.15° at the Z = 10-, 20-, and 30-ft heights, respectively.

The growth of a thinner boundary layer on the ceiling than the floor may be another source of upflow. Data and observations made during tests after installation of the acoustic liner indicate that the floor boundary layer may be as much as three times thicker than the ceiling boundary layer. The cause of this difference is not clear.

Yaw angle distributions at the Z = 10-, 20-, and 30-ft boom heights show little variation with tunnel speed. Some of the yaw distributions show that the flow is turned toward the walls on both sides of the centerline (i.e., positive beta on the inside of the circuit, and negative beta on the outside of the circuit). This is true mostly for the 10-ft boom height data at U_{ts} > 100 knots. This may be caused by flow deflections around the instrumentation boom.

Temperature Distribution

Total temperature measurements were made at each multiprobe station to document cross-stream variations in temperature due to the air exchange system. Another goal of the measurements was to provide a local temperature measurement for the calculation of local density.

There was no significant temperature gradient at 0% air exchange, as was expected, but at 5 and 10% air-exchange rates spanwise variations were as much as 10°F over 60 ft. Figure 56 shows the total temperature distributions at 0, 5, and 10% air exchange for the three boom heights (Z = 10-, 20-, and 30-ft). These plots represent the temperature variation from the mean after the tunnel has reached steady conditions at the maximum flow velocity.

Figure 57 illustrates how the temperature gradient grows as the flow velocity is increased. Data are shown for a 10% air exchange run at the X = 0-ft boom position for all three boom heights. These results necessitated a method of correcting data for the effects of a temperature gradient.

The derivation of the temperature gradient calibration (TGC) shown as figure 58 was performed as follows. First, a straight-line curve fit was applied to the temperature distributions at the Z = 20-ft level for 0, 5, and 10% air exchange. The slope of the straight-line curve fit was then divided by the amount that the tunnel temperature had increased since the start of the wind tunnel run. This quantity (TGC) was then plotted against the air-exchange rate. Figure 58 allows the cross-stream temperature gradient to be estimated without having to make any test section measurements.

Boundary Layer Profiles

Two fixed rakes of total and static pressure probes were used to measure the pressure distribution and the thickness of the boundary layer on the floor of the test section. The location of the rakes is shown in figure 6. The 48-in. tall rake was mounted upstream of the 32-in. tall rake to document separated flow from the acoustic liner leading edge ramp if it existed.

Figure 59 shows the dynamic pressure profiles measured using the two rakes. These profiles did not change significantly with any of the tunnel operational variables. The boundary-layer thickness grows from approximately 10 to 18 in. between the two rakes.

At the 48 in. rake location, the dynamic pressure at Z = 10 in. was approximately 7% below the tunnel centerline value. The dynamic pressure above Z = 10 in. remained constant for approximately 24 in. and then continued to approach the free-stream level. At the 32-in. rake location, the dynamic pressure at Z = 32-in. was also about 7% below the tunnel centerline value. This rake was not tall enough to show how the boundary layer reached the tunnel centerline level. A possible cause for these defects in the boundary-layer profiles is the acoustic liner ramp. The velocity profile for each rake is included as figure 60.

The thickness of the boundary layers on the ceiling and side walls was not measured during the FLOCAL. The ceiling boundary layer is believed to be approximately one third as thick as the floor boundary layer based on oil-flow studies that were done after the acoustic liner was installed. The side-wall boundary layers are believed to be thicker than the floor boundary layer because of the shape of the test section.

DYNAMIC FLOW-QUALITY PARAMETERS

Turbulence Intensity Distribution

Axial turbulence intensity was measured in the test section using hot-wire anemometry. Lateral and vertical turbulence intensity was also measured on the centerline using a cross-wire probe.

A standard, constant-temperature, DISA, hot-wire system was used during the FLOCAL. Instrumentation setup diagrams for the 9-μm single and cross-wire probes are shown as figure 61. A 1-kHz low-pass filter was placed on the output of the linearizer since most of the turbulence energy was below 1000 Hz. This also eliminated the effects of high-frequency instrumentation noise on the signal. A spectrum analyzer was positioned on the output of the anemometer unit.

Temperature fluctuations are believed to have had an effect on the hot-wire measurements. When the tunnel is run at 5 and 10% air-exchange, a cool jet from the air exchange inlet mixes with the warm tunnel flow. If this mixing is not complete, it would be a source of temperature fluctuations. Since the hot wire responds to both temperature and velocity fluctuations, the FLOCAL turbulence intensity would be artificially high. Magnitude of the temperature fluctuation was not measured during the FLOCAL. Estimates show, however, that a temperature fluctuation of only ±1°F could cause the increases in turbulence intensity that were recorded.

Data taken with a large difference between the air-exchange inlet jet temperature and the tunnel mean temperature could not be corrected. For this reason, only data taken below approximately 225 knots after the initial start of the wind tunnel were reliable.

No effect of the air-exchange rate or the streamwise position of the instrumentation boom on turbulence intensity could be resolved. Data collected over three speed ranges and at three air exchange rates were averaged to obtain the final results.

Figure 62 shows the axial turbulence intensity distribution below U_{ts} = 75 knots for the 10-, 20-, and 30-ft boom heights. Figures 63 and 64 are the same plot groups for the U_{ts} = 75- to 150-knot and U_{ts} = 150- to 225-knot speed ranges respectively. A statistical analysis was performed on a set of repeat data points collected at fixed conditions. The mean value was found to be within ±10% of the sample range, 90% of the time.

The plots of figures 62, 63, and 64 also show the lateral turbulence intensity on the centerline. The cross wire on the centerline was rotated 90° to measure the difference between lateral and vertical turbulence intensity. There was no discernible difference between lateral and vertical turbulence intensity. Both had a mean level of around 0.6%. The higher level of lateral and vertical turbulence intensity than axial turbulence intensity is typical of subsonic wind tunnels.

Axial Turbulence Intensity Energy Spectra

Axial turbulence intensity energy spectra were recorded from the hot wire located at the center station of the boom. These data were collected to determine the frequency range of the highest energy flow disturbances.

The nonlinear output of the hot-wire anemometer was fed directly to a spectrum analyzer. An assumption was made that since the turbulence levels were low, the RMS voltage fluctuation was linear over the range of anemometer output. The analyzer was set up to provide plots with a decibel range from -10 to -70 and a linear frequency range from 0 to 2000 Hz.

Spectra recorded at various boom positions and air-exchange rates were compared and no significant differences were visible. Figures 65, 66, and 67 show energy spectra taken with the hot wire located on the tunnel centerline at six test section speeds up to 244 knots. Data above this speed were influenced by temperature fluctuations as discussed previously.

The spectra grew to incorporate higher-frequency flow disturbances as the speed of the tunnel was increased. There was also a rapid decay in energy between 0 and 200 Hz. This is typical of most large-scale subsonic wind tunnels where most of the flow unsteadiness is caused by large-scale velocity fluctuations. Large-scale flow disturbances could be caused by the fan drive, the vane sets, or areas of flow separation in the circuit. The most important feature of the spectra recorded during the FLOCAL was that they were smooth and had no significant peaks.

Flow Meander and Peak-to-Peak Flow Angle

Time history plots of pitch and yaw angle at the five boom stations were collected during the FLOCAL. These data were collected with the boom at the Z = 10-ft height. The sampling period was 90 sec, and no signal filtering was used. A typical pitch and yaw time history is shown as figure 68. Since the flow direction vanes have a limited aerodynamic frequency response, probably less than 5 Hz, much of the unsteadiness was due to vane overshoot, instrumentation noise, and support vibration. If there was a low-frequency meander of the flow, however, it would manifest itself as a variation of the mean in figure 68. No significant meander of the flow was documented at any of the five probe stations.

The peak-to-peak pitch and yaw angles were estimated from each time history plot. Results are shown in figure 69. The pitch-angle plot shows a peak-to-peak variation of around $\pm 1^\circ$ on the centerline, with higher values on each side. The yaw-angle plot has the same shape, with around $\pm 0.75^\circ$ on centerline and with higher levels on each side. Some of the higher pitch and yaw angle variations at each end of the boom may have been caused by higher boom vibrations. The ends of the boom were not constrained.

The pitch and yaw angle variations were higher on the outside wall than on the inside wall of the tunnel. This was confirmed by observations of the flow-angle vanes during tunnel operation. The higher flow unsteadiness on the outside of the circuit could be caused by flow disturbances generated by the new acoustic barrier at the air-exchange exhaust.

SUMMARY OF RESULTS

Objectives of the 40- by 80-Foot Wind Tunnel performance and test section FLOCAL were to

1. Calibrate the windspeed system
2. Document tunnel performance
3. Document the detailed spatial variations in test section flow quality throughout the tunnel operational envelope

The windspeed measurement system was calibrated to accurately measure tunnel speed on the centerline directly above the center of the turntable. Because of the presence of the instrumentation supports and fairings, this calibration was not performed with the test section completely empty.

The tunnel performance calibration documented how the dynamic pressure and velocity in the test section vary with fan blade angle, fan revolutions per minute and tunnel power. This calibration also documented how the test section dynamic pressure and temperature level vary with tunnel operating condition.

Before the test, the following tunnel operational variables were identified as having the potential to affect the test section flow quality.

1. Air-exchange rate
2. Fan blade angle and revolutions per minute
3. Atmospheric temperature
4. Aerodynamic performance of the fan drive, vane sets, and other structures in the tunnel circuit

These tunnel variables were found to have no significant effect on pressure distributions, flow-angle distributions, turbulence distributions, and boundary-layer thickness. A cross-stream temperature gradient caused by the air-exchange system was documented and a correction method was established.

A streamwise wall static pressure gradient was measured during the FLOCAL. On the centerline, this gradient was estimated to be 1% of the dynamic pressure level ($C_{p,cl} = 0.01$) over a 30-ft length of the test section.

RECOMMENDATIONS

Results of a wind tunnel flow calibration (FLOCAL) are not supposed to surprise the reader. If a serious flow-quality anomaly does present itself, the tunnel is generally modified to correct the

problem. This report deals with the flow-quality anomalies that are not serious enough to warrant modification of the wind tunnel, yet should be documented for future tunnel users.

After a test, when the data are being carefully analyzed, one always seems to discover a parameter that should have been measured during the test. This parameter was often eliminated early in test planning because of time or resource constraints. Parameters that were not measured during the FLOCAL were in the area of unsteady flow.

Free-stream flow disturbances in the test section should be well documented. These disturbances have the potential of affecting steady and dynamic measurements made in the wind tunnel. The author recommends that the pressure, temperature, and turbulence-intensity fluctuations with time be measured. More testing that would document the effect of temperature fluctuations on hot-wire turbulence measurements is also recommended to obtain the full-speed turbulence intensity level in the test section.

An accurate measurement of the streamwise static pressure gradient (horizontal buoyancy) in the 40- by 80-ft test section is also required. The 40- by 80-ft test section is relatively short (80 ft) and has an acoustic liner with leading- and trailing-edge ramps. Vortex generators have also been added near the exit of the test section. All of these factors influence the streamwise static pressure distribution. The variation in static pressure coefficient of 0.01 over 30 ft of test section length measured during the FLOCAL was only an estimate based on limited data.

It is important that flow-quality information be available to the users of all wind tunnels. These calibrations must be performed carefully and be well documented for those who must interpret the results. For more detailed information about any particular section of this report, consult the NFAC Documentation Archives located at NASA Ames Research Center.

REFERENCES

1. Olson, Lawrence E.; Zell, Peter T.; Soderman, Paul T.; Falarski, Michael D.; Corsiglia, Victor R.; and Edenborough, H. Kipling: Aerodynamic Flow Quality and Acoustic Characteristics of the 40- by 80-Foot Test Section Circuit of the National Full-Scale Aerodynamic Complex. SAE Tech Paper 872328, 1987.

2. Rossow, V. J.; Schmidt, G. I.; Meyn, L. A.; Ortner, K. R.; and Holmes, R. E.: Aerodynamic Characteristics of an Air Exchanger System for the 40- by 80-Foot Wind Tunnel at Ames Research Center. NASA TM 88192, 1987.

3. Zell, Peter T.; and McMahon, Robert D.: A Free-Trailing Vane Flow Direction Indicator Employing a Linear Output Hall Effect Transducter. Proc. 34th Intern. Instrumentation Symp., 1988, pp. 429-436.

4. Pressure Systems Incorporated: Model 780B/T Pressure Measurement System Users Manual. Sept. 1983.

5. Benedict, Robert P.: Fundamentals of Temperature, Pressure and Flow Measurements, Third Ed. John Wiley and Sons, 1984, pp. 172.

6. Tolhurst, W. H.: The Fundamentals of Measuring Dynamic Pressure and Velocity in the Ames 40- by 80-Foot Wind Tunnel. NFAC Documentation Archives, Dec. 1987.

7. Rae, William H., Jr.; and Pope, Alan: Low-Speed Wind Tunnel Testing, Second Ed. John Wiley and Sons, 1984.

TABLE 1.– 40- BY 80- FLOCAL TEST MATRIX

Date 1987	Run #	Boom pos.	Power mode	Air ex., %	RPM	Blade angle, deg	Max. vel., knots	Comments
5/4	1	-	-	-	-	-	-	Instrument check-out
5/7	2	A	Utility	10	180	0 - 40	240	Abbreviated run
5/8	3	A	Utility	10	180	0 - 48	300	
5/9	4	A	Utility	10	180	0 - 48	300	Flow angle vanes inverted
5/9	5	-	-	-	-	-	-	Run cancelled
5/11	6	A	Utility	5	180	0 - 48	300	
5/12	7 a	A	Utility	0	180	0 - 26	175	First half of run
5/12	7 b	A	IFC	0	90 135 175	8 - 28 8 - 28 8 - 22	90 140 145	Second half of run
5/14	8	A	IFC	5	37 90 135 175	16 - 46 8 - 28 8 - 28 8 - 22	55 90 135 140	

TABLE 1.– Continued

Date 1987	Run #	Boom pos.	Power mode	Air ex., %	RPM	Blade angle, deg	Max. vel., knots	Comments
5/14	9	A	IFC	10	37 90 135 175	16 - 46 8 - 28 8 - 28 8 - 22	55 85 130 135	
5/15	10	A	Utility	5	180	32	-	Instrument check-out, no data
5/19	11	B	Utility	10	180	0 - 48	300	New boom position
5/19	12	B	Utility	0	180	0 - 24	165	
5/20	13	B	Utility	5	180	0 - 48	300	
5/21	14	B	Utility	10	180	0 - 48	300	
5/27	15	D	Utility	10	180	0 - 48	300	New boom position
5/27	16	D	Utility	0	180	0 - 24	165	
5/28	17	D	Utility	5	180	0 - 48	300	
6/1	18	-	-	-	-	-	-	Run cancelled
6/2	19	C	Utility	10	180	0 - 48	300	New boom position
6/3	20 a.	C	Utility	0	180	0 - 24	165	First half of run

TABLE 1.– Concluded

Date 1987	Run #	Boom pos.	Power mode	Air ex., %	RPM	Blade angle, deg	Max. vel., knots	Comments
6/3	20 b.	C	Utility	5	180	0 - 48	300	Second half of run
6/6	21 a.	E	Utility	0	180	0 - 24	165	New boom position First half of run
6/6	21 b.	E	Utility	5	180	0 - 48	300	Second half of run
6/8	22	E	Utility	10	180	0 - 48	300	
6/9	23	F	Utility	0	180	0 - 23	160	New boom position
6/11	24	F	Utility	10	180	0 - 48	300	
6/12	25	F	Utility	5	180	0 - 48	300	
6/15	26	F	Utility	5	180	0 - 48	300	Flow angle vanes inverted

TABLE 2.– PROBE DESCRIPTIONS

PITOT/STATIC PROBE	
Maunufacturer:	United Sensor
Specifications:	Model PAE-12-M-W Probe length, 12 in Sensing stem diameter, 1/4 in.
Accuracy:	±0.5% of full scale
Additional Info:	Part of multiprobe assembly
THERMOCOUPLE	
Manufacturer:	United Sensor
Specifications:	Model TU-12-C/C-36-F Wire Type, CU/CON Maximum temperature, 400°F Probe diameter, 1/4 in.
Accuracy:	±1°F
Additional Info:	Part of multiprobe assembly
HOT-WIRE PROBE	
Manufacturer:	DISA Electronics
Specifications:	Model 55P01 (Single Sensor) Model 55P51 (Dual Sensor) Platinum-plated tungsten wire-diameter = 9 μm
Additional Info:	Part of multiprobe assembly
FLOW-ANGLE VANES	
Manufacturer:	Specially designed and built in-house
Specifications:	Airspeed range, 5 to 300 knots Angle range, ±40°
Accuracy:	Angle resolution, ±0.1°
Additional Info:	Part of multiprobe assembly pitch and yaw vanes contained on each multiprobe
WALL PRESSURE TAP	
Manufacturer:	In-house design
Specifications:	1-ft-diameter plate with 1/8-in.-diameter orifice in center
Accuracy:	±0.5% of full scale
Additional Info:	Nine static pressure taps mounted flush on the west test section wall
STATIC PRESSURE PROBE	
Manufacturer:	In-house design
Specification:	0.250 diameter x 0.035 wall tubing Four pressure ports, radially 90° apart, 10 diameters from the tip of the probe
Accuracy:	±0.5% of full scale
Additional Info:	Probes were mounted on two fixed rakes, 48 in. and 32 in. tall.

TABLE 2.– Concluded

TOTAL PRESSURE PROBE	
Manufacturer:	In-house design
Specification:	0.125 diameter x 0.028 wall tubing 30° beveled tip
Accuracy:	±0.5% of full scale
Additional Info:	Probes were mounted on two fixed rakes, 48 in. and 32 in. tall.
HUMIDITY SENSOR	
Manufacturer:	General Eastern
Specifications:	Model 400 CD Range: 0-100% relative humidity Temperature span for relative humidity, 0-140°F
Accuracy:	±3%, between 15% and 95% relative humidity
Additional Info:	Temperature-induced humidity changes are eliminated by employing a compensating thermistor.
BAROMETER	
Manufacturer:	Datametrics
Specifications:	Type 1400 Electronic Manometer
Accuracy:	±15% of reading
Additional Info:	Located in control room.

Figure 1.– Aerial view of the NASA 40- by 80-/80- by 120-Foot Wind Tunnels at Ames Research Center.

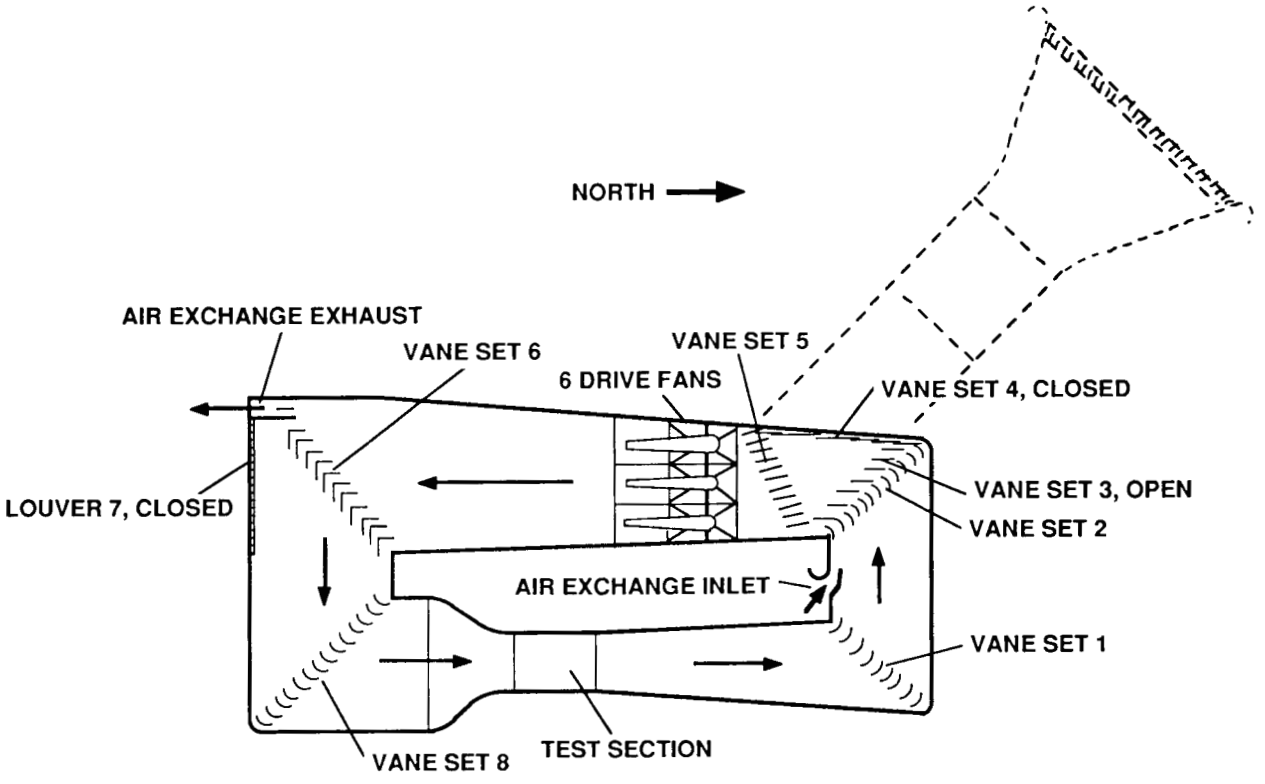

Figure 2.– 40- by 80-Foot Wind Tunnel circuit.

ORIGINAL PAGE IS
OF POOR QUALITY

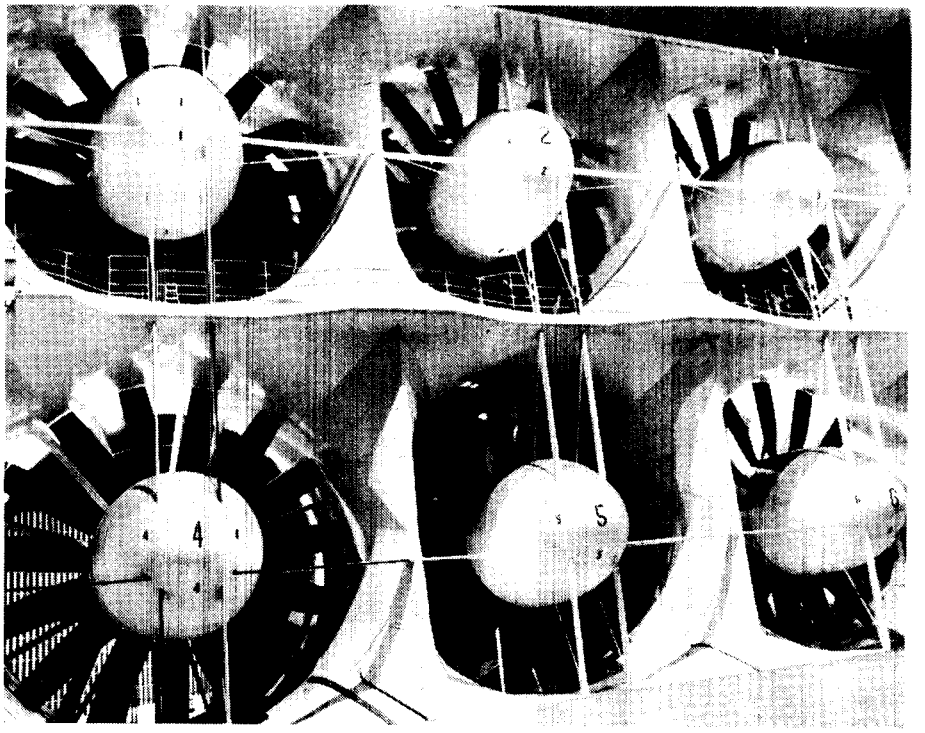

Figure 3.– 40- by 80-Foot Wind Tunnel fan drive system.

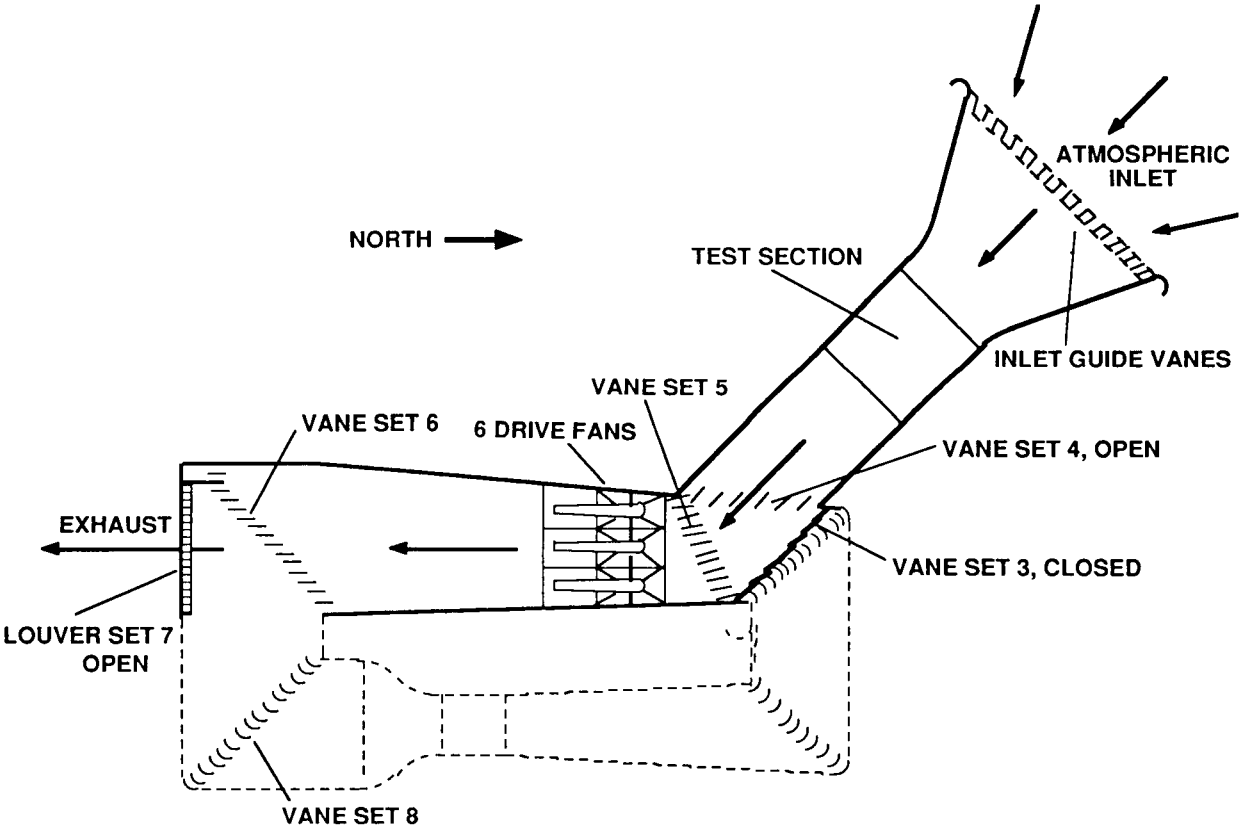

Figure 4.– 80- by 120-Foot Wind Tunnel circuit.

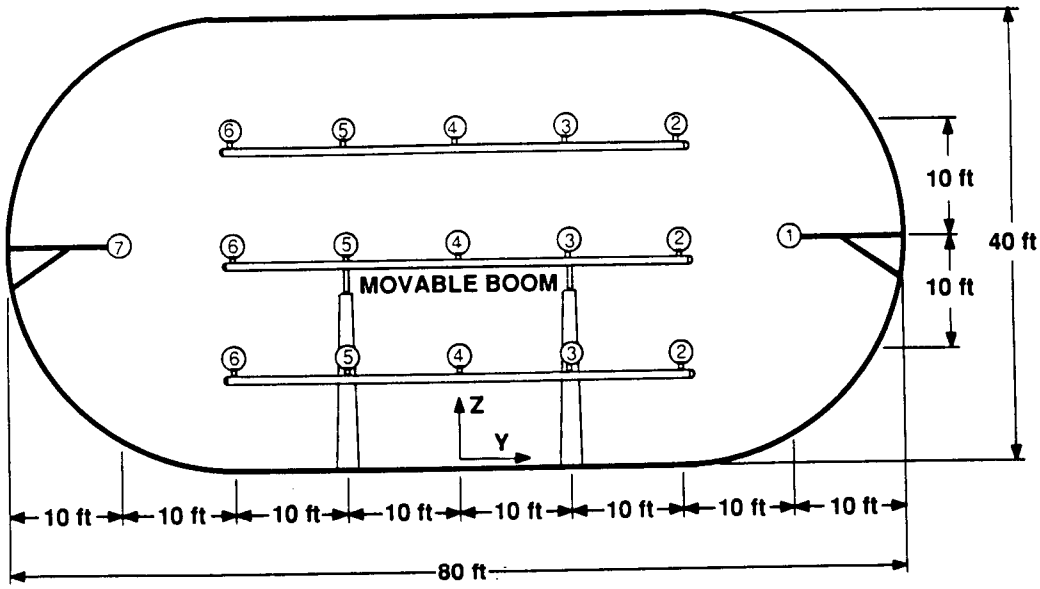

INSTRUMENTATION DISTRIBUTION

STATION	PITOT-STATIC PROBE	PITCH/YAW VANES	THERMO-COUPLE	HOT WIRE X PROBE	HOT WIRE SINGLE
1	X		X		X
2	X	X	X		X
3	X	X	X		X
4	X	X	X	X	
5	X	X	X		X
6	X	X	X		X
7	X		X		X

Figure 5.– Location of instrumentation in the 40- by 80-Foot Wind Tunnel test section (pilot's view).

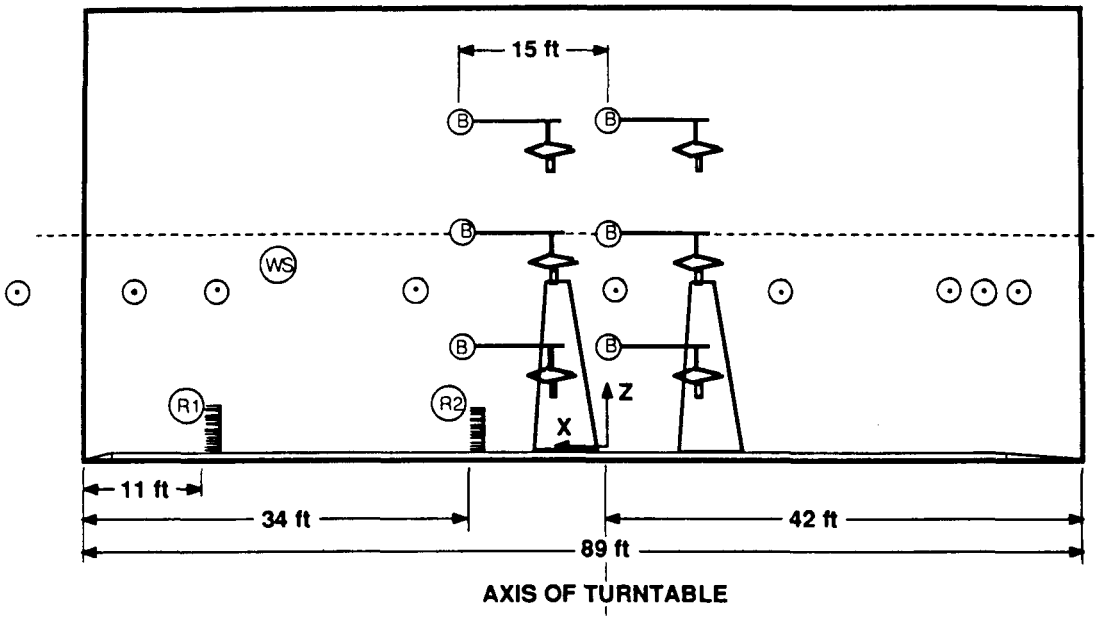

INSTRUMENTATION DISTRIBUTION

STATION	INSTRUMENTATION
B	7 STING MOUNTED MULTI-PROBES (SEE PILOT'S VIEW)
R1	1 48 in., 19 TUBE BOUNDARY LAYER RAKE (19 TOTALS & 5 STATICS)
R2	1 36 in., 15 TUBE BOUNDARY LAYER RAKE (15 TOTALS & 3 STATICS)
WS	9 WALL STATIC PRESSURE TAPS

Figure 6.– Location of instrumentation in the 40- by 80-Foot Wind Tunnel test section (view looking west).

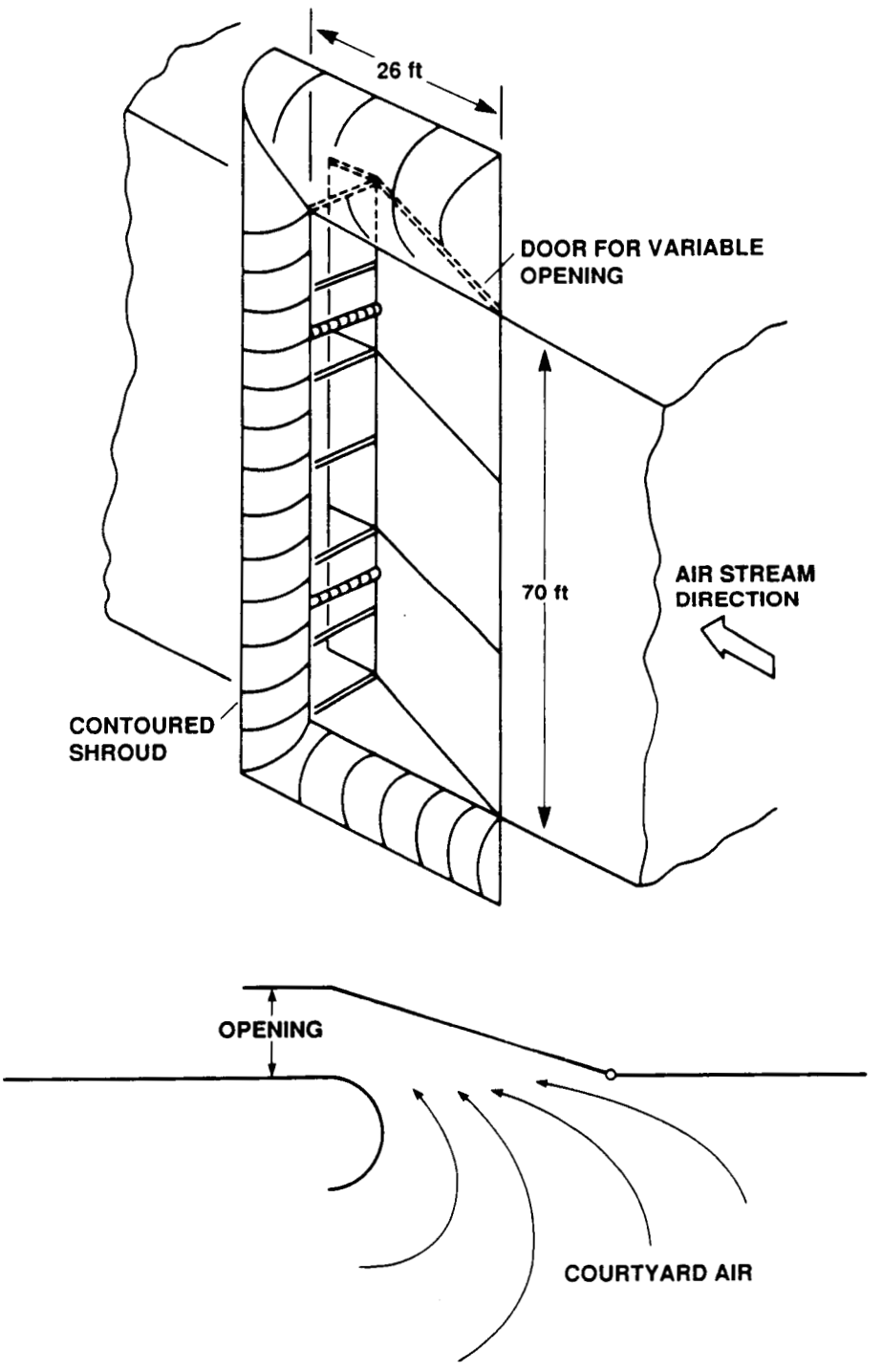

Figure 7.– Wind tunnel air-exchange system inlet.

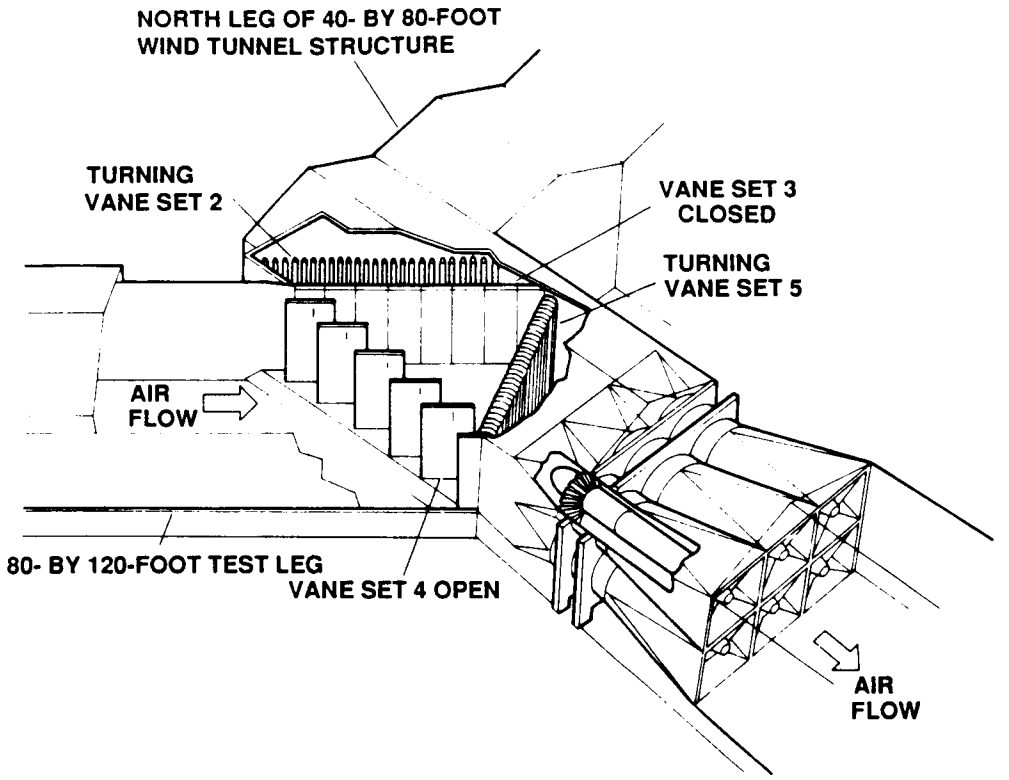

Figure 8.– Intersection between the 40- by 80-Foot and 80- by 120-Foot Wind Tunnels (80- by 120-Foot Wind Tunnel mode).

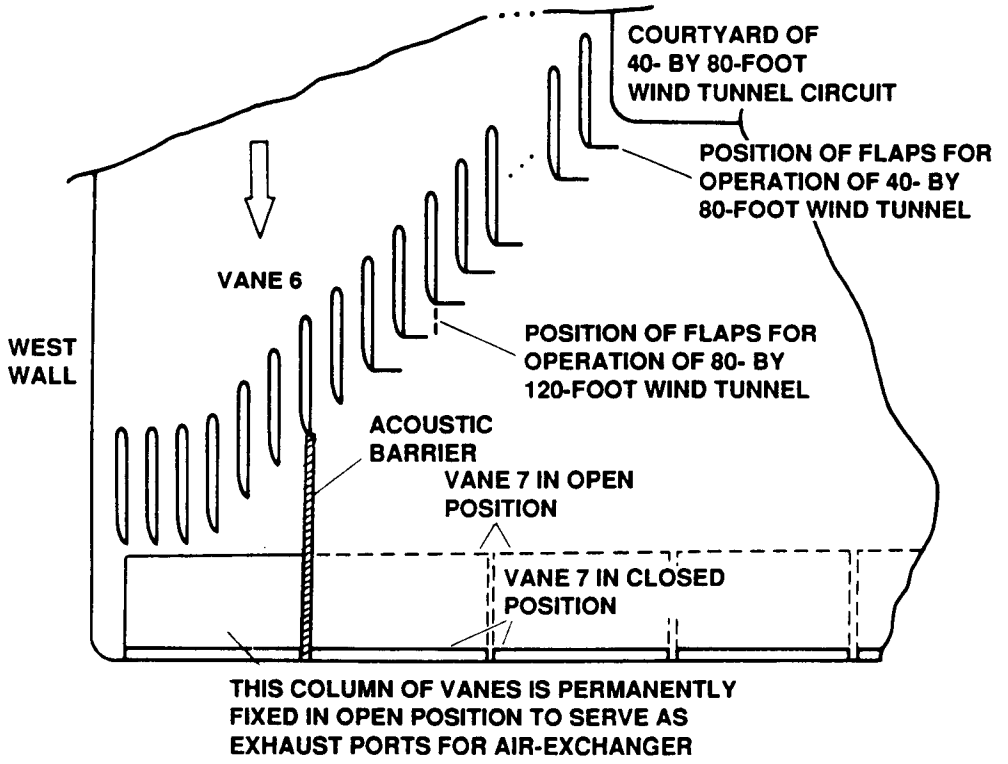

Figure 9.– Van set #6, air-exchange exhaust and acoustic barrier (positioned for 40- by 80-Foot Wind Tunnel operation).

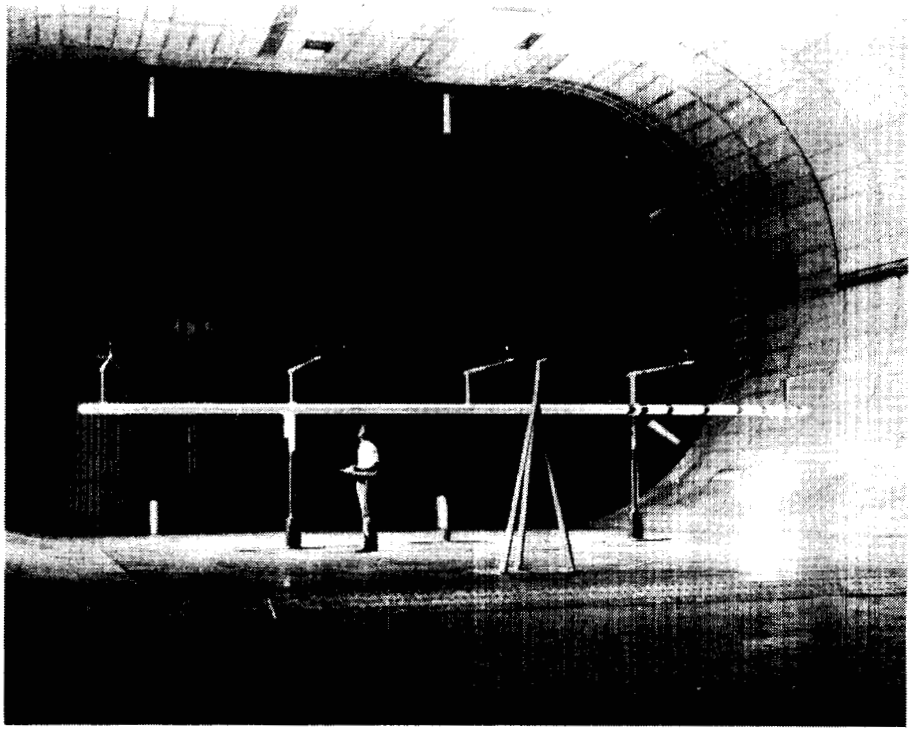

Figure 10.– Instrumentation boom at Z = 10 ft height.

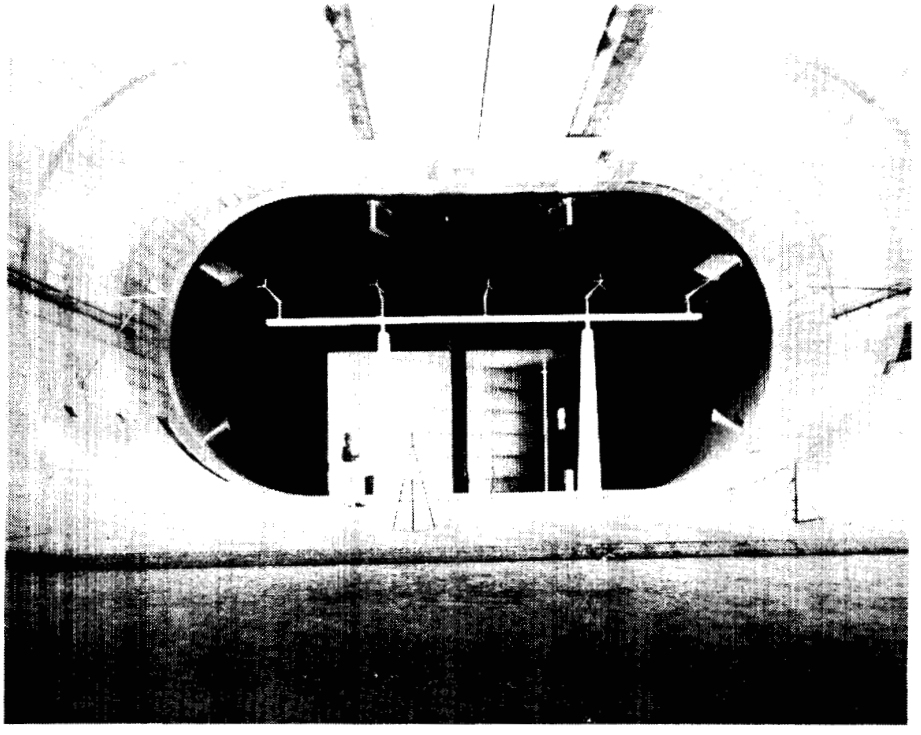

Figure 11.– Instrumentation boom at Z = 20 ft height.

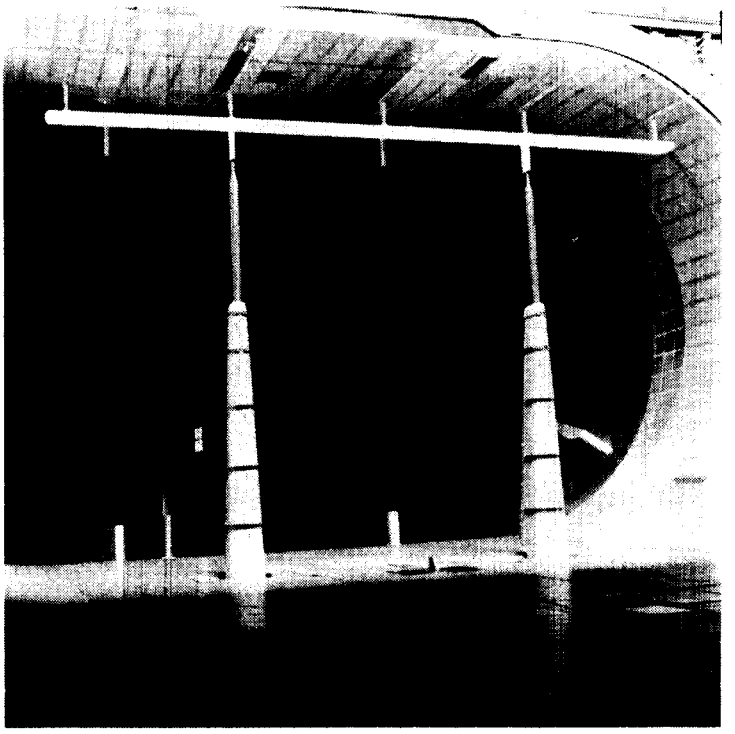

Figure 12.– Instrumentation boom at Z = 30 ft height.

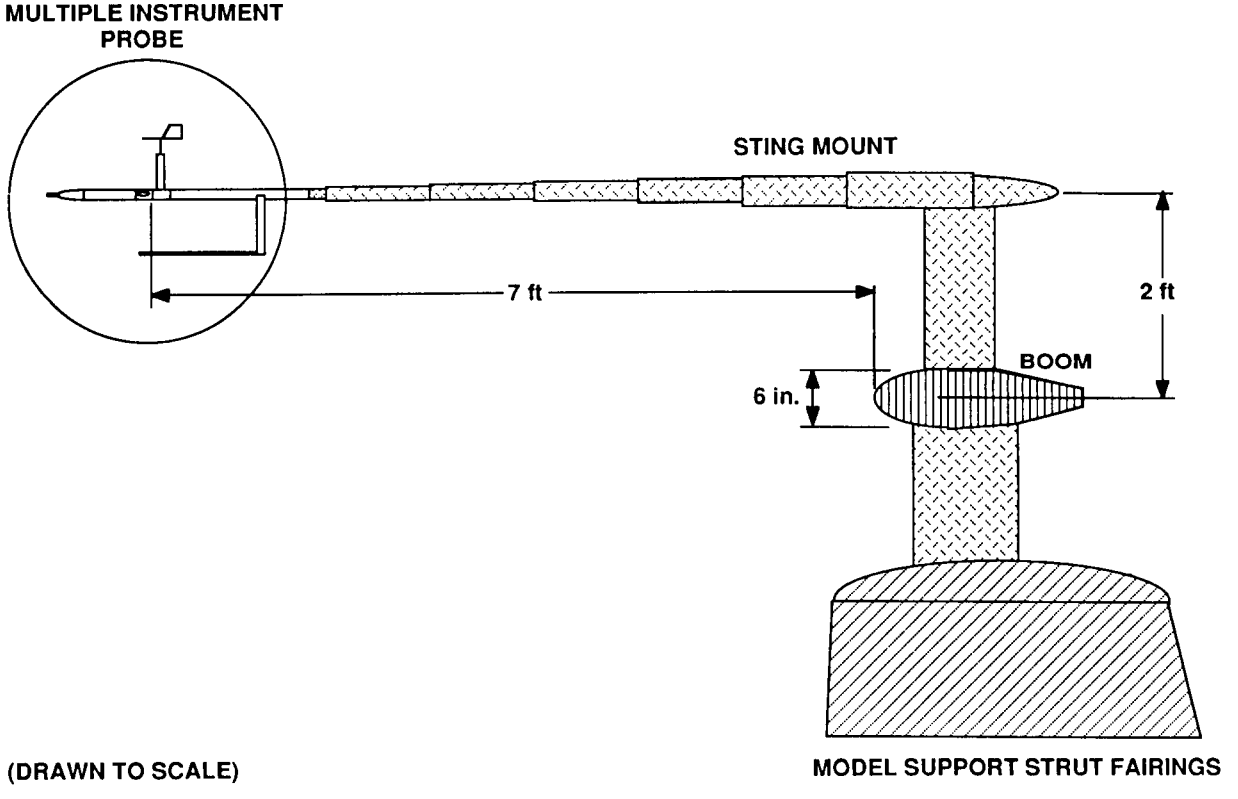

Figure 13.– Multiprobe positioned ahead of the instrumentation boom.

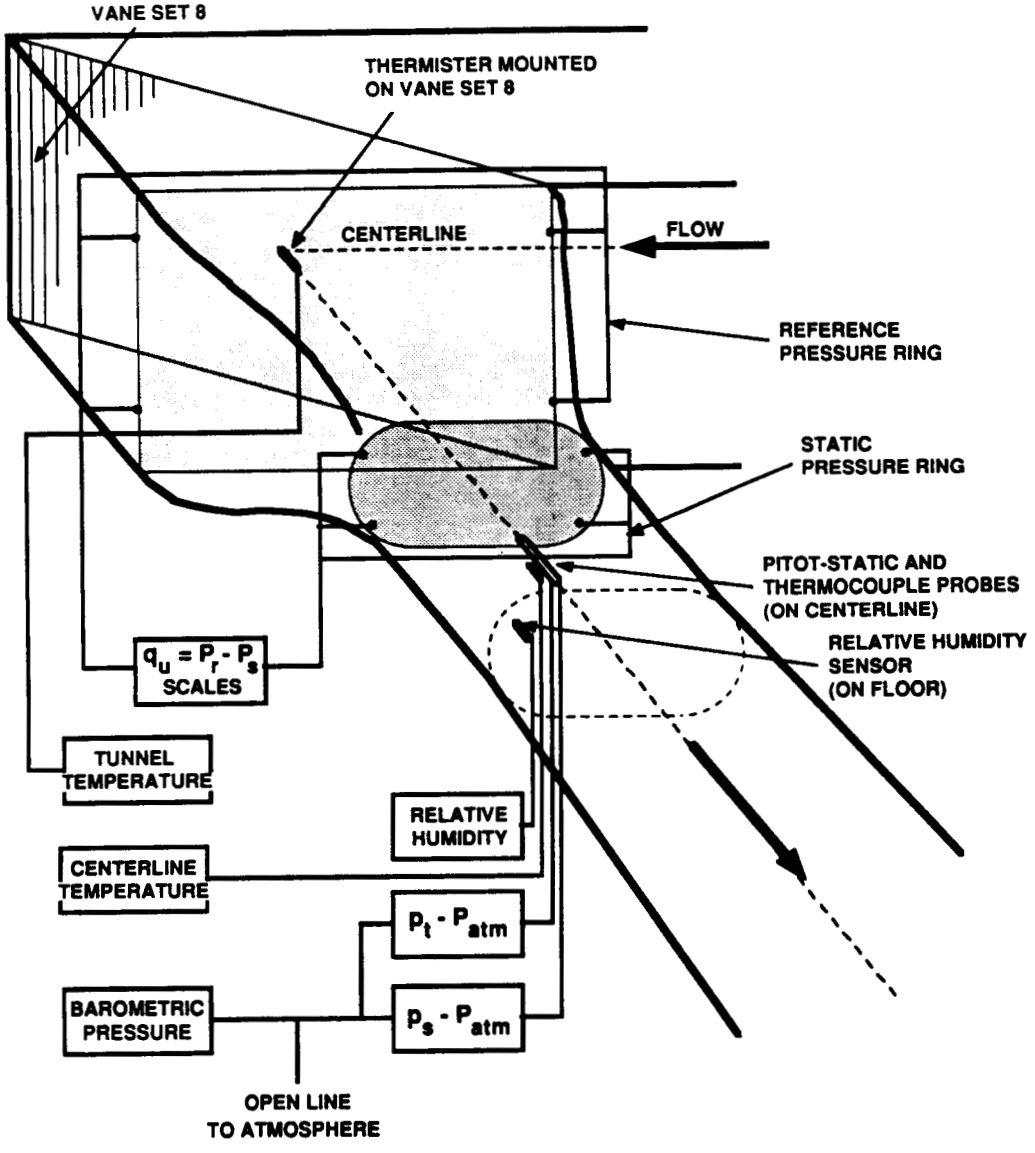

Figure 14.– Standard wind tunnel instrumentation for the 40- by 80-Foot Wind Tunnel.

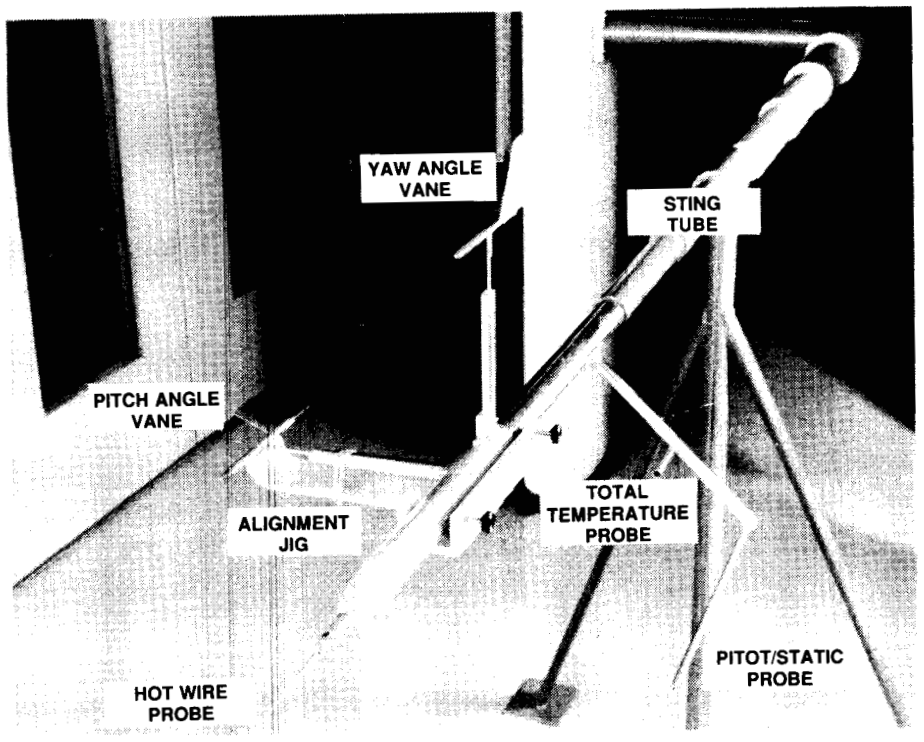

Figure 15.– Multiprobe mounted on sting tube (note alignment jig on pitch vane).

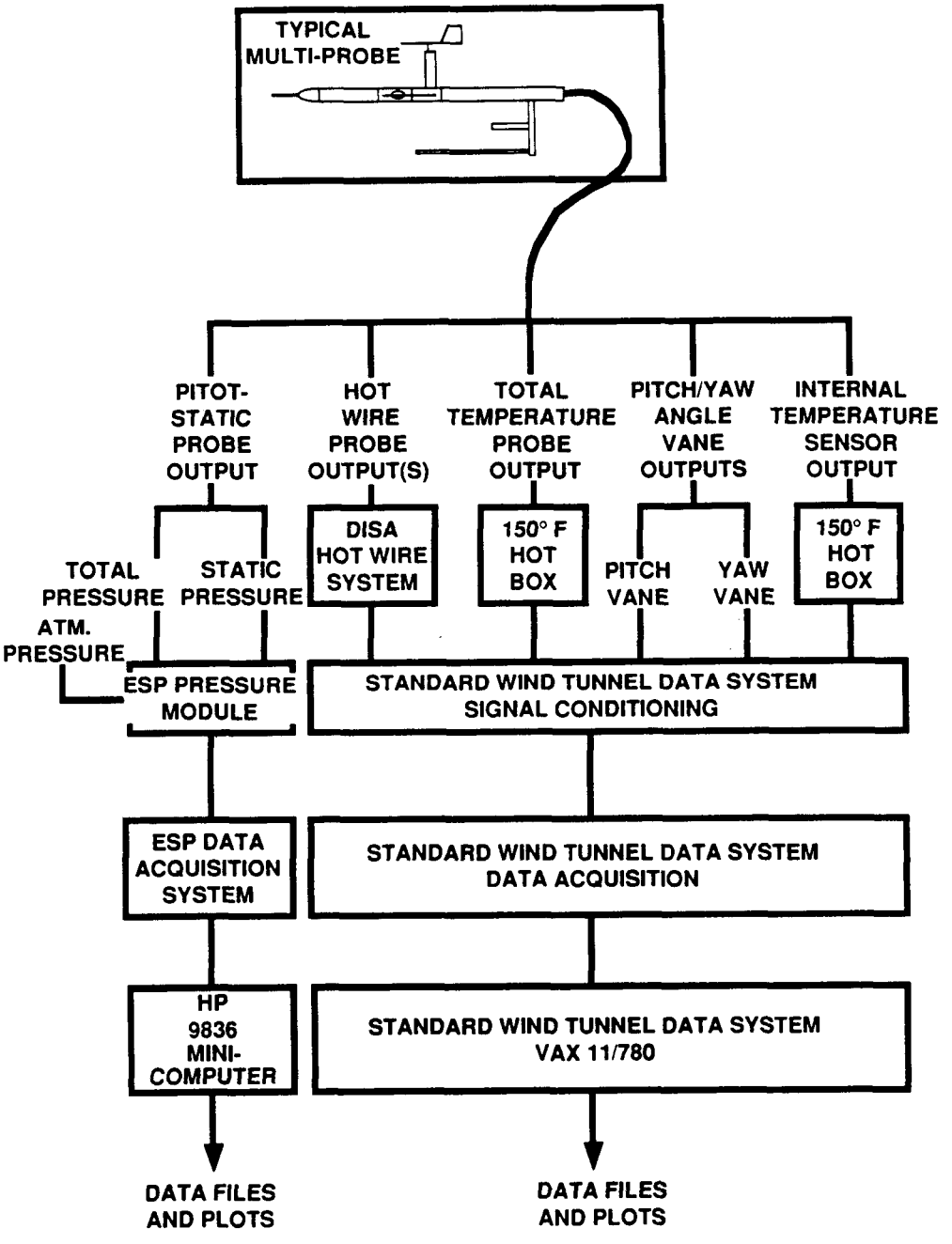

Figure 16.– Data system flow chart for a typical multiprobe.

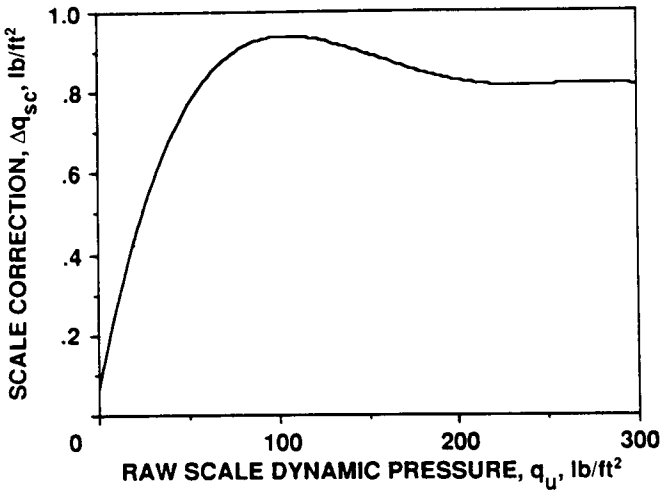

$$\Delta q_{sc} = 0.0659 + 0.022(q_u) - 1.906E\text{-}4(q_u)^2 + 6.562E\text{-}7(q_u)^3 - 7.933E\text{-}10(q_u)^4$$

Figure 17.– Dynamic pressure scale correction versus scale dynamic pressure.

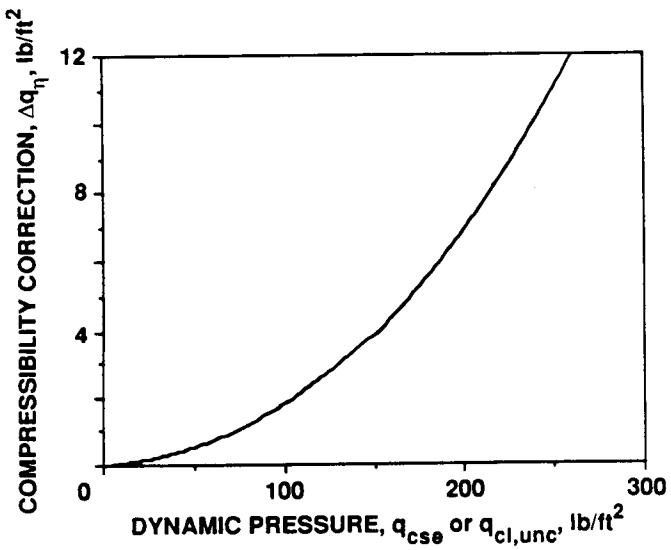

$$\Delta q_\eta = 0.0089 + 0.0033(q_{cse}) + 1.319E\text{-}4(q_{cse})^2 + 1.240E\text{-}7(q_{cse})^3$$

Figure 18.– Dynamic pressure compressibility correction versus scale dynamic pressure.

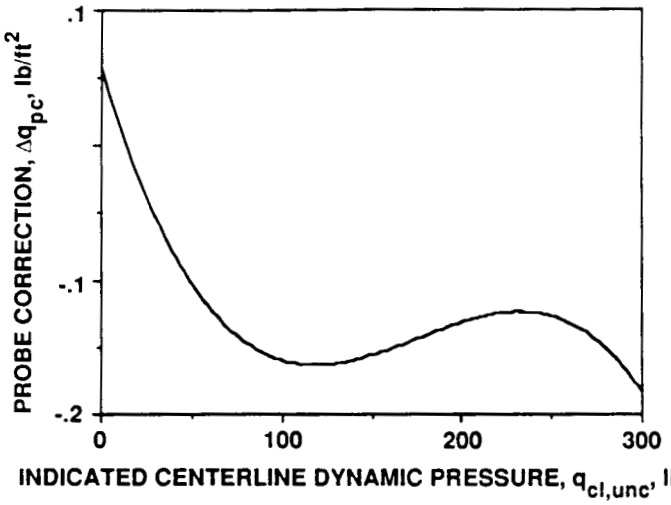

$$\Delta q_{pc} = 0.0569 - 0.0045(q_{cl,unc}) + 2.853E\text{-}5(q_{cl,unc})^2 - 5.425E\text{-}8(q_{cl,unc})^3$$

Figure 19.– Dynamic pressure probe correction versus indicated centerline dynamic pressure.

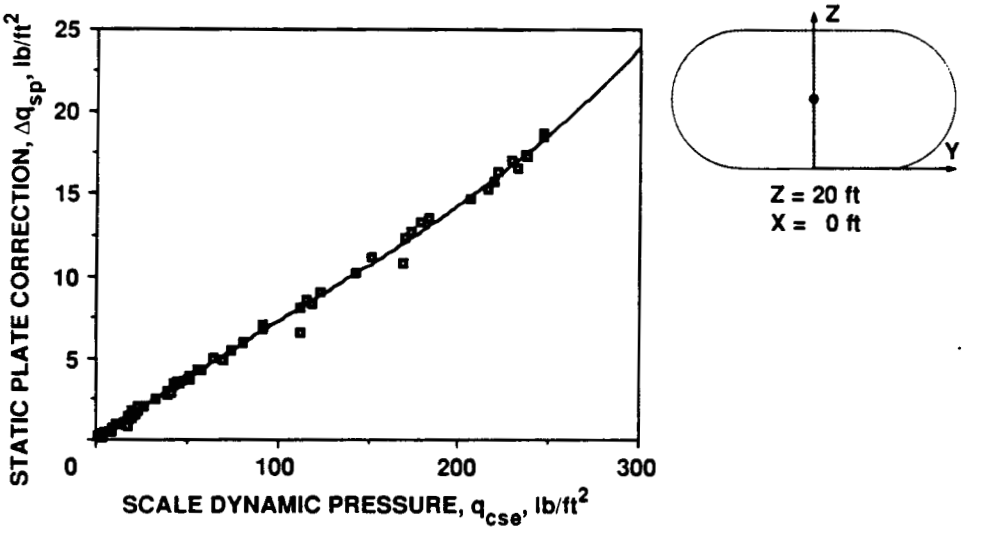

$$\Delta q_{sp} = -0.024 + 0.0804(q_{cse}) - 1.238E\text{-}4(q_{cse})^2 + 4.051E\text{-}7(q_{cse})^3$$

Figure 20.– Dynamic pressure static plate correction versus scale dynamic pressure.

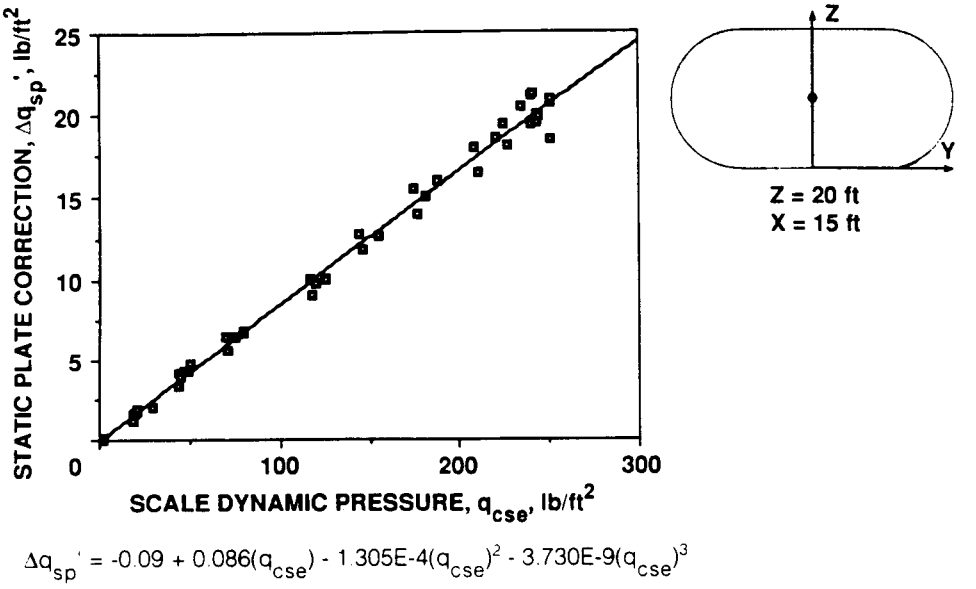

Figure 21.– Dynamic pressure static plate correction versus scale dynamic pressure (X = 15 ft).

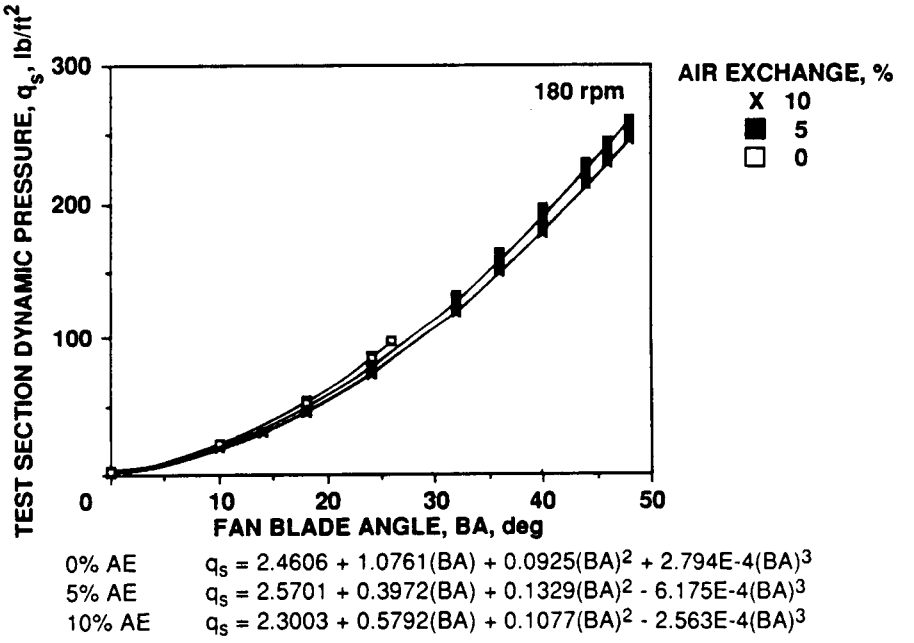

Figure 22.– Corrected dynamic pressure on centerline versus fan blade angle (utility mode).

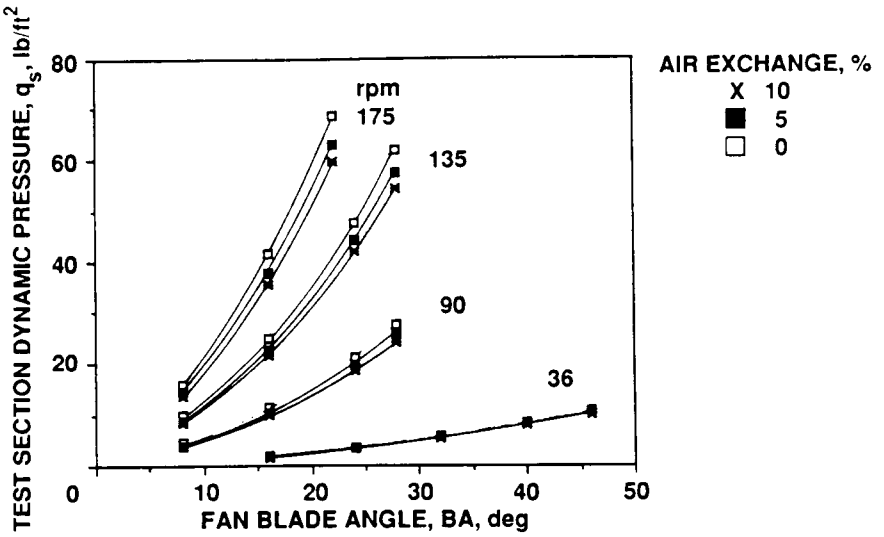

0% AE	175 rpm	$q_s = 2.2841 + 0.9354(BA) + 0.0955(BA)^2 - 3.968E\text{-}5(BA)^3$
	135 rpm	$q_s = 1.5746 + 0.5750(BA) + 0.0527(BA)^2 + 1.340E\text{-}4(BA)^3$
	90 rpm	$q_s = 0.6915 + 0.2589(BA) + 0.0243(BA)^2 + 2.617E\text{-}5(BA)^3$
5% AE	175 rpm	$q_s = 2.2560 + 0.8406(BA) + 0.0797(BA)^2 + 3.550E\text{-}4(BA)^3$
	135 rpm	$q_s = 1.3069 + 0.5143(BA) + 0.0511(BA)^2 + 6.767E\text{-}5(BA)^3$
	90 rpm	$q_s = 0.6513 + 0.2369(BA) + 0.0216(BA)^2 + 6.610E\text{-}5(BA)^3$
	36 rpm	$q_s = 0.0608 + 0.0347(BA) + 0.0045(BA)^2 - 8.737E\text{-}6(BA)^3$
10% AE	175 rpm	$q_s = 2.1199 + 0.799(BA) + 0.0764(BA)^2 + 2.852E\text{-}4(BA)^3$
	135 rpm	$q_s = 1.3473 + 0.493(BA) + 0.0456(BA)^2 + 1.599E\text{-}4(BA)^3$
	90 rpm	$q_s = 0.6329 + 0.226(BA) + 0.0202(BA)^2 + 6.594E\text{-}5(BA)^3$
	36 rpm	$q_s = 0.0578 + 0.033(BA) + 0.0043(BA)^2 - 7.194E\text{-}6(BA)^3$

Figure 23.– Corrected dynamic pressure on centerline versus fan blade angle (IFC mode).

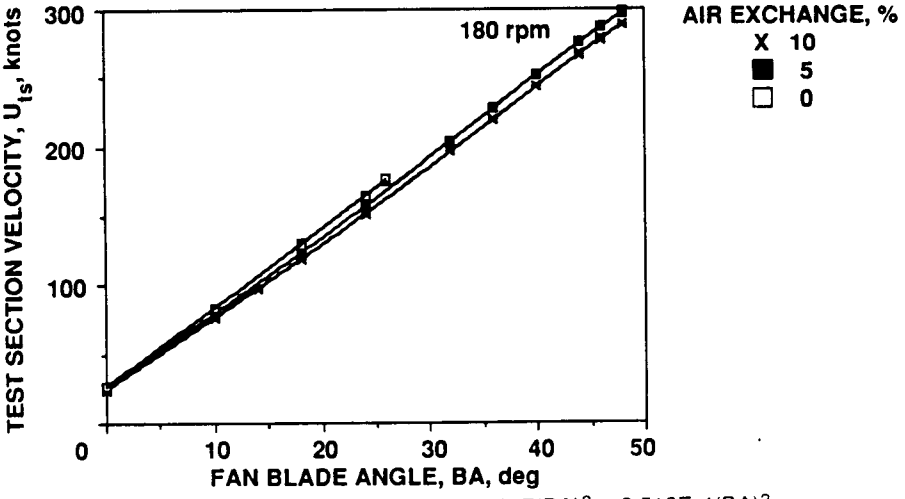

0% AE	$U_{ts} = 27.2900 + 5.6810(BA) - 0.0047(BA)^2 + 2.518E\text{-}4(BA)^3$
5% AE	$U_{ts} = 26.2285 + 5.0471(BA) + 0.0232(BA)^2 - 2.150E\text{-}4(BA)^3$
10% AE	$U_{ts} = 25.1336 + 4.9577(BA) + 0.0154(BA)^2 - 8.267E\text{-}5(BA)^3$

Figure 24.– Corrected test section velocity on centerline versus fan blade angle (utility mode).

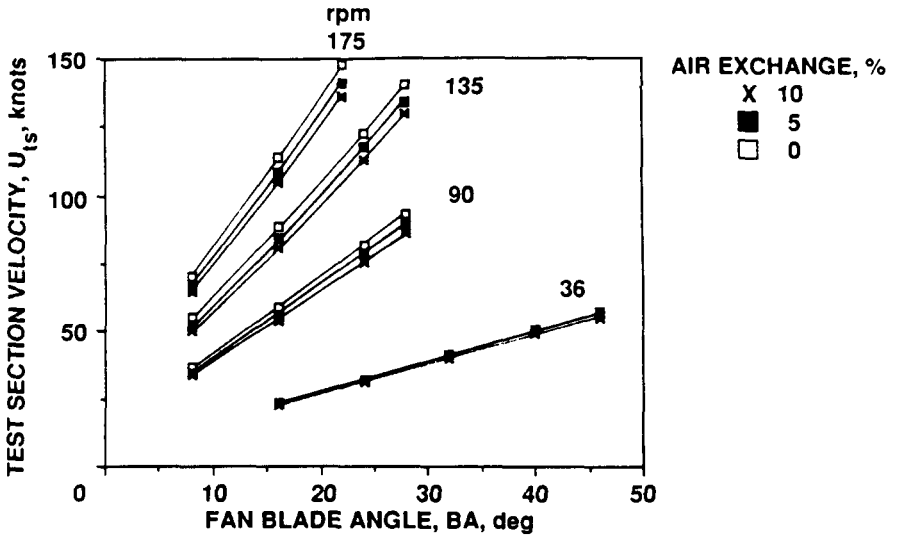

0% AE	175 rpm	$U_{ts} = 26.9493 + 5.3946(BA) + 0.0015(BA)^2 + 1.129E\text{-}4(BA)^3$
	135 rpm	$U_{ts} = 21.2798 + 4.2201(BA) - 0.0057(BA)^2 + 2.385E\text{-}4(BA)^3$
	90 rpm	$U_{ts} = 14.3117 + 2.8341(BA) - 0.0048(BA)^2 + 1.345E\text{-}4(BA)^3$
5% AE	175 rpm	$U_{ts} = 25.6082 + 5.1129(BA) - 3.009E\text{-}4(BA)^2 + 2.886E\text{-}4(BA)^3$
	135 rpm	$U_{ts} = 19.9034 + 3.9764(BA) + 2.376E\text{-}5(BA)^2 + 1.226E\text{-}4(BA)^3$
	90 rpm	$U_{ts} = 13.4965 + 2.6802(BA) - 0.0032(BA)^2 + 1.261E\text{-}4(BA)^3$
	36 rpm	$U_{ts} = 5.3543 + 1.0805(BA) + 0.0020(BA)^2 - 2.963E\text{-}5(BA)^3$
10% AE	175 rpm	$U_{ts} = 24.7038 + 4.9300(BA) - 8.064E\text{-}4(BA)^2 + 2.6928E\text{-}4(BA)^3$
	135 rpm	$U_{ts} = 19.3743 + 3.8476(BA) - 0.0040(BA)^2 + 2.411E\text{-}4(BA)^3$
	90 rpm	$U_{ts} = 13.1181 + 2.5957(BA) - 0.0047(BA)^2 + 1.629E\text{-}4(BA)^3$
	36 rpm	$U_{ts} = 5.2120 + 1.0512(BA) + 0.0018(BA)^2 - 2.565E\text{-}5(BA)^3$

Figure 25.– Corrected test section velocity on centerline versus fan blade angle (IFC mode).

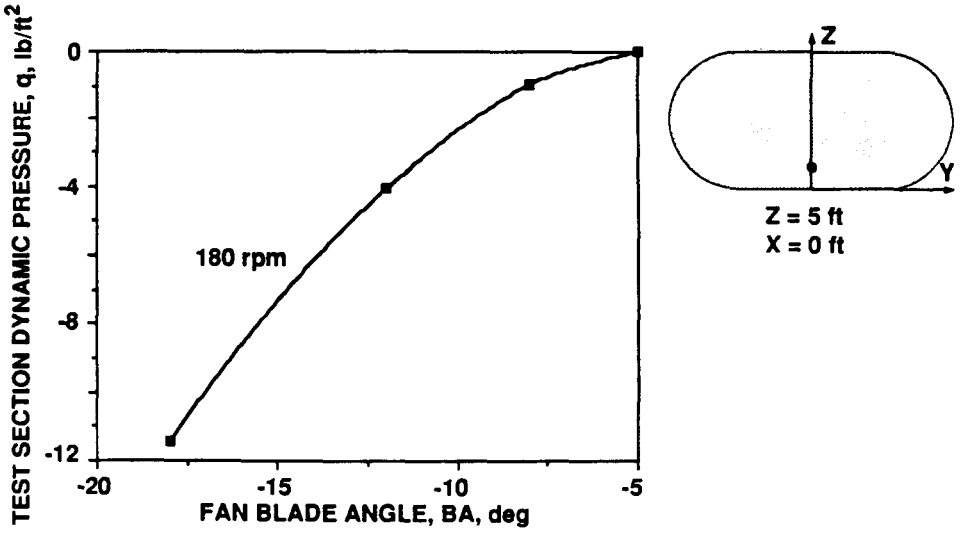

Figure 26.– Reverse flow dynamic pressure versus fan blade angle (utility mode).

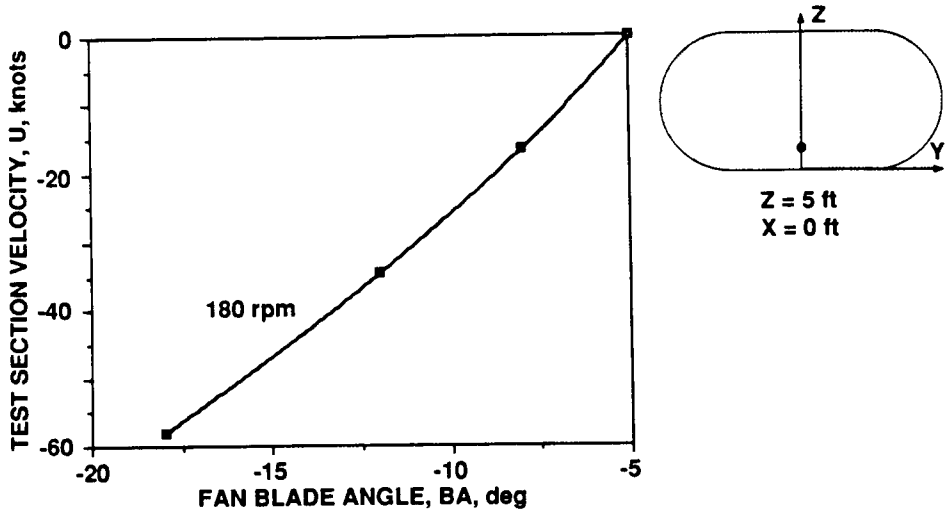

Figure 27.– Reverse flow velocity versus fan blade angle (utility mode).

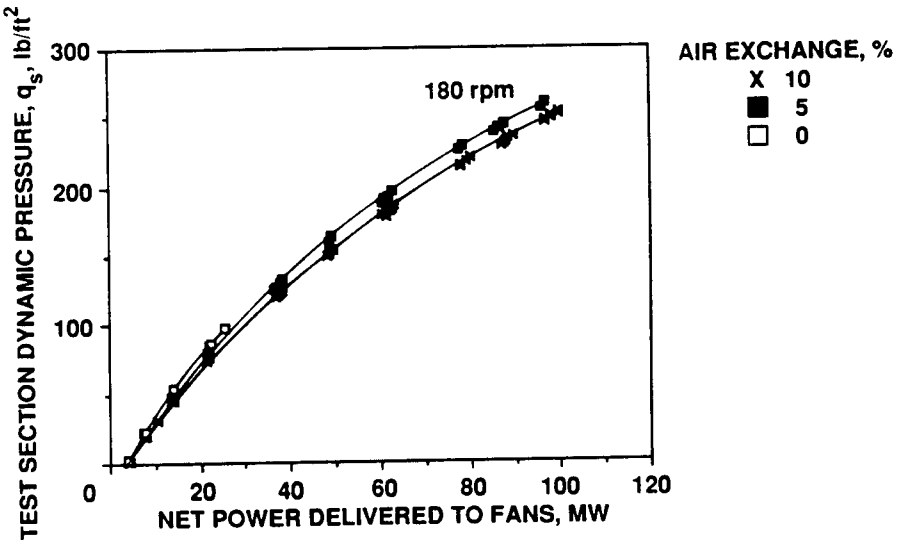

Figure 28.– Corrected dynamic pressure on centerline versus net power delivered to fans (utility mode).

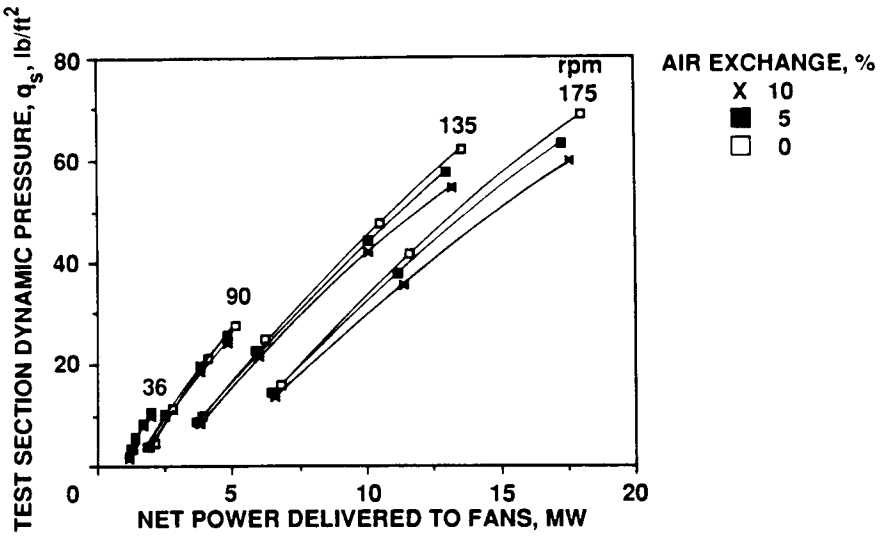

Figure 29.– Corrected dynamic pressure on centerline versus net power delivered to fans (IFC mode).

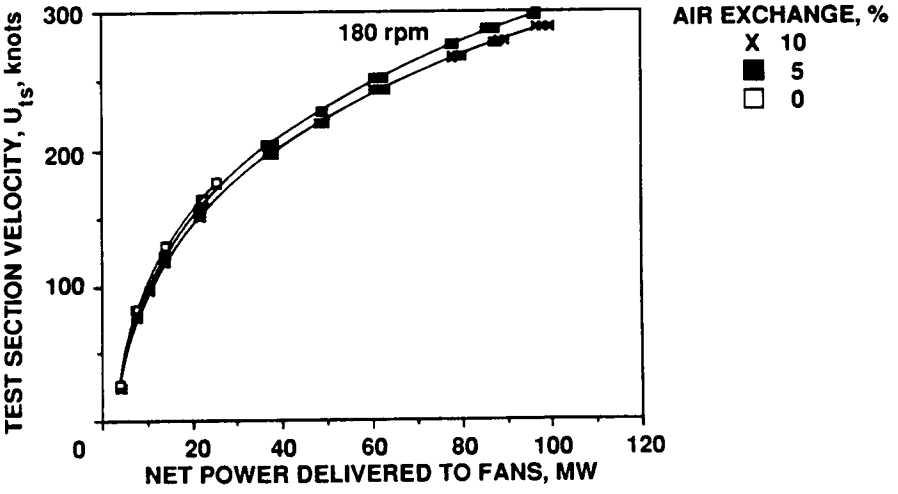

Figure 30.– Corrected test section velocity on centerline versus net power delivered to fans (utility mode).

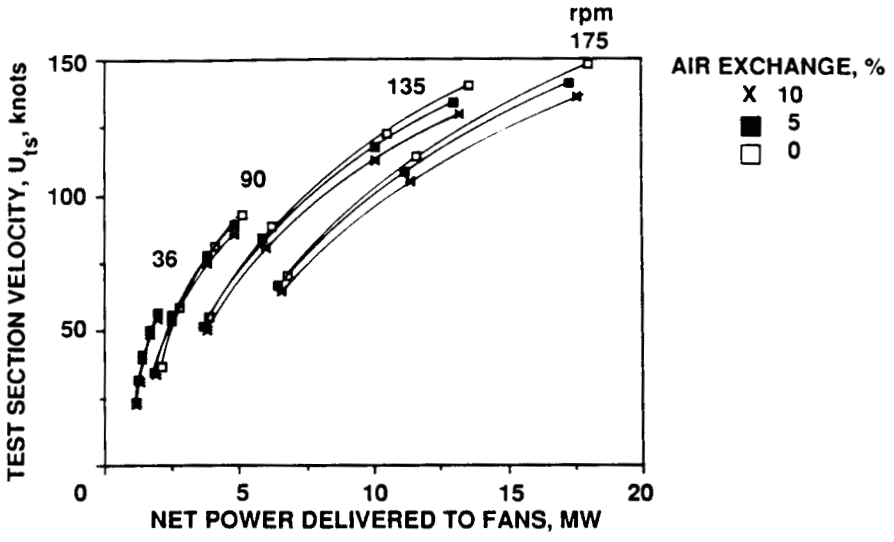

Figure 31.– Corrected test section velocity on centerline versus net power delivered to fans (IFC mode).

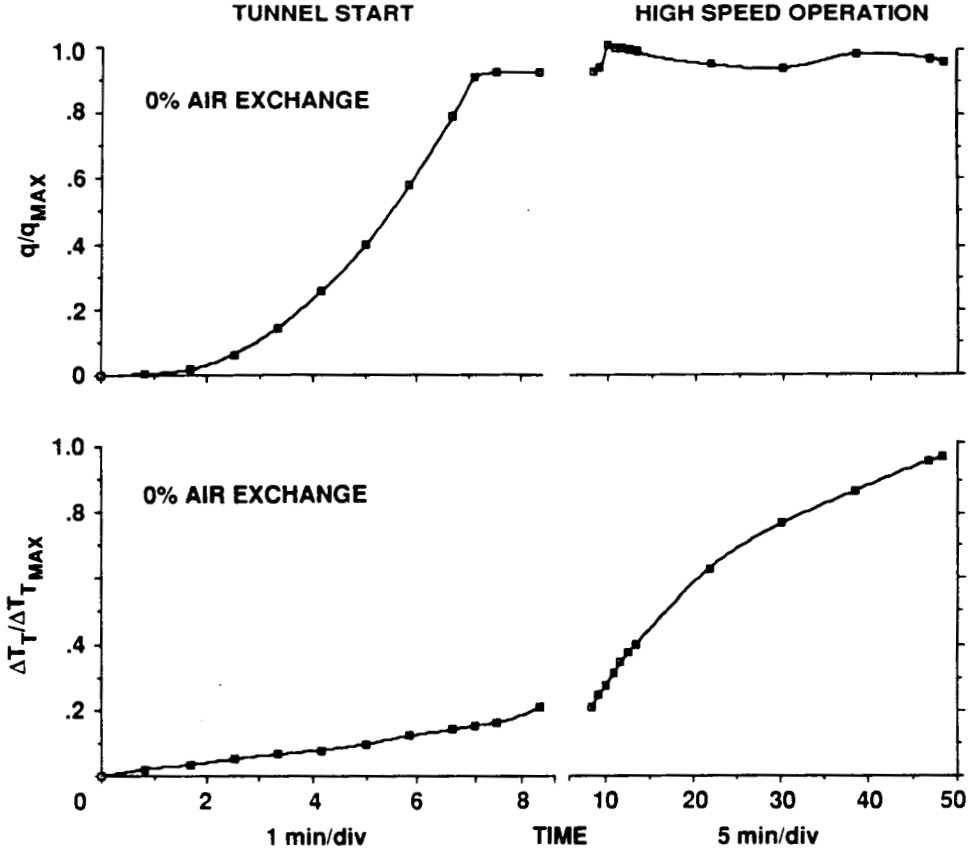

Figure 32.– Dynamic pressure and temperature time history (0% air exchange, q_{max} = 100 psf).

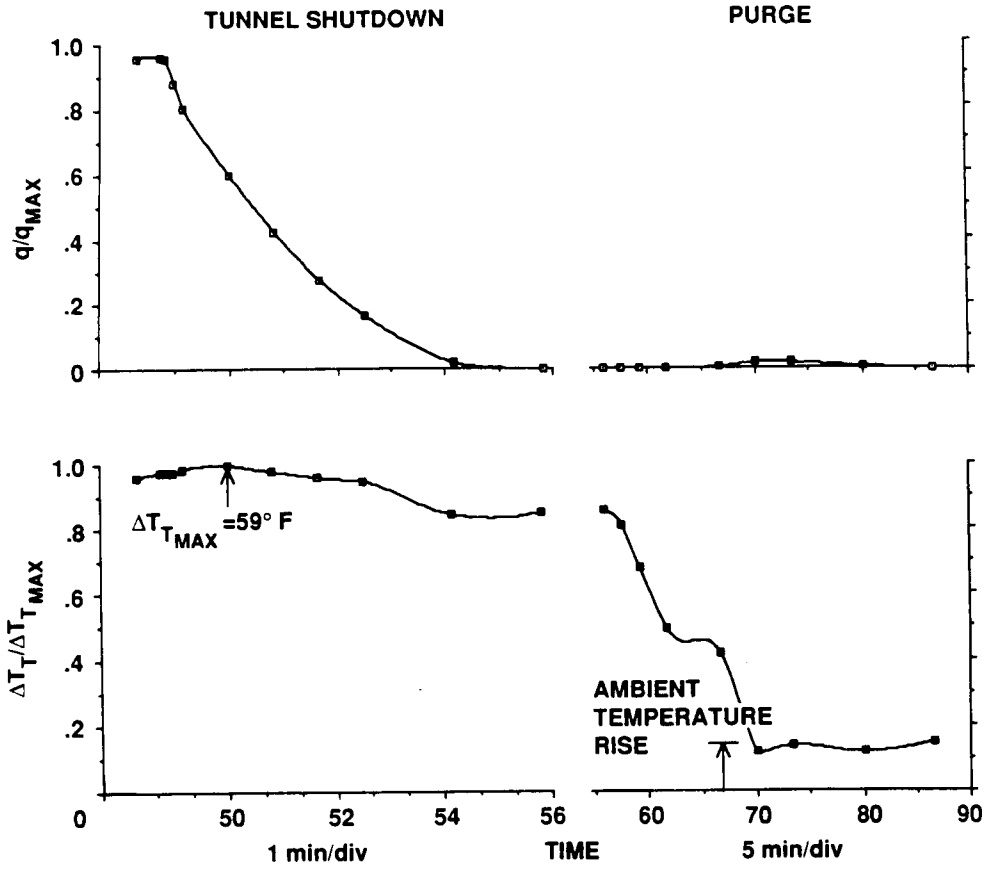

Figure 32.– Concluded.

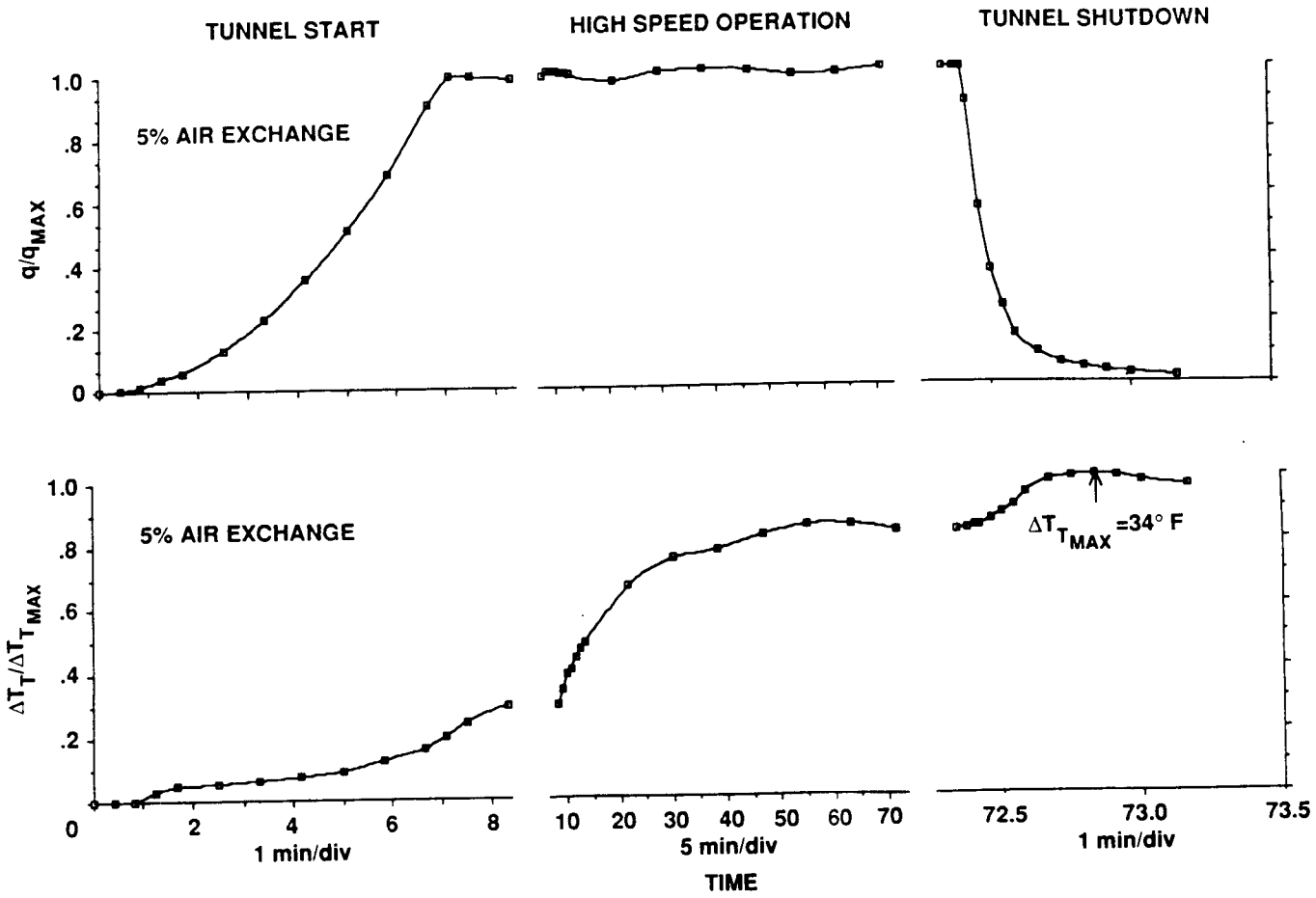

Figure 33.– Dynamic pressure and temperature time history (5% air exchange, q_{max} = 262 psf).

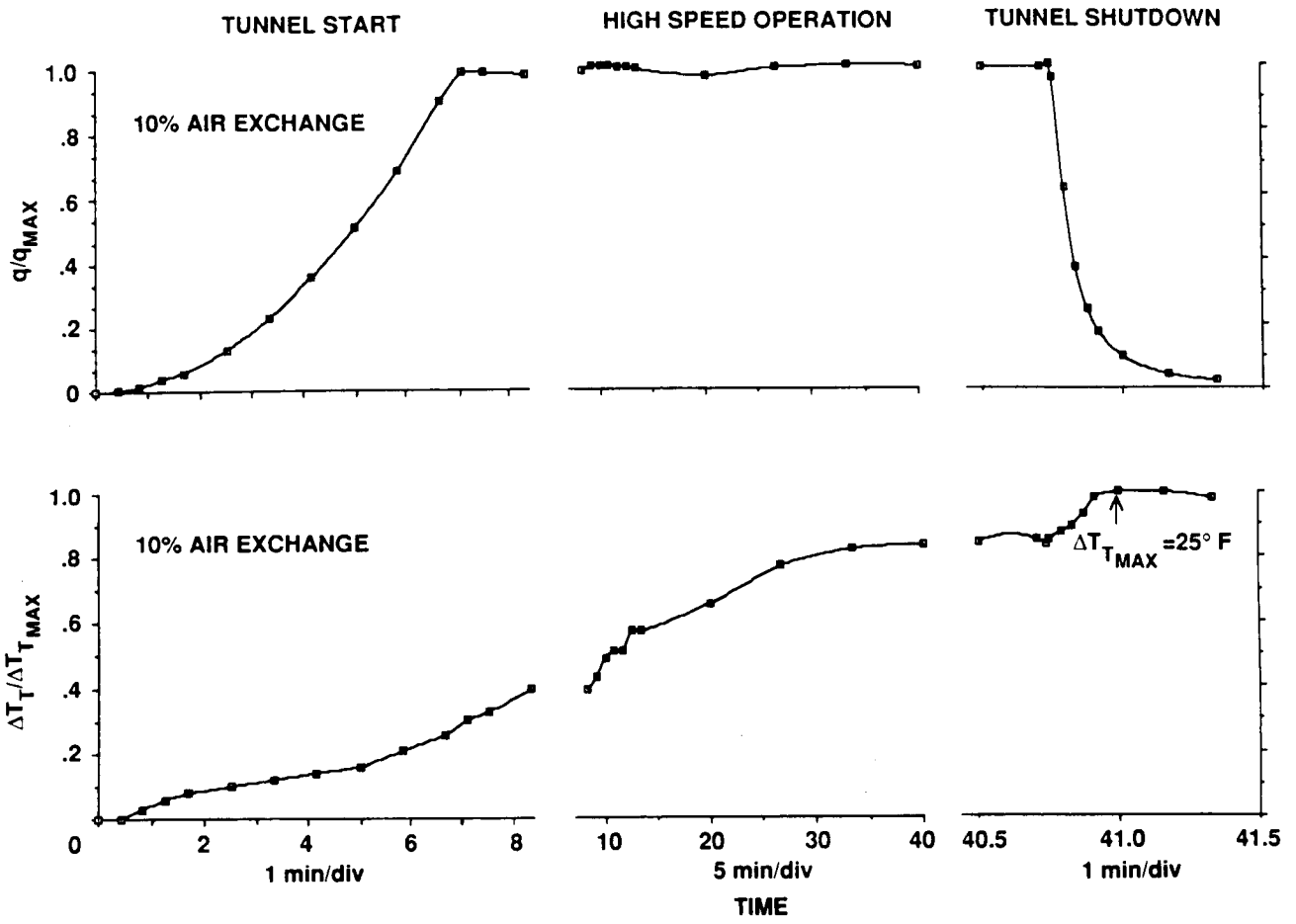

Figure 34.– Dynamic pressure and temperature time history (10% air exchange, q_{max} = 262 psf).

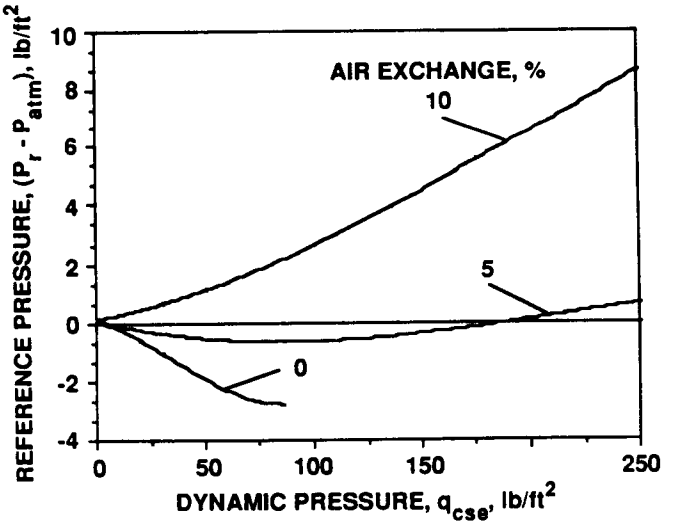

10% AE $(P_r - P_{atm}) = 0.1435 + 0.0133(q_{cse}) + 1.343E\text{-}4(q_{cse})^2 - 2.046E\text{-}7(q_{cse})^3$

5% AE $(P_r - P_{atm}) = 0.0824 - 0.0182(q_{cse}) + 1.317E\text{-}4(q_{cse})^2 - 1.998E\text{-}7(q_{cse})^3$

0% AE $(P_r - P_{atm}) = 0.0918 - 0.0226(q_{cse}) - 6.659E\text{-}4(q_{cse})^2 + 6.294E\text{-}6(q_{cse})^3$

Figure 35.– Settling chamber static pressure level versus scale dynamic pressure.

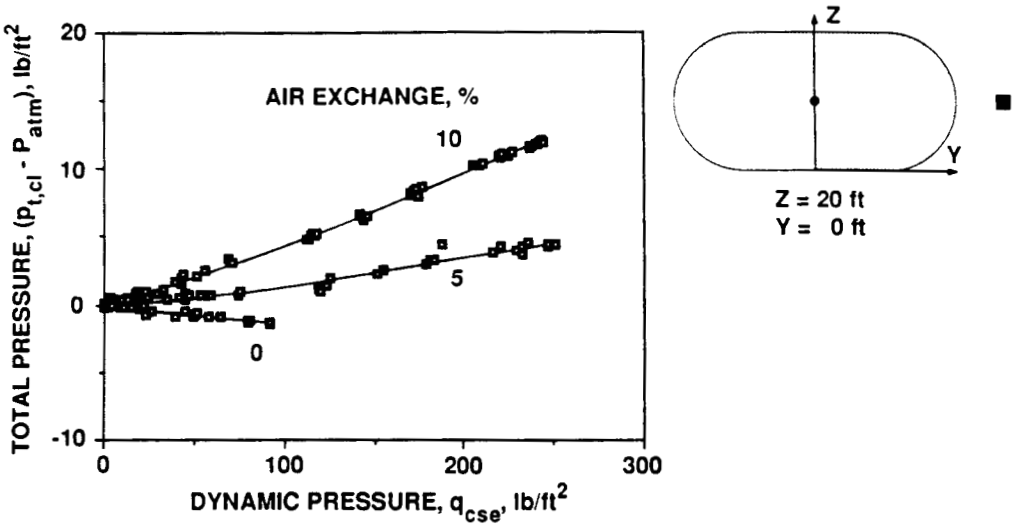

10% AE $(p_{t,cl} - P_{atm}) = 0.0168 + 0.041(q_{cse}) + 3.492E\text{-}5(q_{cse})^2$
5% AE $(p_{t,cl} - P_{atm}) = 0.089 + 0.0094(q_{cse}) + 3.468E\text{-}5(q_{cse})^2$
0% AE $(p_{t,cl} - P_{atm}) = 1.349E\text{-}4 - 0.0174(q_{cse}) + 3.275E\text{-}5(q_{cse})^2$

Figure 36.– Indicated total pressure on centerline versus scale dynamic pressure (Z = 20 ft).

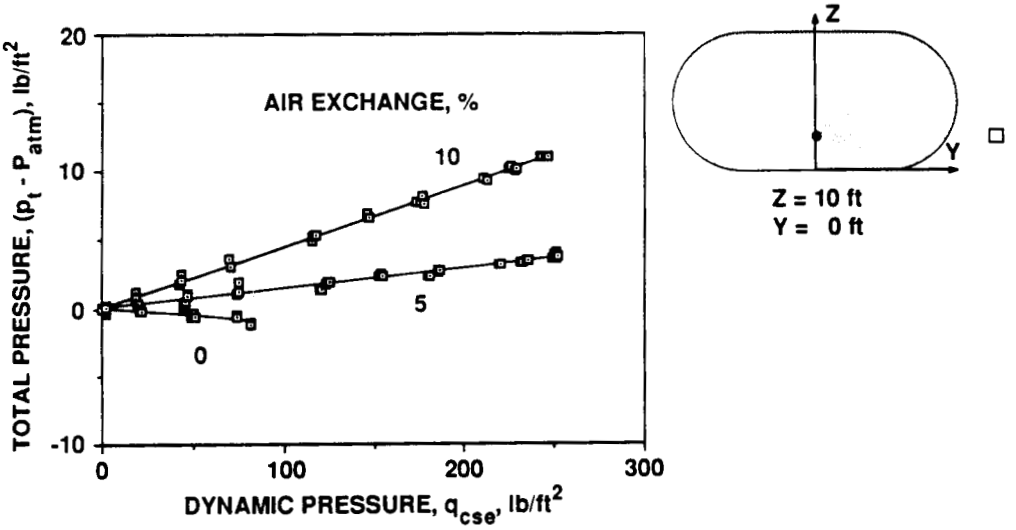

10% AE $(p_t - P_{atm}) = -0.0058 + 0.0462(q_{cse}) - 5.799E\text{-}6(q_{cse})^2$
5% AE $(p_t - P_{atm}) = -0.0499 + 0.014(q_{cse}) + 4.760E\text{-}6(q_{cse})^2$
0% AE $(p_t - P_{atm}) = 0.0135 - 0.0066(q_{cse}) - 6.277E\text{-}5(q_{cse})^2$

Figure 37.– Indicated total pressure on centerline versus scale dynamic pressure (Z = 10 ft).

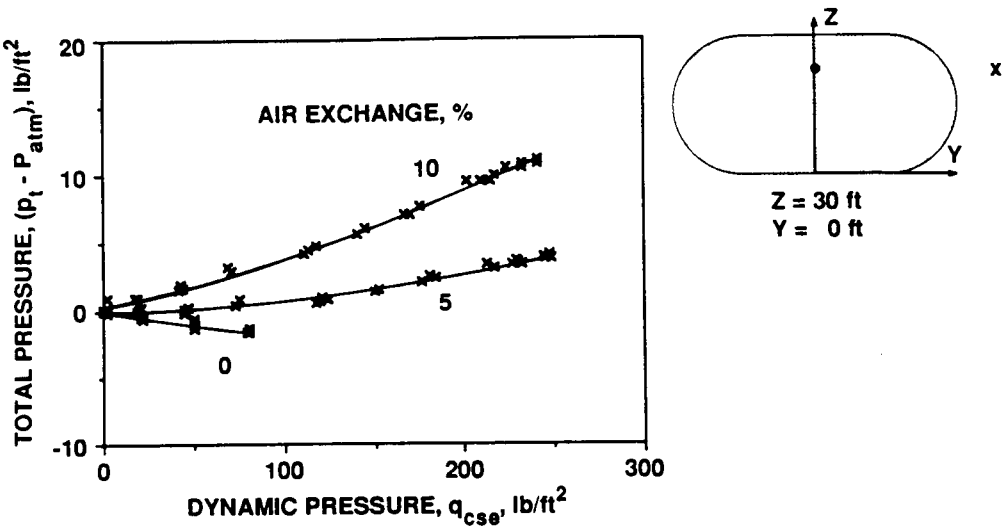

10% AE $(p_t - P_{atm}) = 0.1459 + 0.0344(q_{cse}) + 4.543E\text{-}5(q_{cse})^2$

5% AE $(p_t - P_{atm}) = -0.0273 + 5.760E\text{-}4(q_{cse}) + 6.361E\text{-}5(q_{cse})^2$

0% AE $(p_t - P_{atm}) = 0.0121 - 0.0184(q_{cse}) - 8.587E\text{-}6(q_{cse})^2$

Figure 38.– Indicated total pressure on centerline versus scale dynamic pressure (Z = 30 ft).

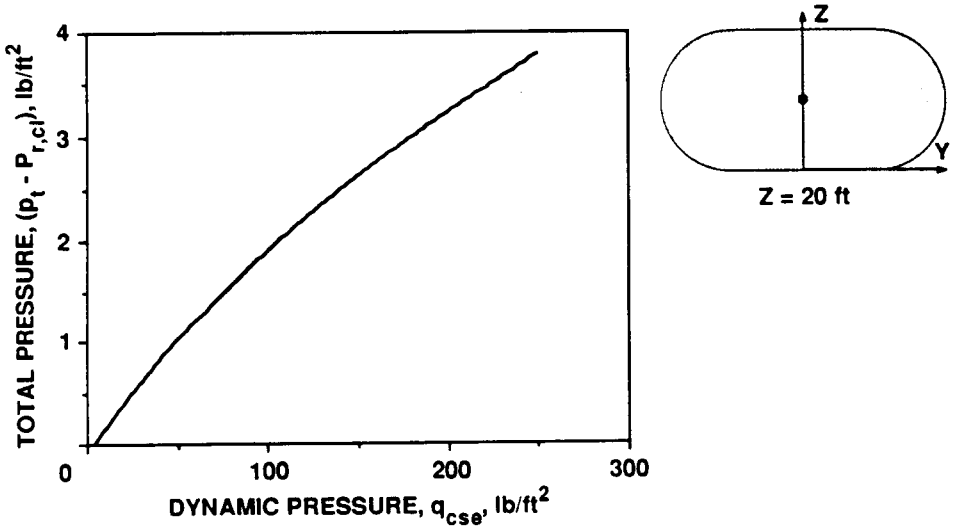

$(p_t - P_r) = -0.0898 + 0.0251(q_{cse}) - 5.855E\text{-}5(q_{cse})^2 + 8.156E\text{-}8(q_{cse})^3$

Figure 39.– Total pressure on centerline (referenced to P_r ring) versus scale dynamic pressure (Z = 20 ft).

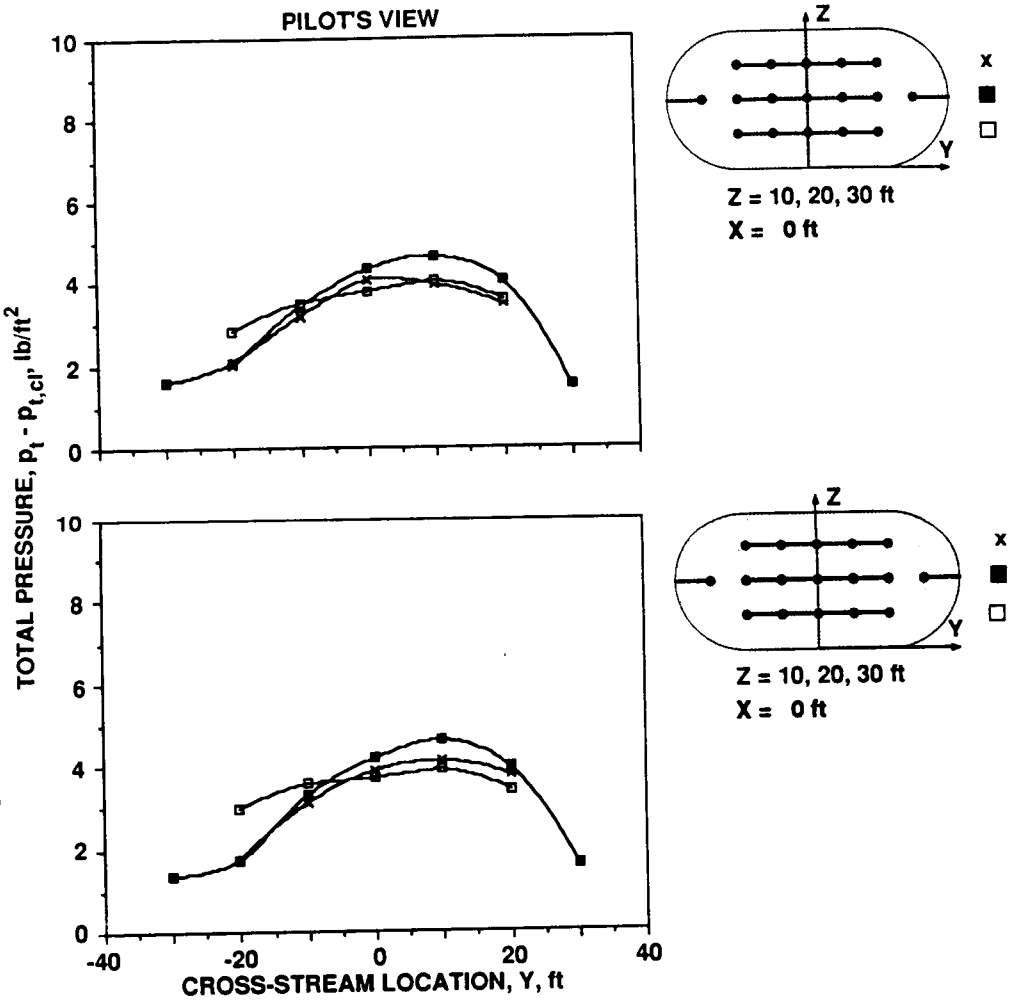

Figure 40.– Effect of streamwise location on total pressure distribution ($p_t - p_{t,cl}$ at U_{ts} = 300 knots).

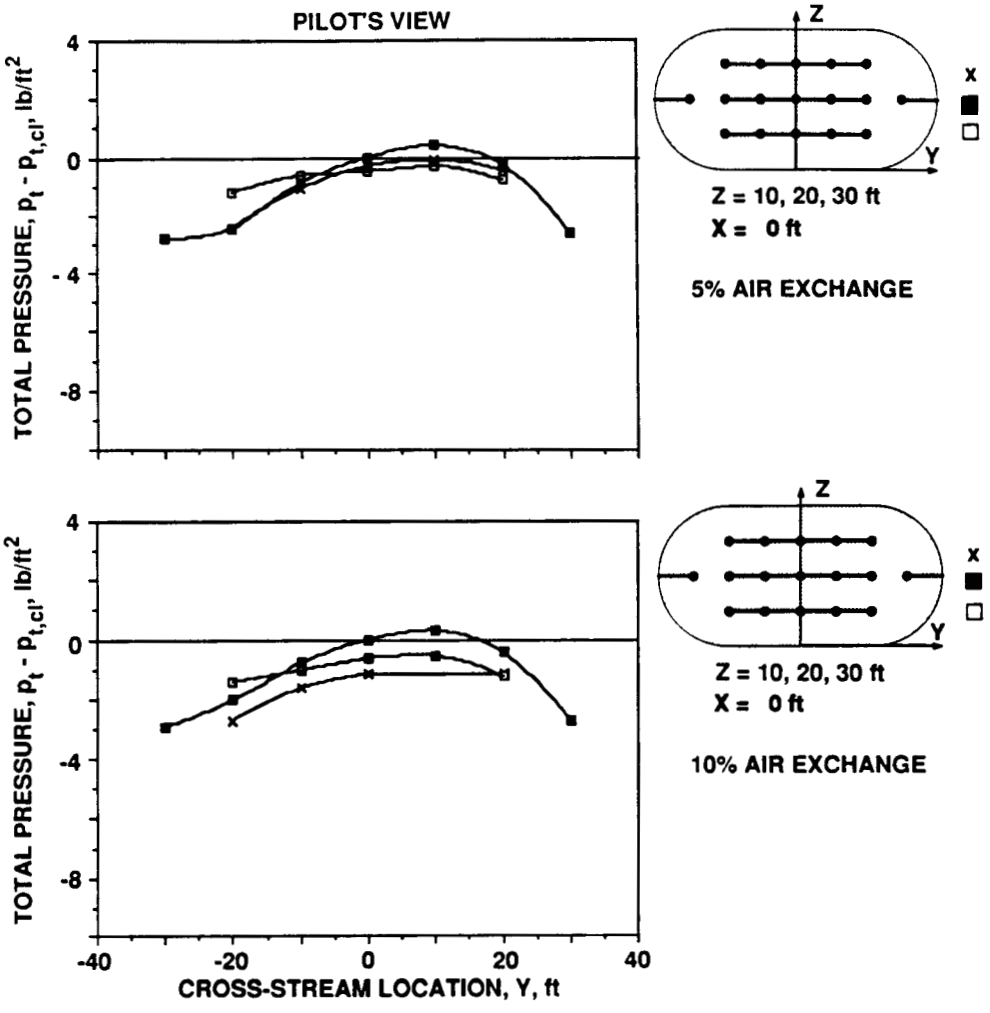

Figure 41.– Effect of air exchange on total pressure distribution (p_t - $p_{t,cl}$ at U_{ts} = 300 knots).

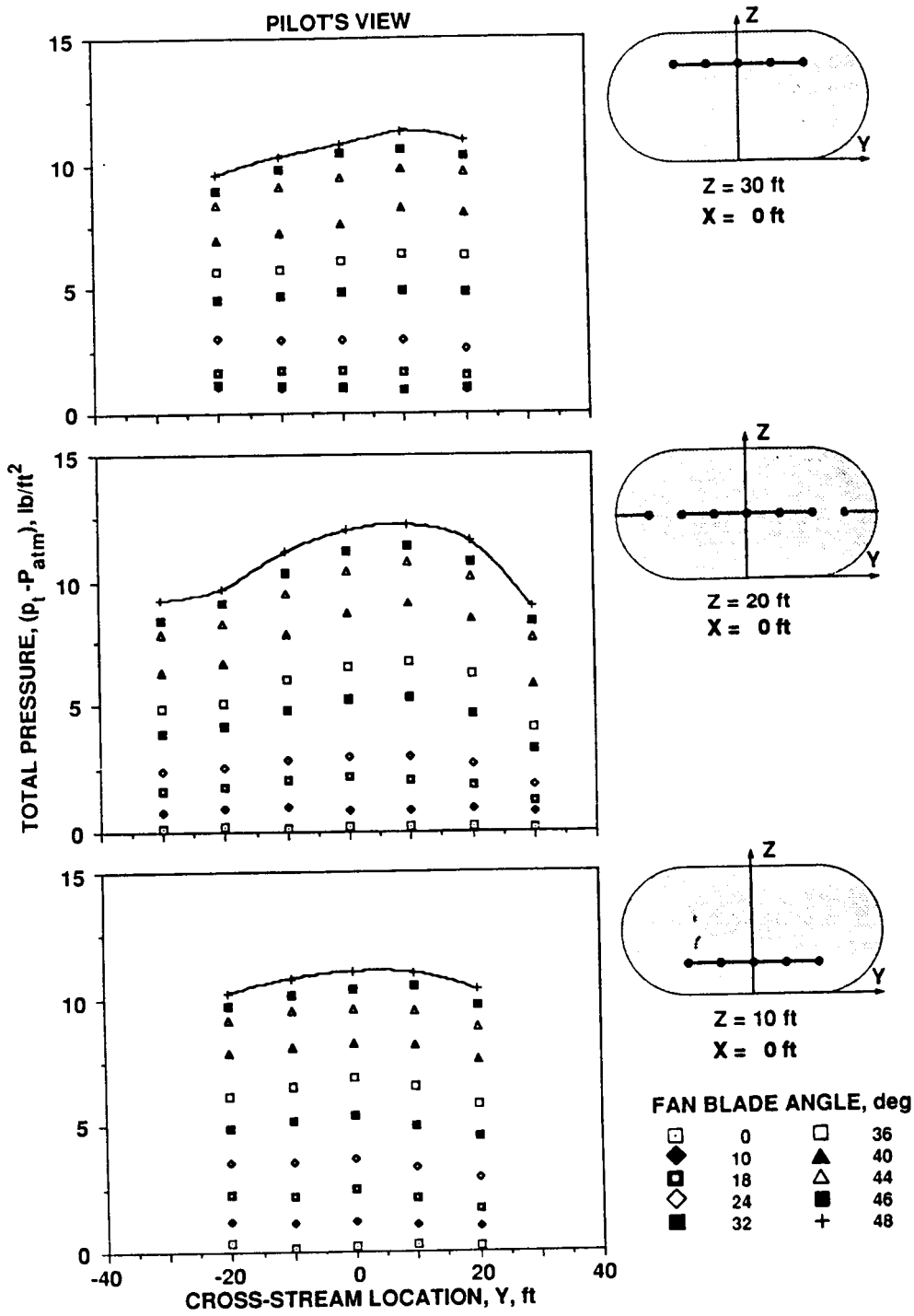

Figure 42.– Total pressure distributions for various fan blade angle settings at 10% air exchange.

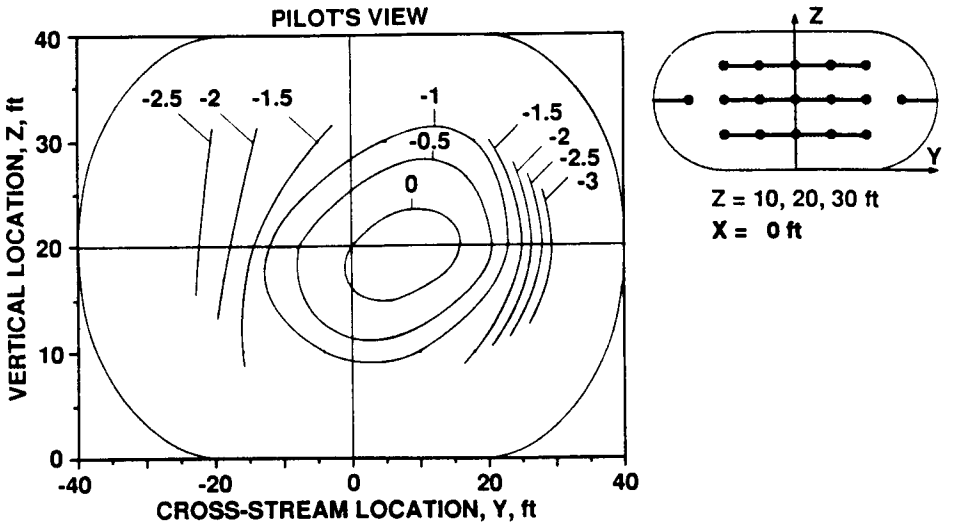

Figure 43.– Total pressure contour plot (lines of equal (p_t - $p_{t,cl}$ at U_{ts} = 300 knots, 10% air exchange)).

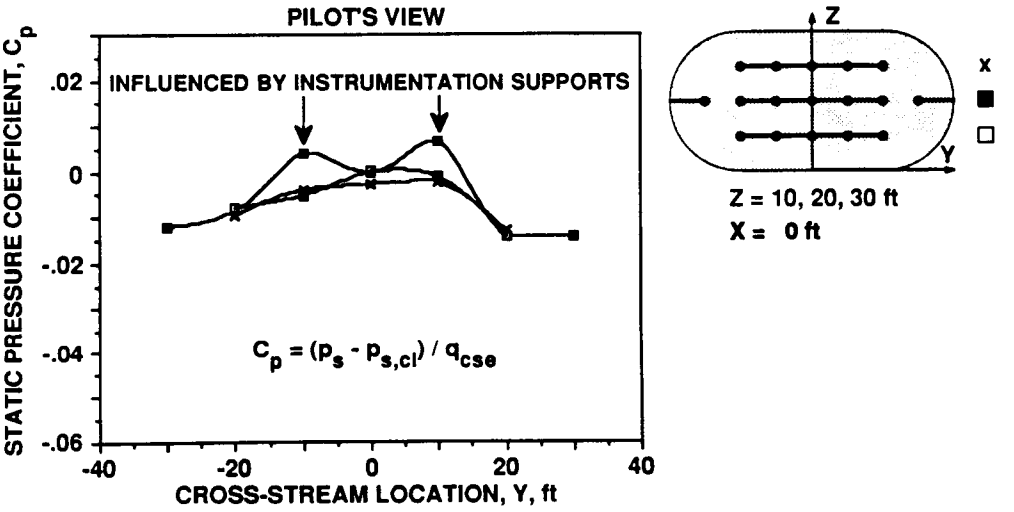

Figure 44.– Static pressure coefficient distribution.

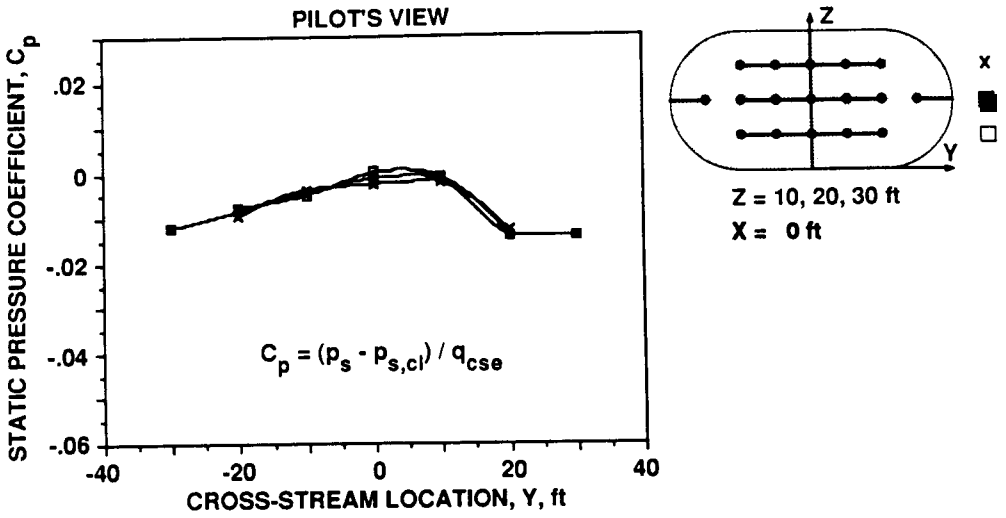

Figure 45.– Static pressure coefficient distribution (correction for aerodynamic interference of the instrumentation supports applied).

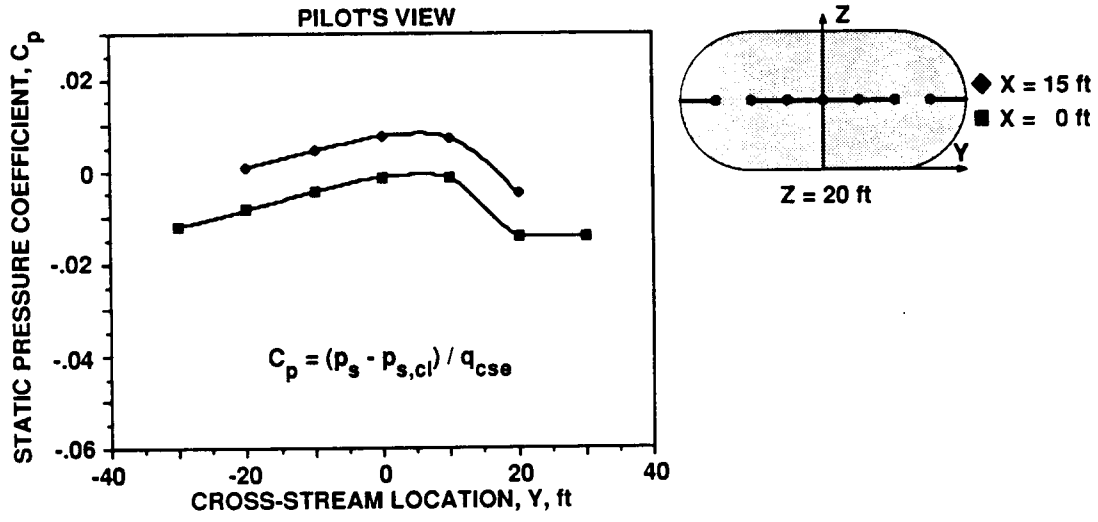

Figure 46.– Comparison between the static pressure coefficient distributions at X = 0 ft and X = 15 ft.

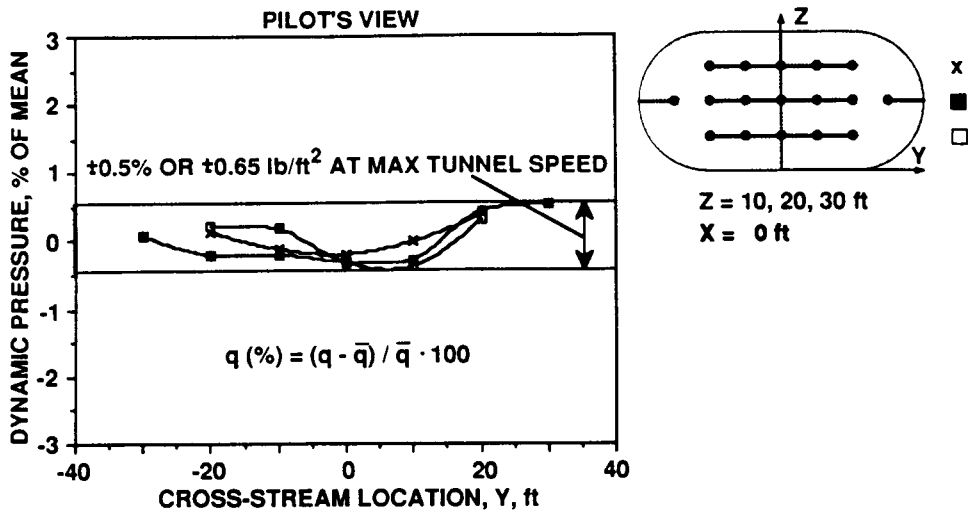

Figure 47.– Dynamic pressure distribution for maximum tunnel speed (10% air exchange).

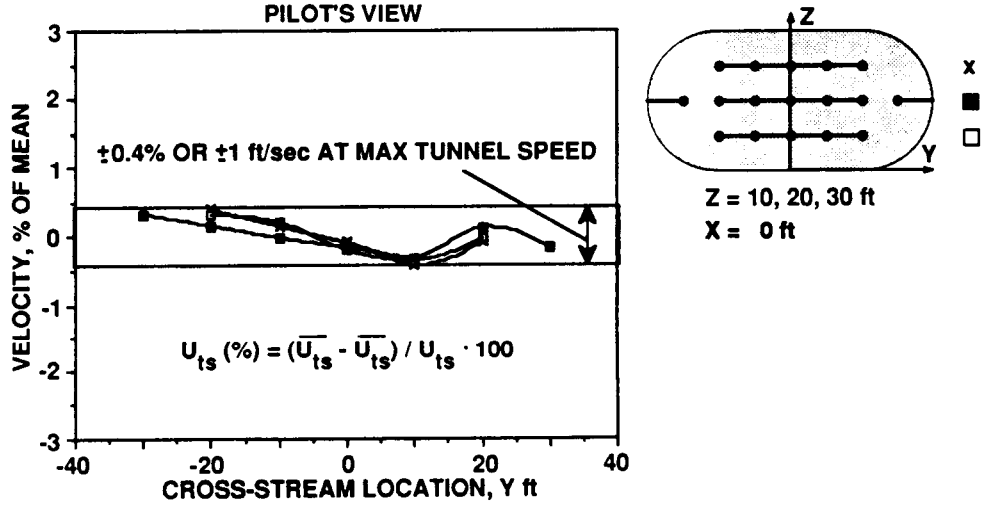

Figure 48.– Velocity distribution for maximum tunnel speed (10% air exchange).

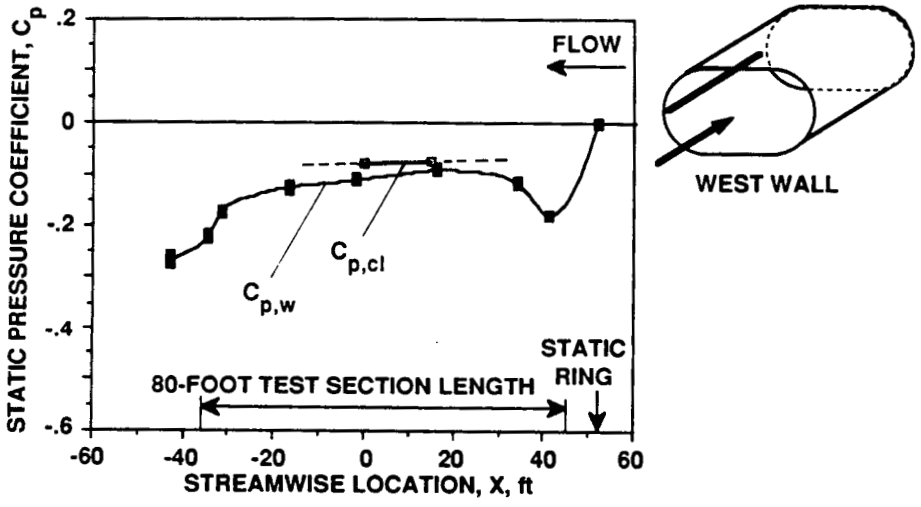

Figure 49.– Streamwise static pressure coefficient distribution (U_{ts} = 300 knots).

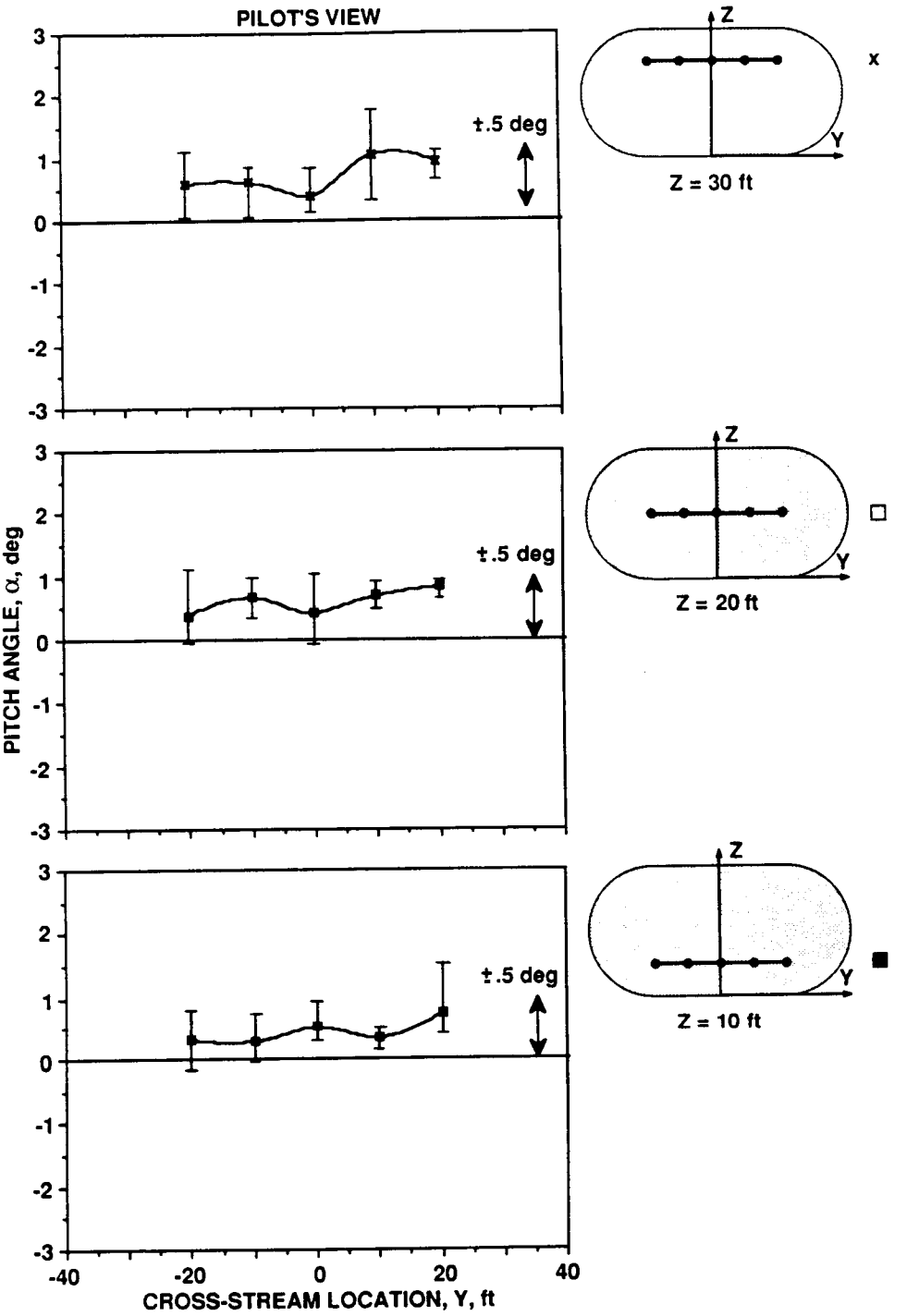

Figure 50.– Pitch angle distributions (U_{ts} > 200 knots).

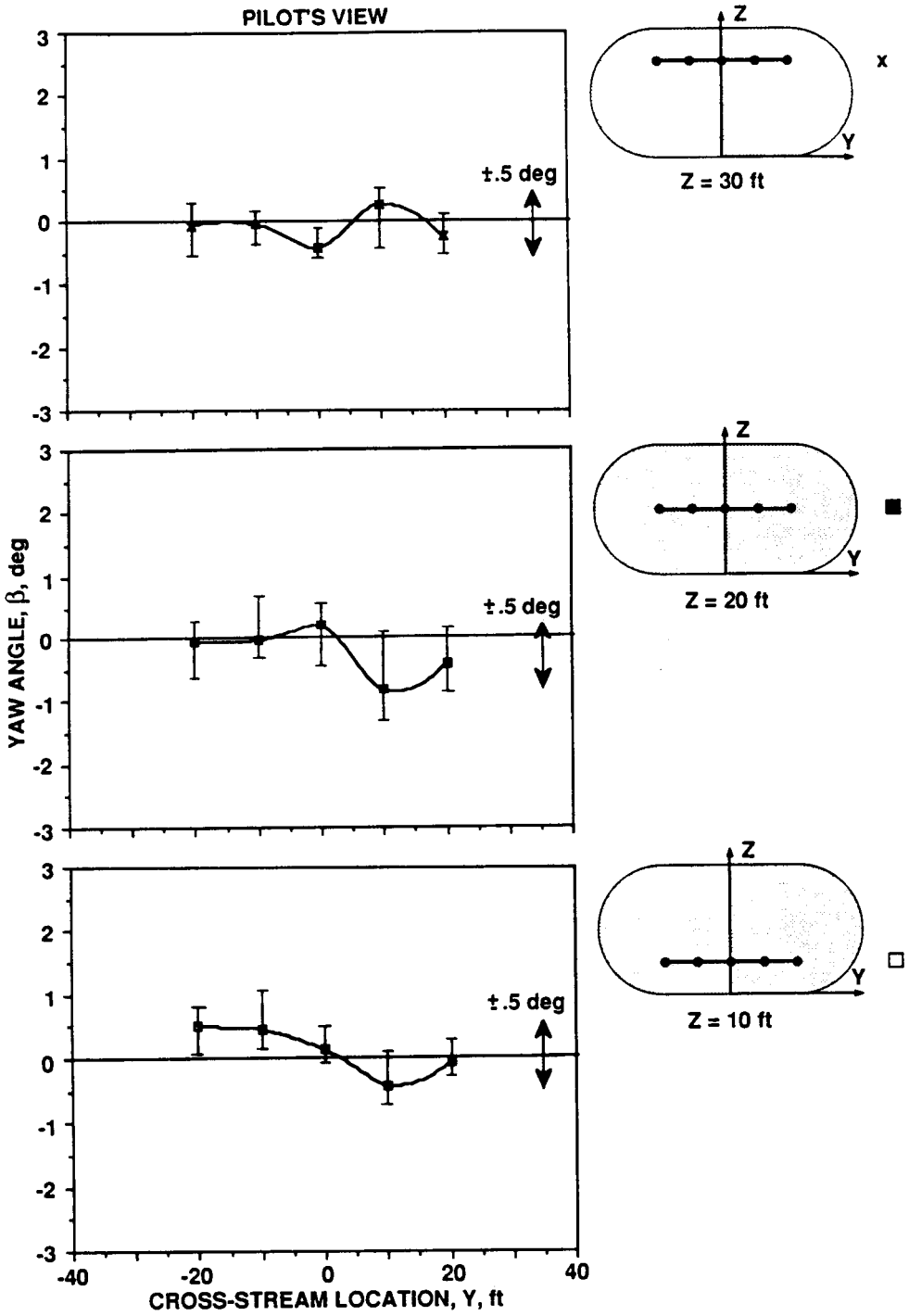

Figure 51.– Yaw angle distributions (U_{ts} > 200 knots).

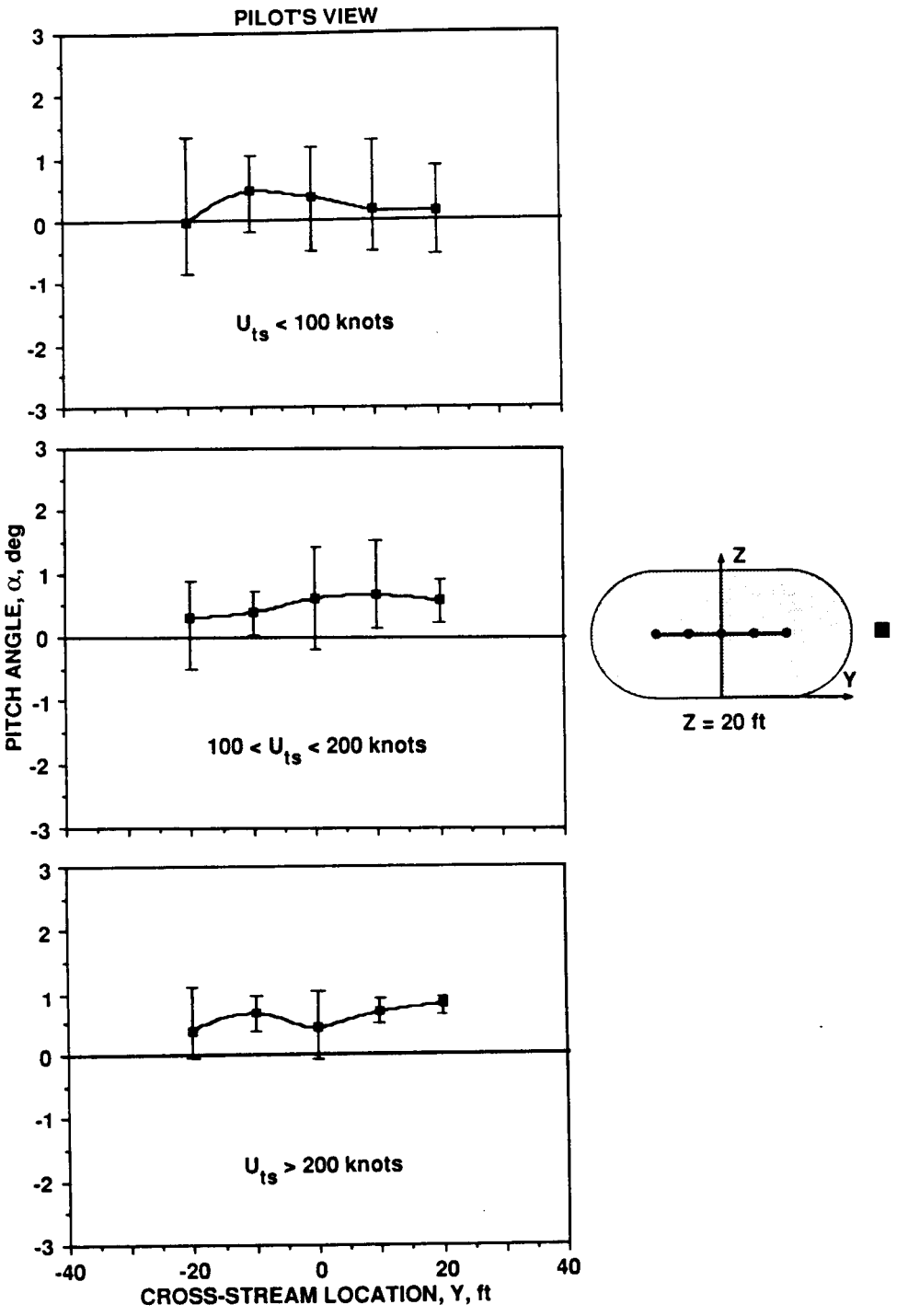

Figure 52.– Pitch angle distributions for three speed ranges.

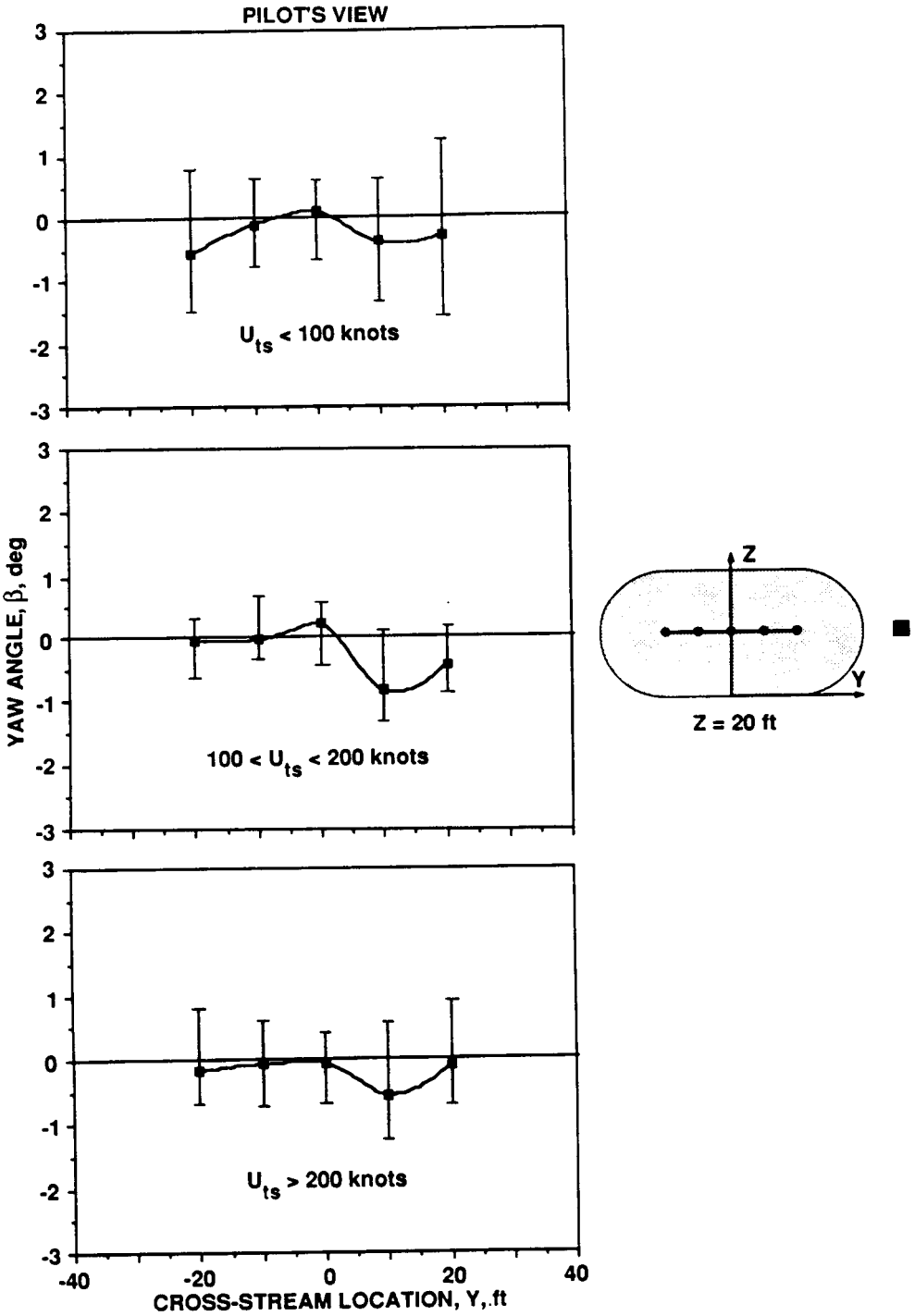

Figure 53.– Yaw angle distributions for three speed ranges.

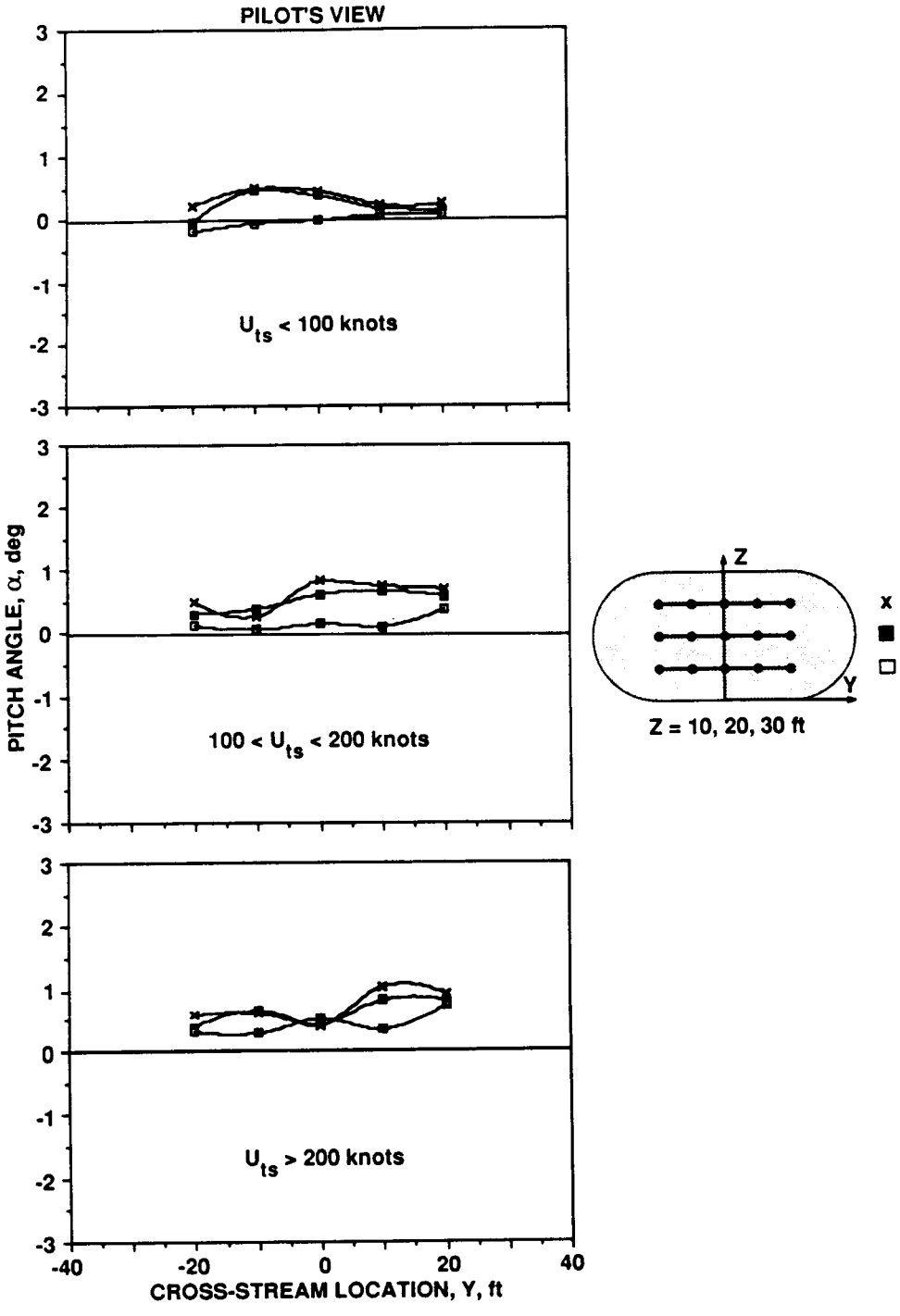

Figure 54.– Overall pitch angle distributions for three speed ranges.

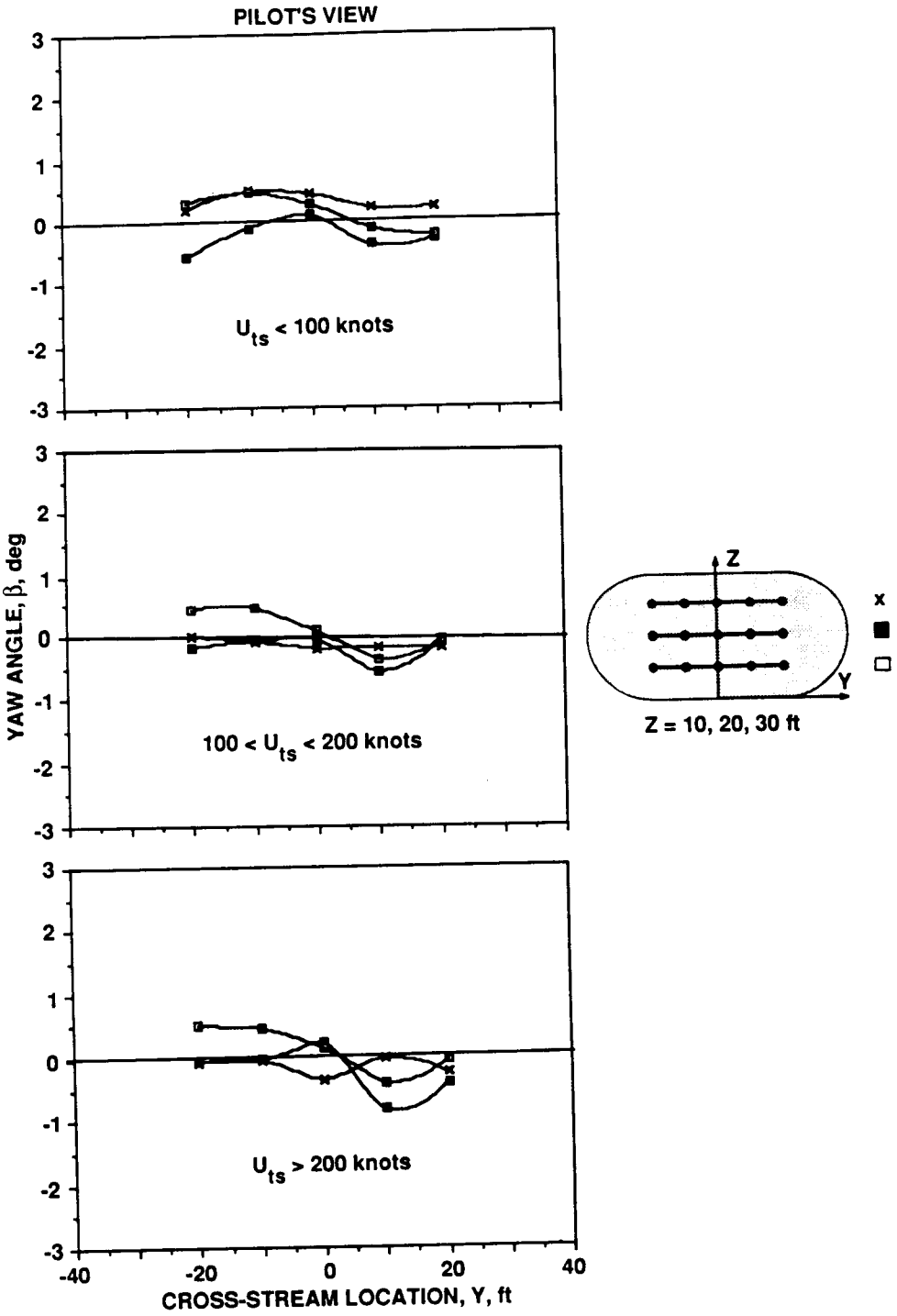

Figure 55.– Overall yaw angle distributions for three speed ranges.

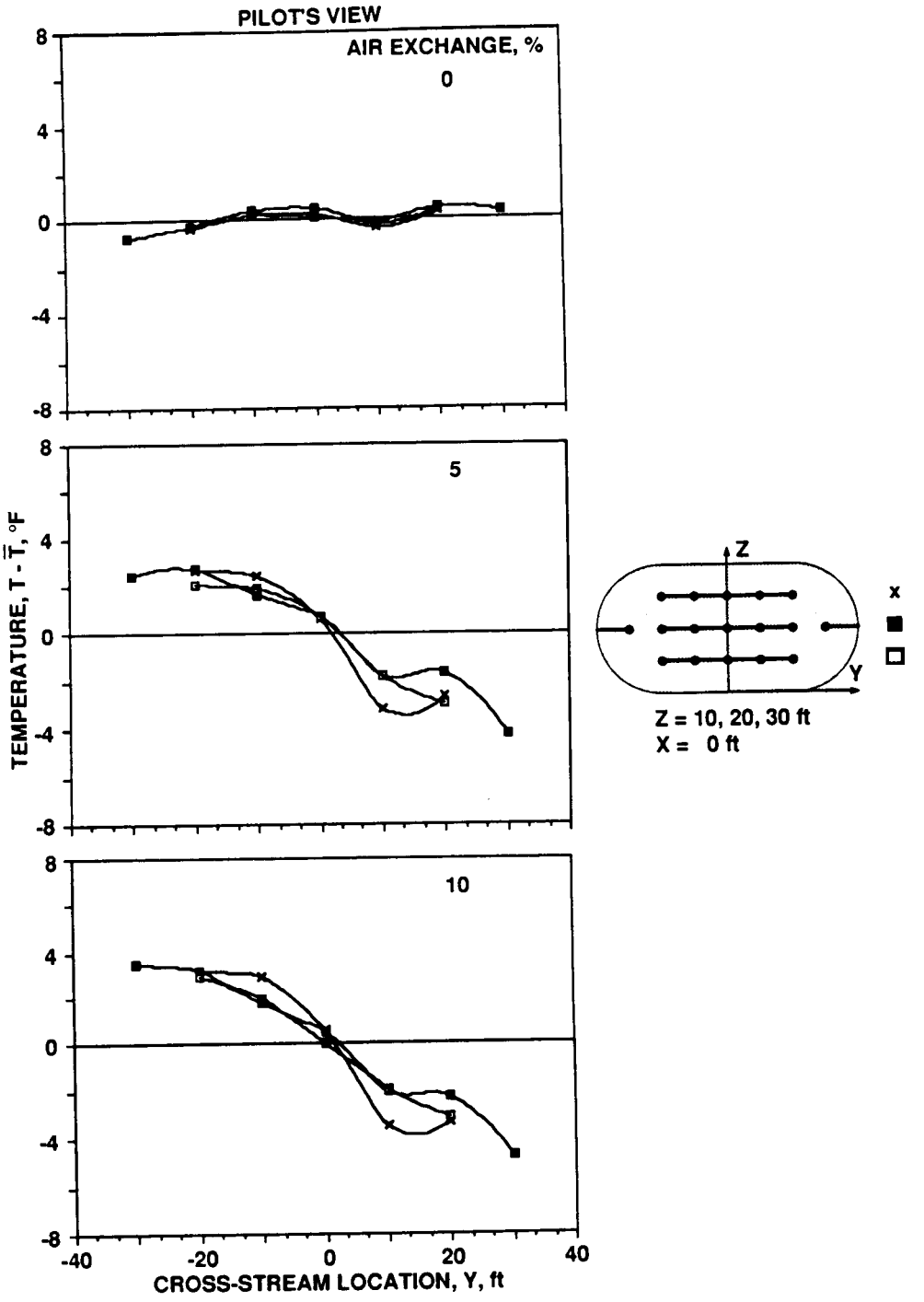

Figure 56.– Total temperature distributions at steady tunnel conditions (U_{ts} = 300 knots).

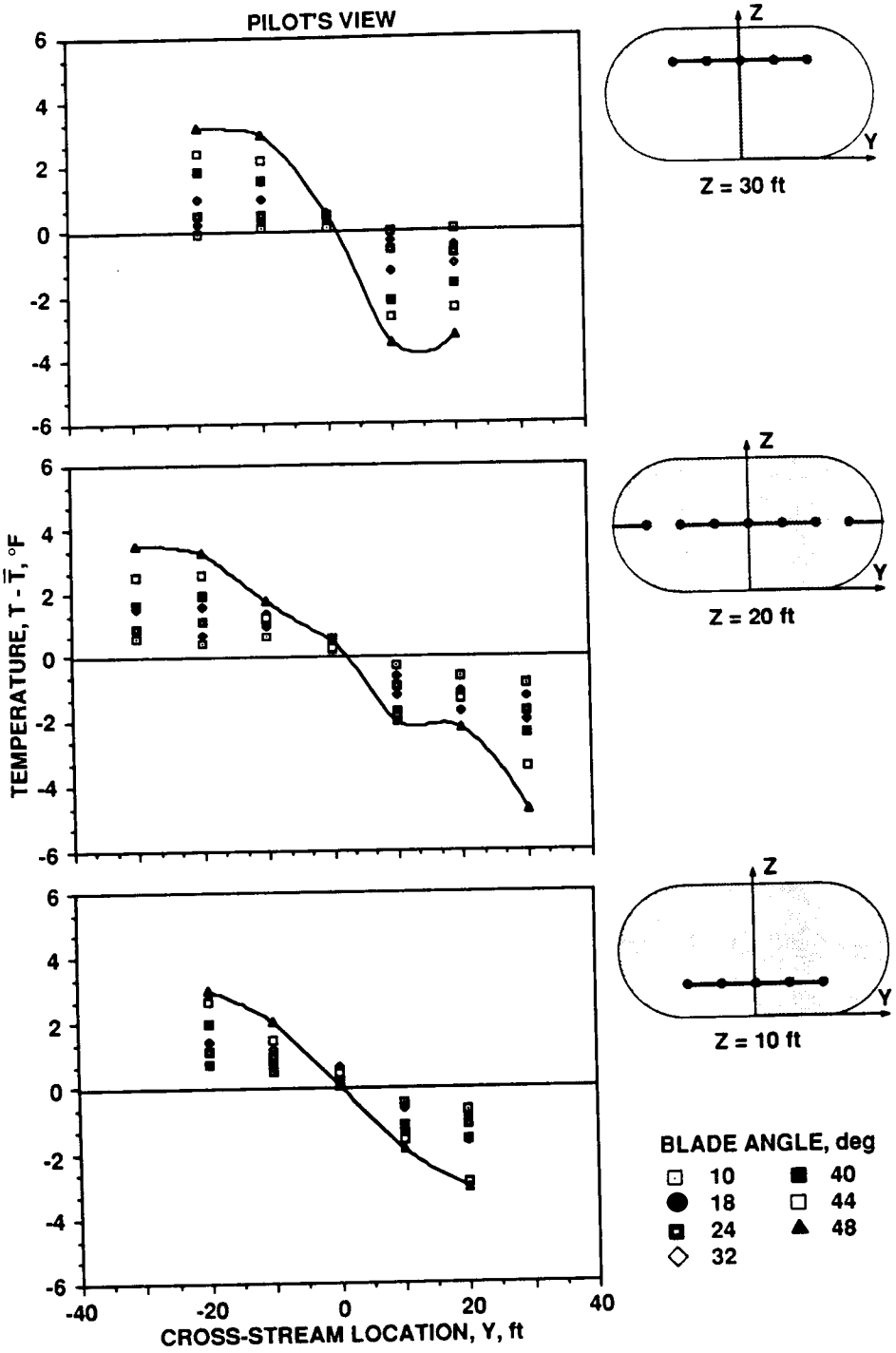

Figure 57.– Total temperature distribution variation with increasing fan blade angle (10% air exchange).

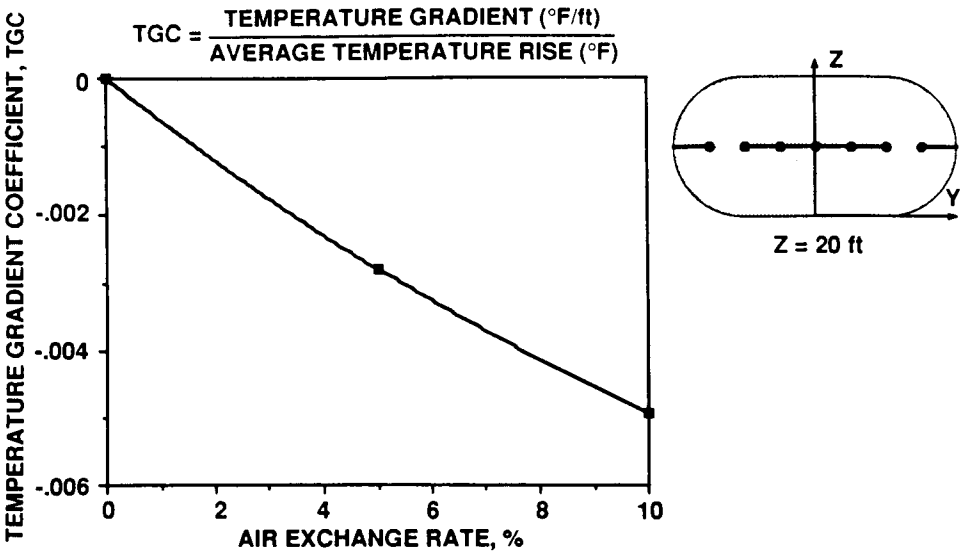

Figure 58.– Temperature gradient calibration.

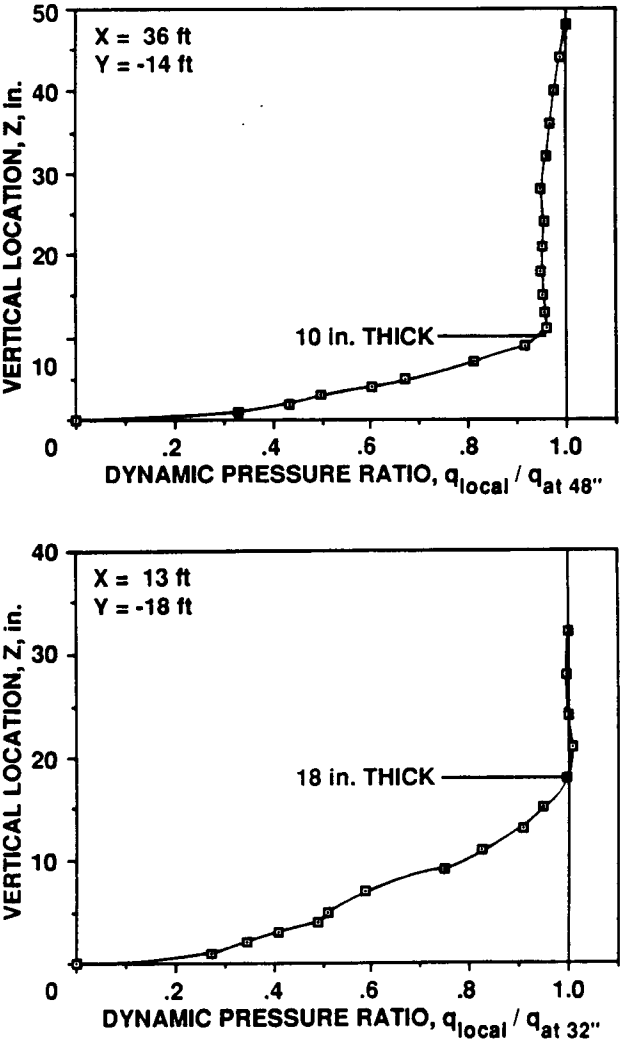

Figure 59.– Dynamic pressure profiles from the fixed rakes on the test section floor.

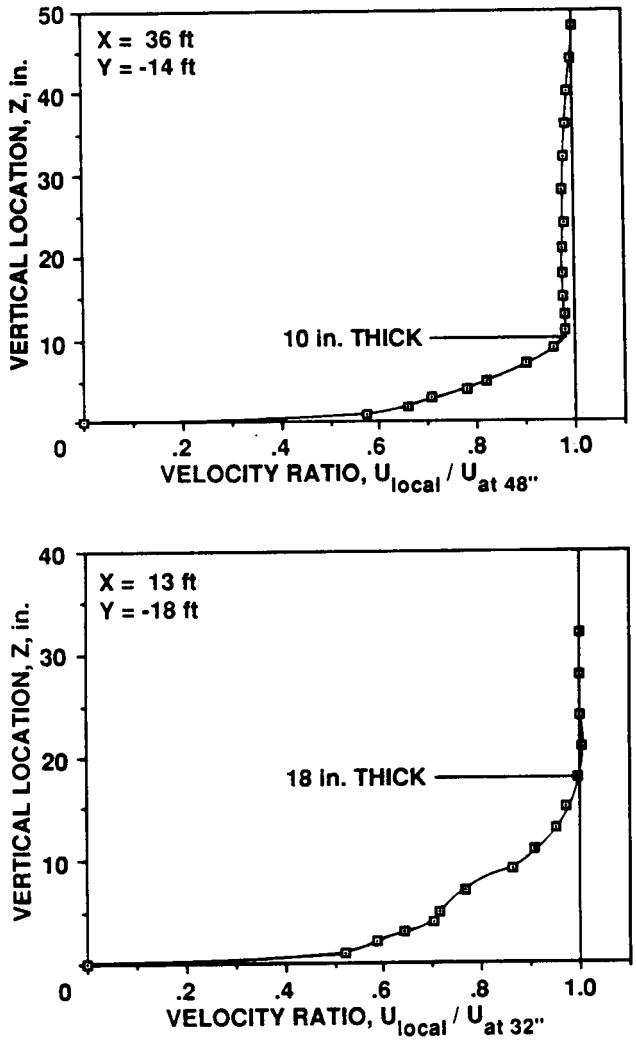

Figure 60.– Velocity profiles from the fixed rakes on the test section floor.

SINGLE HOT WIRE
HOOK-UP DIAGRAM

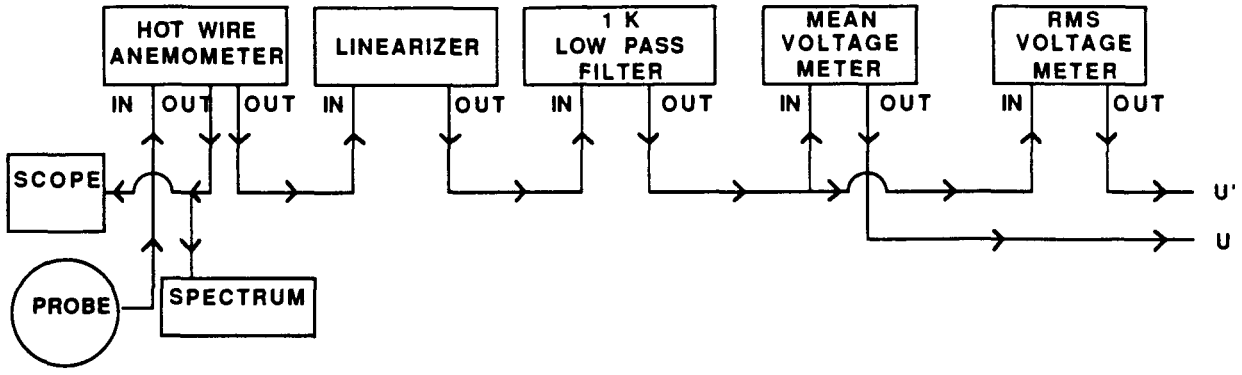

DUAL HOT WIRE
HOOK-UP DIAGRAM

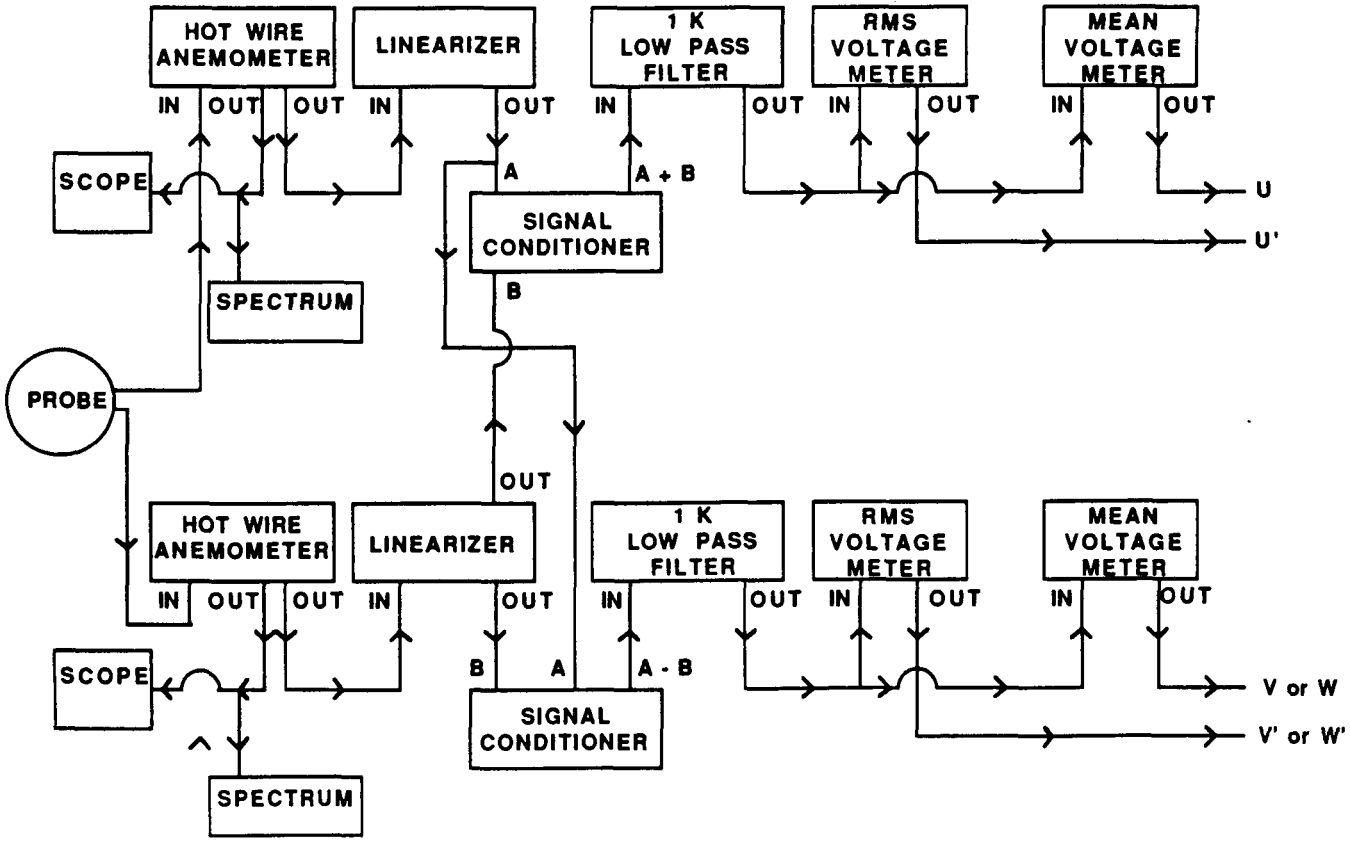

Figure 61.– Hot wire anemometer instrumentation diagrams.

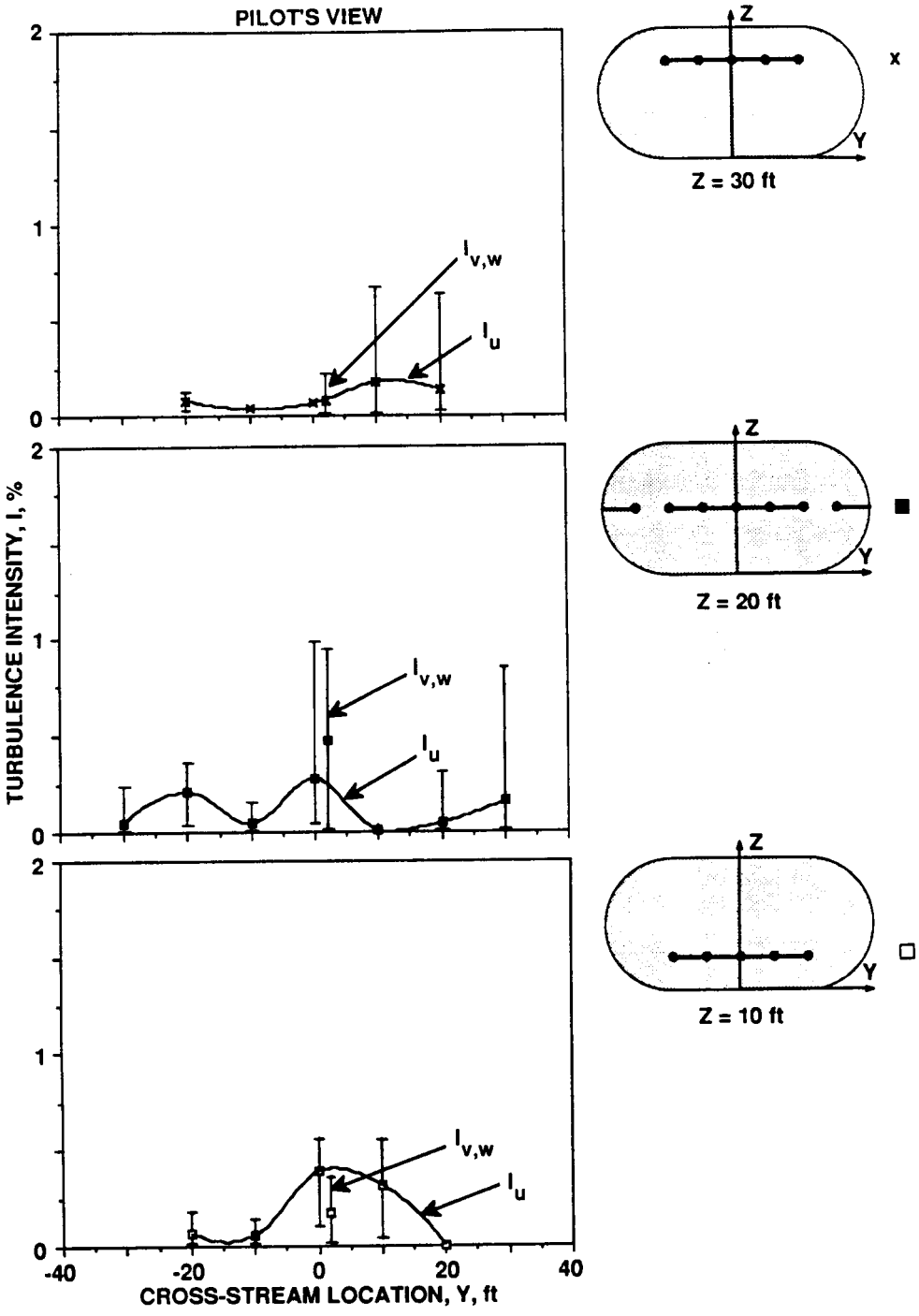

Figure 62.– Turbulence intensity distribution (U_{ts} < 75 knots).

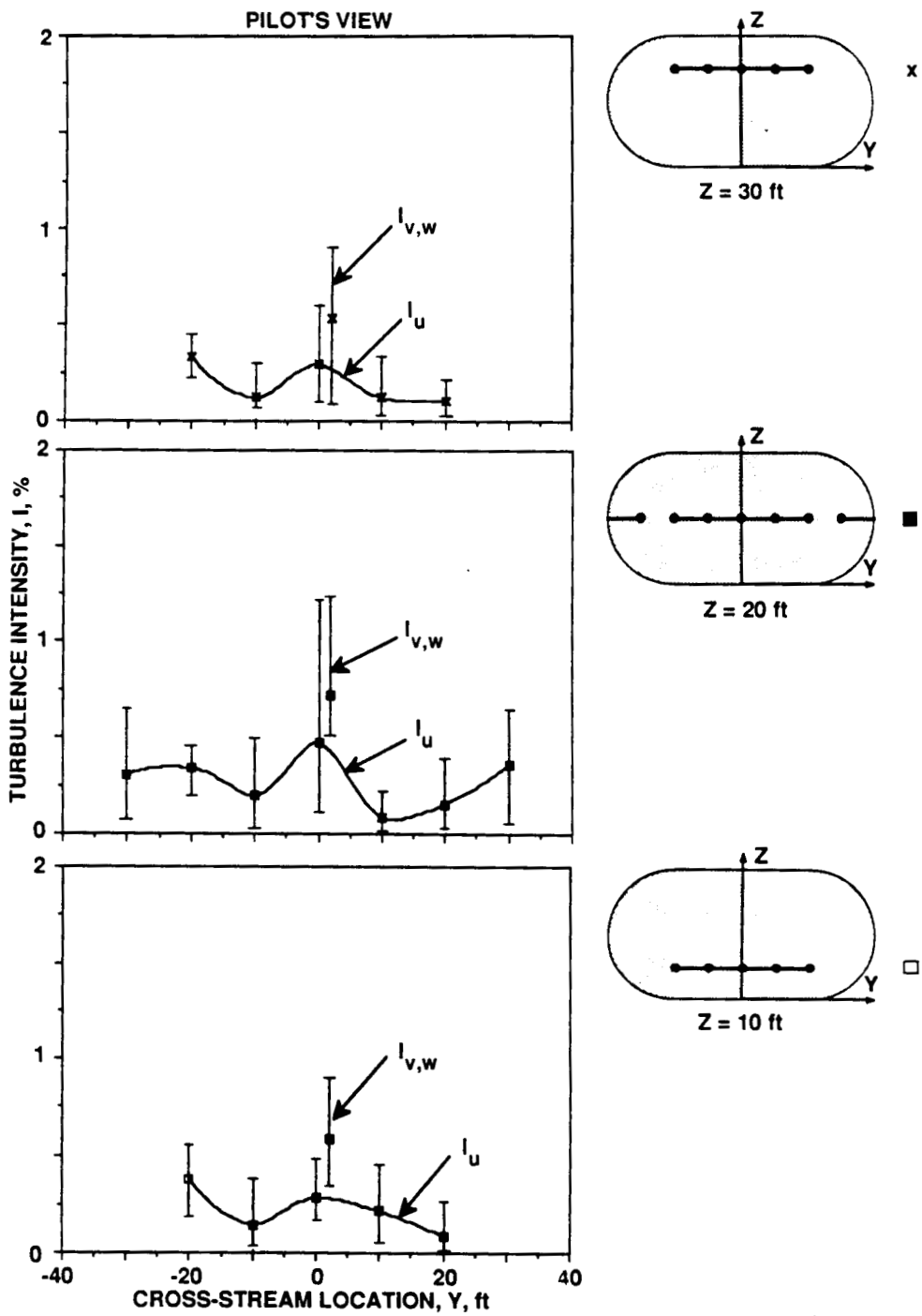

Figure 63.–Turbulence intensity distribution (75 knots < U_{ts} < 150 knots).

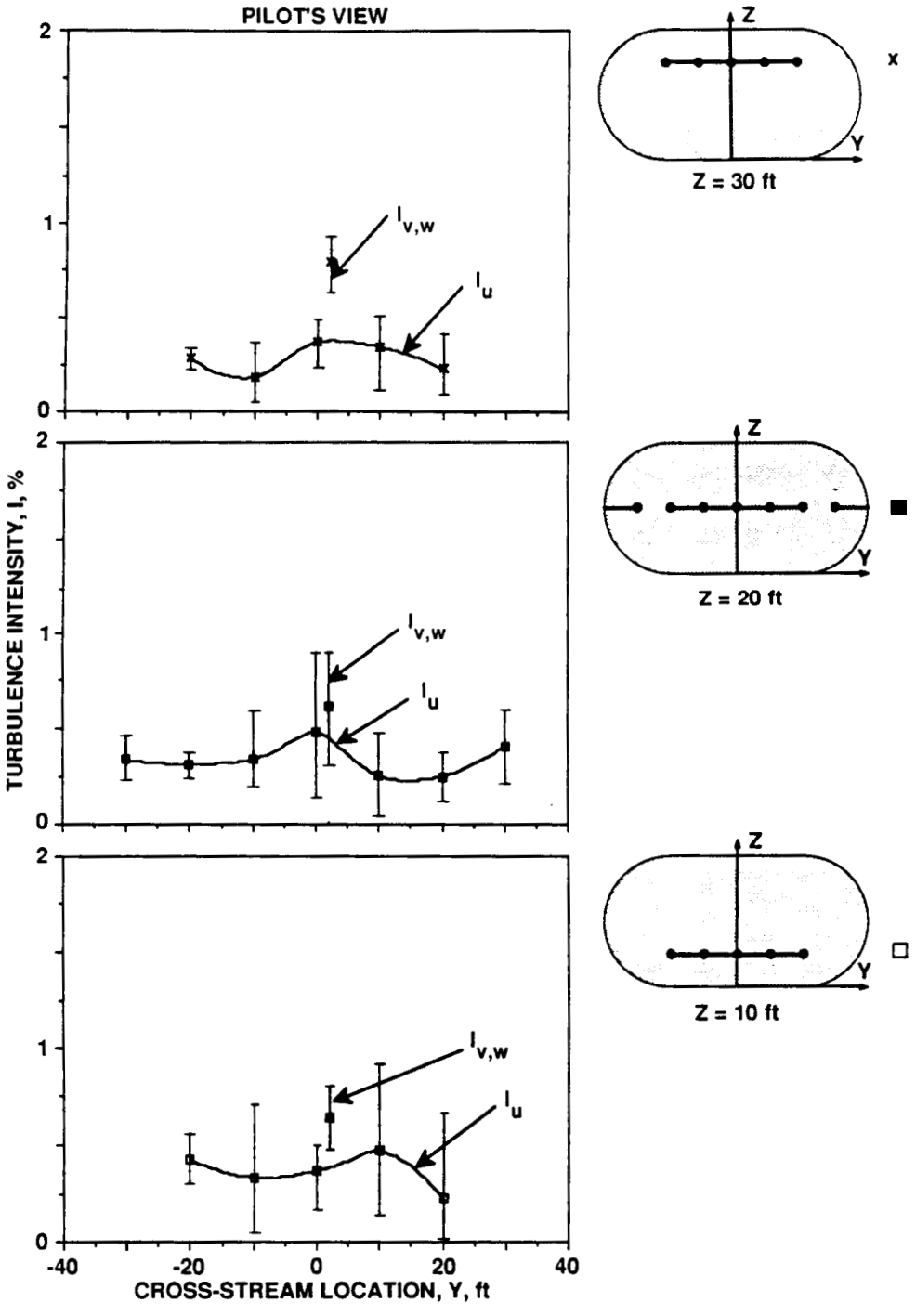

Figure 64.– Turbulence intensity distribution (150 knots < U_{ts} < 225 knots).

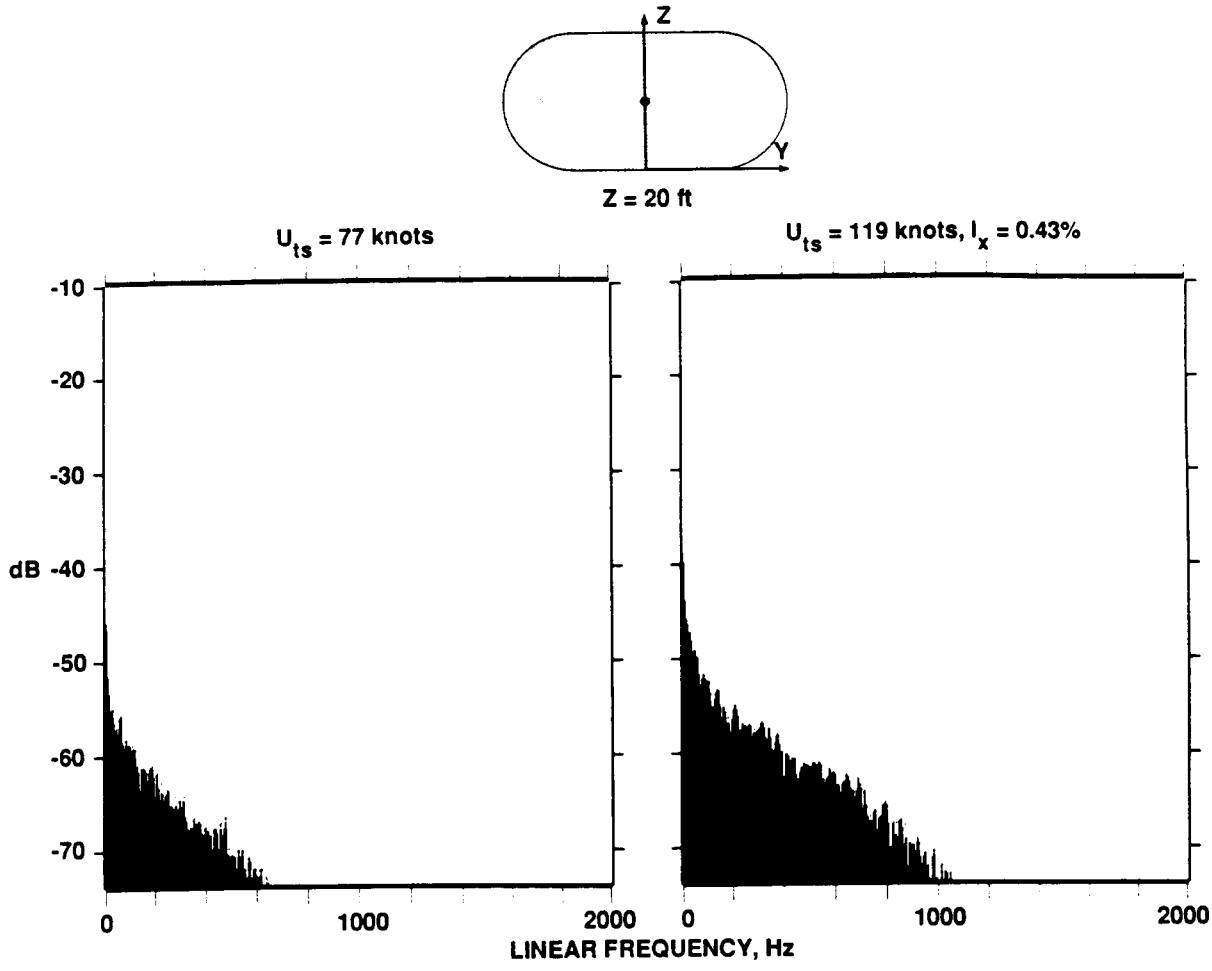

Figure 65.– Energy spectra (U_{ts} = 77 and 119 knots).

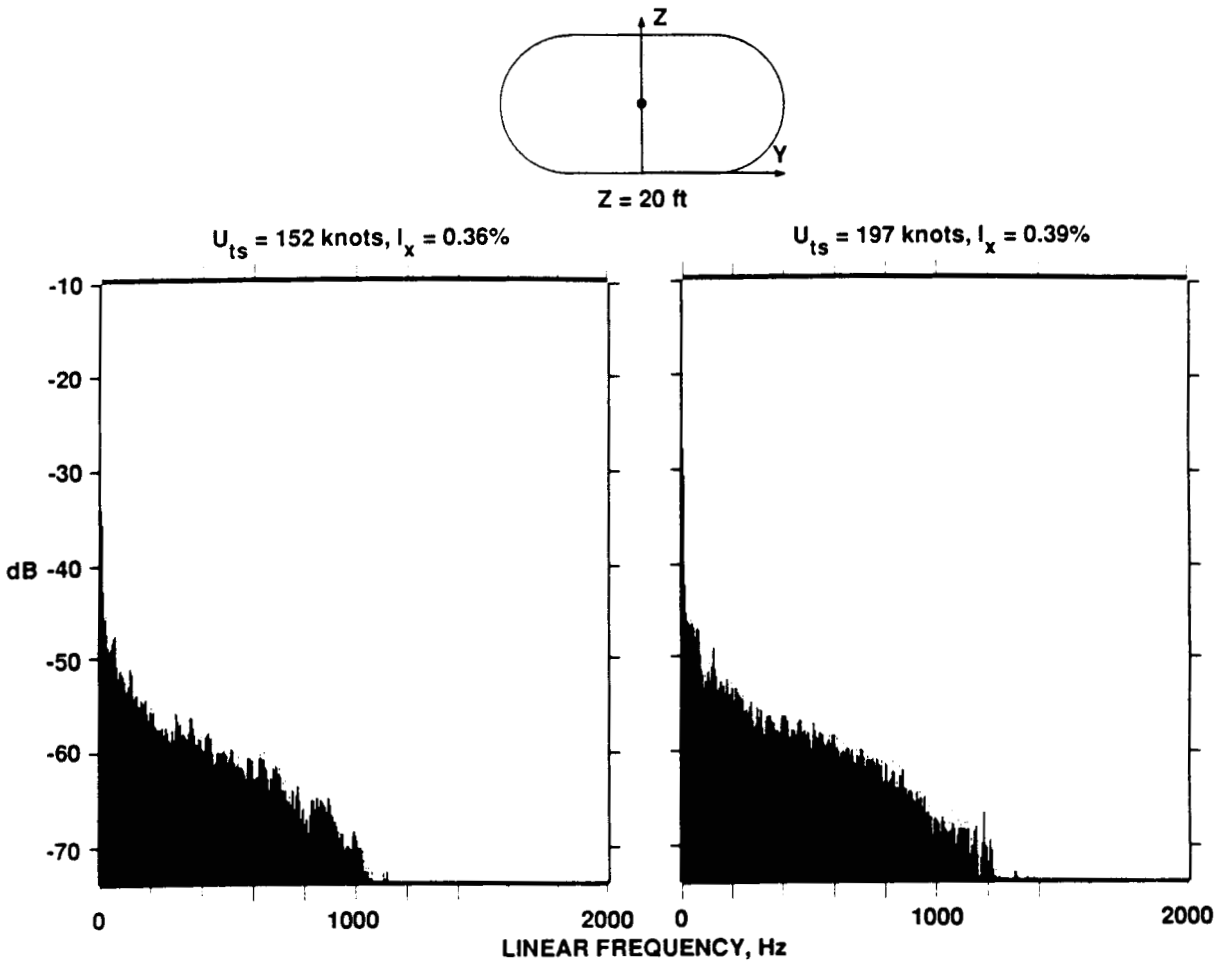

Figure 66.– Energy spectra (U_{ts} = 152 and 197 knots).

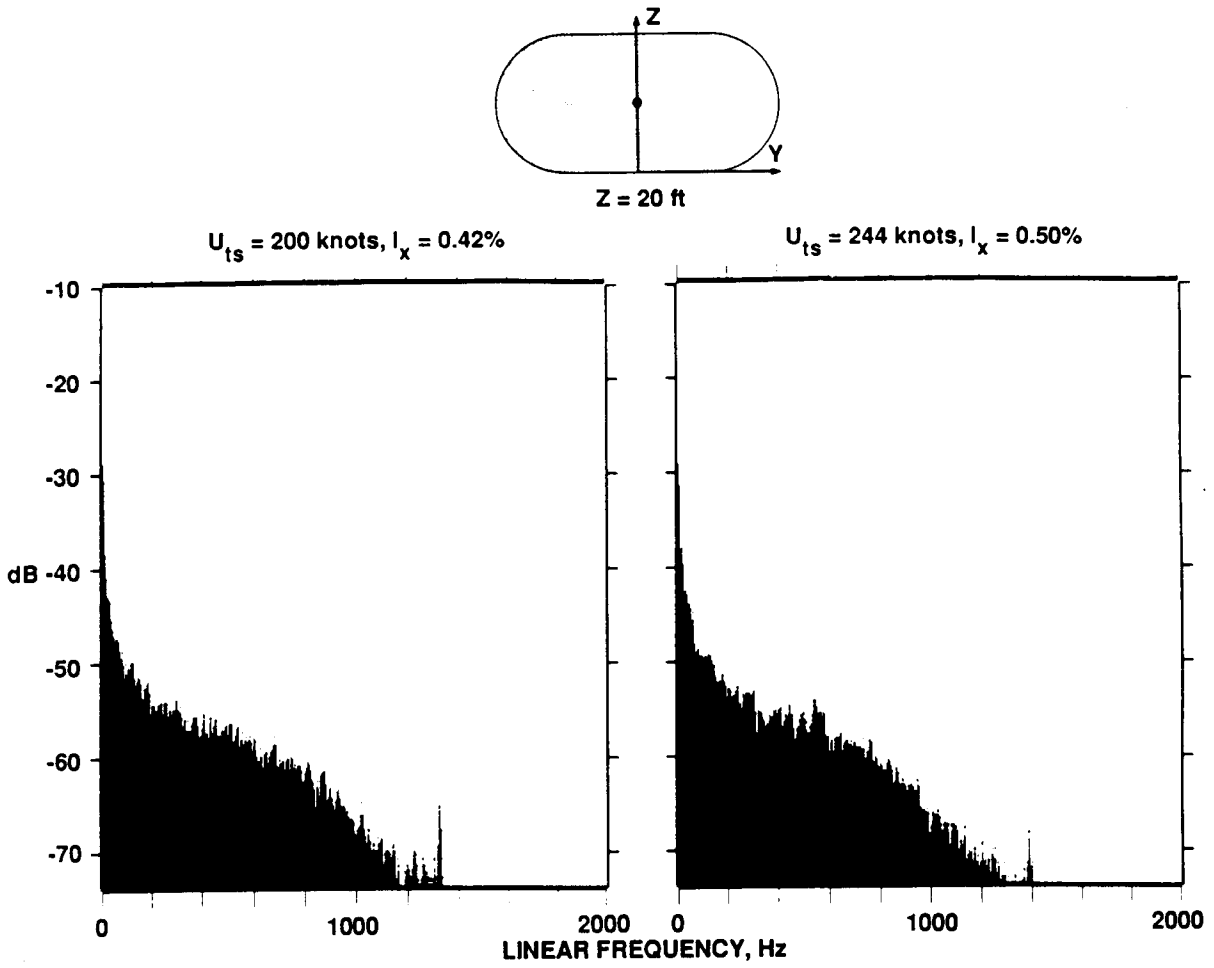

Figure 67.– Energy spectra (U_{ts} = 220 and 244 knots).

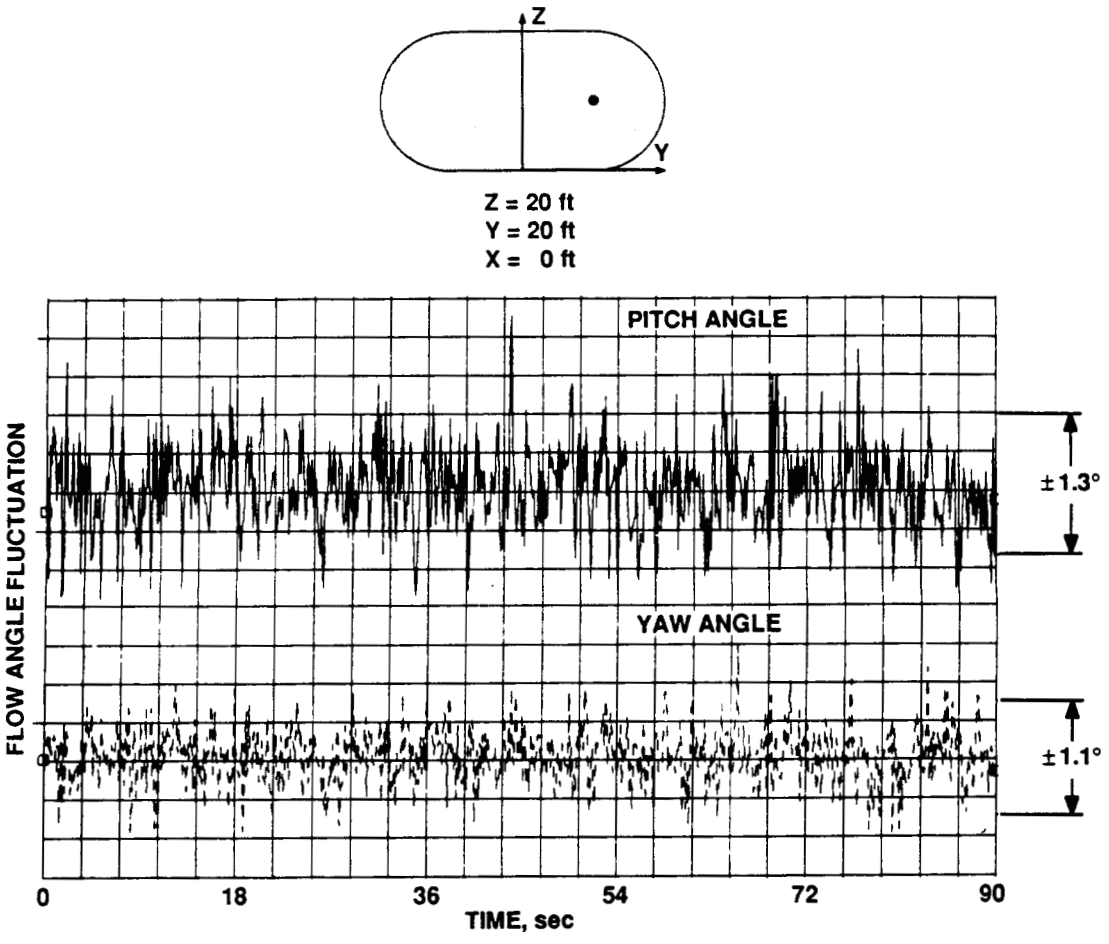

Figure 68.– 90 sec pitch and yaw angle time history for Y = 20 ft station (U_{ts} = 300 knots).

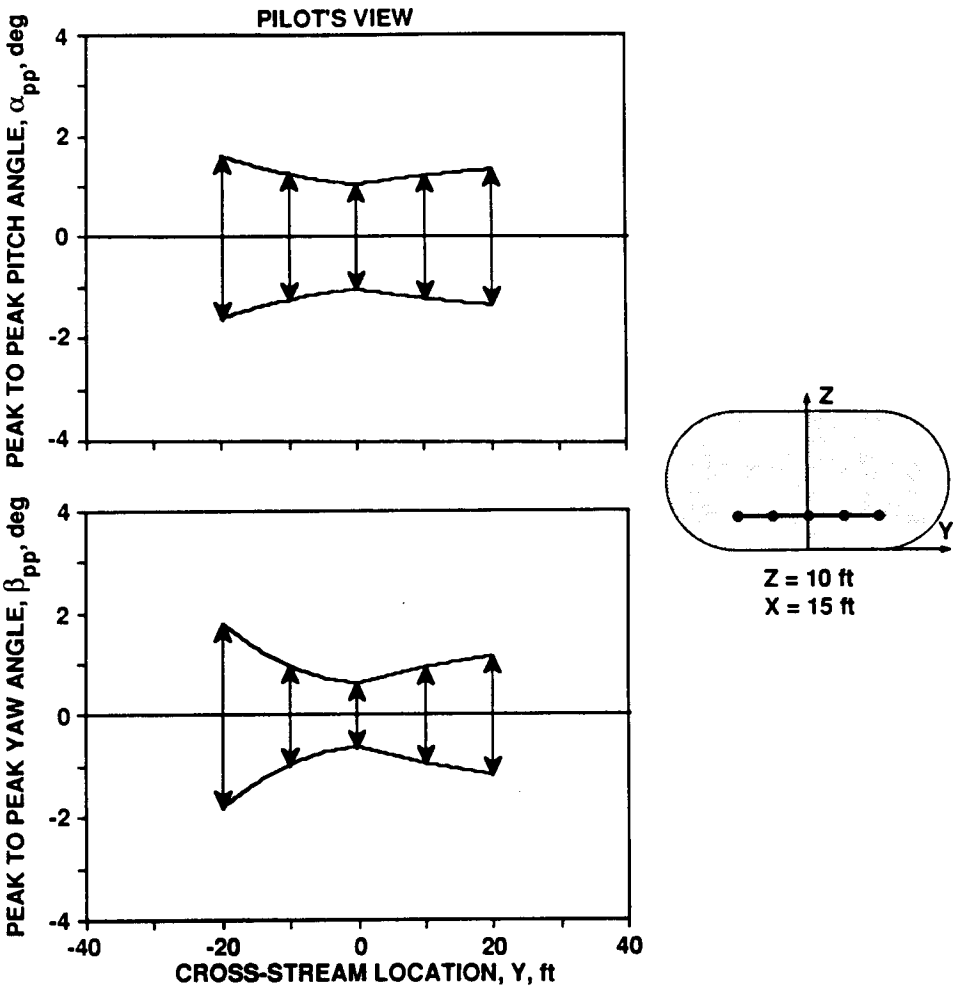

Figure 69.– Peak to peak pitch and yaw angles.

NASA
National Aeronautics and Space Administration

Report Documentation Page

1. Report No.	2. Government Accession No.	3. Recipient's Catalog No.
NASA TM-101065		

4. Title and Subtitle

Performance and Test Section Flow Characteristics of the National Full-Scale Aerodynamics Complex 40- by 80-Foot Wind Tunnel

5. Report Date

February 1989

6. Performing Organization Code

7. Author(s)

Peter T. Zell and Karen Flack

8. Performing Organization Report No.

A-89028

10. Work Unit No.

505-61-28

9. Performing Organization Name and Address

Ames Research Center
Moffett Field, CA 94035

11. Contract or Grant No.

13. Type of Report and Period Covered

Technical Memorandum

12. Sponsoring Agency Name and Address

National Aeronautics and Space Administration
Washington, DC 20546-0001

14. Sponsoring Agency Code

15. Supplementary Notes

Point of Contact: Peter T. Zell, Ames Research Center, MS 221-5, Moffett Field, CA 94035
(415) 694-3690 or FTS 464-3690

16. Abstract

Results from the performance and test section flow calibration of the 40- by 80-Foot Wind Tunnel are presented. A flow calibration test was conducted in May and June 1987. The goal of the flow calibration test was to determine detailed spatial variations in the 40- by 80-ft test section flow quality throughout the tunnel operational envelope. Data were collected for test section speeds up to 300 knots and for air exchange rates of 0, 5, and 10%. The tunnel performance was also calibrated during the detailed mapping of the test section flow field.

Experimental results presented indicate that the flow quality in the test section, with the exception of temperature, is relatively insensitive to the level of dynamic pressure and the air exchange rate. The dynamic pressure variation in the test section is within ±0.5% of mean. The axial turbulence intensity is less than 0.5% up to three-quarters of the maximum test section speed, and the vertical and lateral flow angle variation is within ±0.5° at all test section velocities. Cross-stream temperature gradients in the test section caused by the air exchange system were documented, and a correction method was established. Streamwise static pressure variation on the centerline is about 1% of test section dynamic pressure over 30 ft of the test section length.

17. Key Words (Suggested by Author(s))	18. Distribution Statement
Calibration Wind tunnel Flow quality Test section	Unclassified-Unlimited Subject Category – 01

19. Security Classif. (of this report)	20. Security Classif. (of this page)	21. No. of pages	22. Price
Unclassified	Unclassified	77	A05